DESIGN AND IMPLEMENTATION OF POWER SYSTEM STABILIZERS IN WIND PLANTS

by

Carlos Martinez
B.Eng. Concordia University

A thesis submitted to the Department of Electrical and Computer Engineering in partial fulfillment of the requirements of the degree of Master in Engineering

Department of Electrical and Computer Engineering,
McGill University,
Montréal, Québec, Canada
September 2009

Abstract

Wind energy, increasing its share in the generation mix, is intended to replace fossil fuel plants in order to reduce green house gas emissions. However, the replacement of conventional synchronous units by wind generators reduces the number of online Power Systems Stabilizers (PSS) and may therefore deteriorate the damping of critical swing modes, leading to a reduction of the power transfer capacity in transmission corridors. Several reports indicate that angular instability, due to insufficient damping and inadequate tuning or disabling of power system stabilizers, is one of the major events that lead and/or contributed to wide area blackouts.

Variable speed wind turbine generators are capable of fast decoupled real and reactive power control. A damping torque can be generated by modulating a fraction of the real and reactive power output of the wind farm. Supplementary active and reactive power control loops are designed and integrated in the wind turbine controls. Operating limits are added to restrict the kinetic energy exchange of the supplementary control loop within a specified turbine speed. An analytical method is developed in order to assess the effectiveness of real and reactive power modulation in damping inter-area oscillations and to justify the use and commissioning of wind based PSS. A wide area measurement based power system stabilizer suitable for wind farms is designed and integrated in the global and local controls of wind turbines. Feedback signals are selected based on an observability index of the selected mode(s). The proposed stabilizer transfer function is derived via a constrained H∞ optimization.

The controller is tested in time domain simulations using a two area four generators benchmark suffering from interarea oscillatory mode within the range of 0.4-0.6Hz. Testing scenarios show the resiliency and effectiveness of the wind based PSS in damping angular oscillations and stabilizing the power system. The damping contribution of the wind stabilizer is found to be comparable to two conventional PSS.

Résumé

Possédant un taux de croissance important, la filière éolienne est supposée remplacer des centrales électriques polluantes. La réduction du nombre de machines synchrones entraîne une diminution du nombre de stabilisateurs de réseau conventionnels menant à une dégradation de l'amortissement des oscillations angulaires critiques d'un réseau ce qui pourra limiter la capacité de transfert de puissance des lignes de transports. Plusieurs rapports indiquent que des oscillations angulaires excessives, causées par un manque d'amortissement, ont contribué ou même étaient à l'origine des pertes de charges, déconnection des alternateurs et des blackouts.

La génératrice éolienne, équipée par un contrôleur d'entraînement à vitesse variable, est capable de réguler précisément et rapidement sa puissance active et réactive d'une façon découplée. L'amortissement des oscillations angulaires peut être amélioré en modulant une fraction de la puissance active et/ou réactive des génératrices éoliennes. Des boucles de commandes supplémentaires sont introduites dans la structure de control des éoliennes. Des limites de modulation de puissance active sont ajoutées pour respecter les contraintes opérationnelles de vitesse rotationnelle des turbines. Une méthode analytique est développée pour évaluer le potentiel d'amortissement des oscillations de puissances à travers les interconnections, étant donné le placement d'une ferme éolienne dans un réseau électrique ainsi que le type de modulation. Des indices d'observabilité sont utilisés pour sélectionner les signaux d'entrée du stabilisateur. La fonction de transfert du stabilisateur est dérivée via une optimisation H∞.

Le contrôleur est testé dans un réseau qui consiste de 4 alternateurs séparés en deux zones. Le réseau possède un mode oscillatoire critique qui varie entre 0.4-0.6 Hz. Les scenarios comprennent des tests pour différents placements du parc éolien, niveaux de puissance du parc, et opérations du réseau. Les résultats démontrent l'efficacité des stabilisateurs des éoliennes à amortir les oscillations angulaires et à contribuer à la stabilisation du réseau.

Acknowledgements

I would like to thank Prof. Géza Joós, for his help, and patience during my Master's studies. I am also very grateful for the contributions of Prof. Innocent Kamwa, whose advice and expertise allowed me to improve the work. Through their guidance, I have attained a better grasp on engineering principles and industry needs. Also, I would like to thank Prof. Boon-Teck Ooi for guiding me early in the work.

I would like to extend my thanks to Prof. Francisco Galiana, Prof. Anthony Rodolakis, and Prof. Jorge Marques for sharing some of their experience. I am grateful for the support and friendship of John Chahwan, Jean Morneau, Hamed Golestani Far, Mohamed El Chehaly, Jonathan Robinson, Michael Ross, Sameh El Khatib, Bassam Frem, Omar Saadeh, Chad Abbey, Jose Restrepo, Ali Jahanbani Ardakani, Hugo Gil, Catalina Gomez-Quilles, Li Wei, Rodrigo Hidalgo, Makram de Freige, Saadat Qadri, Amir Kalantari, Moustafa Momen, Yongzheng Zhang and Quanrui Hao.

Special thanks to the *Institut du Génie de L'Énergie Électrique* (IGEE) administration for their continuous help and support. Also, I would like to thank Prof. Chadi Assi and Prof. Luiz Lopes from Concordia University and Prof. Gilles Roy from École Polytechnique de Montréal.

I would like to thank the financial support of the Wind Energy Strategic Network (WESNet), the Natural Sciences and Engineering Research Council of Canada (NSERC) and McGill University.

Finally I would like to thank my parents, Noellie and Raymondo, as well as my two brothers, Ricardo and Miguel. Also, special thanks to Mireille Kisso, Antoine Kassas and Albert Sleiman.

Table of Contents

LIST OF FIGURES

List of Tables

List of Abbreviations

WTG	*Wind Turbine Generator*
PMG	*Permanent Magnet Generator*
SG	*Synchronous Generator*
SCIM	*Squirrel Cage Induction Machine*
DFIG	*Doubly Fed Induction Generator*
VSWTG	*Variable Speed Wind Turbine Generator*
PSS	*Power System Stabilizer*
TCR	*Thyristor Controlled Reactors*
TSC	*Thyristor Switched Capacitor*
STATCOM	*Static Compensator*
HVDC	*High Voltage dc*
HVAC	*High Voltage ac*
VSC-HVDC	*Voltage Source Converter HVDC*
LCC-HVDC	*Line Commutated Converter HVDC*
FACTS	*Flexible ac Transmission System*
SVC	*Static Var Compensator*
PCC	*Point of Common Coupling*
WPSS	*Wind based PSS*
Gk	*Synchronous machine k*
GM	*Gain Margin*
PM	*Phase Margin*
WAMS	*Wide Area Measurements*
ΔP_W	*Active power output of the WPSS*
ΔQ_W	*Reactive power output of the WPSS*
P_{WTG}	*Individual WTG power output*

List of Acronyms

V_{REF}	*Reference synchronous machine voltage*
ΔV_{PSS}	*PSS dependant reference voltage*
ΔV	*SG terminal voltage deviation*
ΔT_m	*SG mechanical torque deviation*
$\Delta\omega_R$	*SG speed deviation*
$\Delta\delta$	*SG internal angle deviation*
V_W	*Wind speed*
Cp	*Power coefficient*
ρ_{air}	*Air density*
λ	*Tip speed ratio*
R	*WTG blade radius*
β	*Pitch angle*
K_G	*Gear constant*
ω_T	*WTG rotational speed*
P_{REF}	*WTG reference active power*
Q_{REF}	*WTG reference reactive power*
X''	*WTG sub-transient impedance*
Xeq''	*Wind farm equivalent sub-transient impedance*
fos	*Interarea oscillation frequency*
HT	*WTG inertia constant*
Pm	*WTG mechanical power*
Pe	*WTG electrical power*
X_T	*Transformer series impedance*
R	*Line resistance*
X_L	*Line impedance*
B	*Line admittance*
$\Delta\delta_k$	*Internal angle deviation of synchronous machine k*
$\Delta\omega_k$	*Speed deviation synchronous machine k*
P_{Gk}	*Electric power output of synchronous unit k*
P_W	*Wind farm active power output*
Q_W	*Wind farm reactive power output*
M_k	*Inertia constant of synchronous units k*
D_k	*Damping constant of synchronous unit k*
V_G	*Synchronous units terminal voltages*
I_G	*Synchronous units current injection*
V_L	*Voltage at load buses*
I_L	*Load current injection*
Y	*Admittance matrix*
Y_R	*Reduced admittance matrix*
Y_{WIND}	*Equivalent wind farm admittance as seen by the power system*
CI_P	*Controllability index of active power PSS*
CI_Q	*Controllability index of reactive power PSS*

OI	*Observability index of interarea mode*
G(s)	*Power System Frequency Domain Transfer Function*
do(s)	*Output Disturbance*
U(s)	*Output of Wind Based Power System Stabilizer*
Y(s)	*Output of the plant G(s)*
S_0	*Output Sensitivity*
T_0	*Output Transmission*
Wu(s)	*Input Weighting Function*
We(s)	*Output Sensitivity Weighting Function*
Wt(s)	*Output Transmission Weighting Function*

Chapter 1: Introduction

1.1 Power Systems Stability

Traditionally, power systems are regional networks providing power to local nearby loads. Early stages of power system evolution occurred following the generation market deregulation. Transmission networks increased in size and interconnection length as a consequence of generation owners' tendency to dispatch generation far from load in order to maximize revenue. Due to the large area that transmission networks occupy, power systems integrity is threatened by natural events, outages of equipments and lines, human factor as well as delays in operation and maintenance.

Following several blackouts, power system stability has seen major interest by the electric utility. As transmission networks increase in size and complexity, it is important from an economical and national security standpoint to operate reliable, secure and stable operation. In today's competitive global market, continuous energy supply to loads is essential to maintain economic growth. Any loss of industrial load leads to a reduction in production, profit and as a result limits the industry's ability to compete on a national and international level. In some regions, social welfare dictates continuous supply of electric energy as residential customers rely heavily on electricity for heating. In essence, the power system must be flexible, stable and robust to meet the needs of current and future customers. In order to achieve such goals, utilities put forth a design philosophy that consists of four principles [1]:

- Service continuity following a set of predefined contingencies/events
- Incorporate means to avoid system wide failure
- Strategic equipment must not be damaged in order to ensure system restoration if needed
- Restore system within minimum delays

Today, power systems are going through another evolution stage as renewable energies, distributed and centralized, are increasing their penetration into the generation

mix. Renewable generation adds more complexity to the design and operation of a power system as they are inflexible, intermittent or variable yet reliability, stability and security requirements must be upheld. Among the different renewable technologies, wind energy is rapidly increasing its share in the generation mix [2], Figure 1.1.

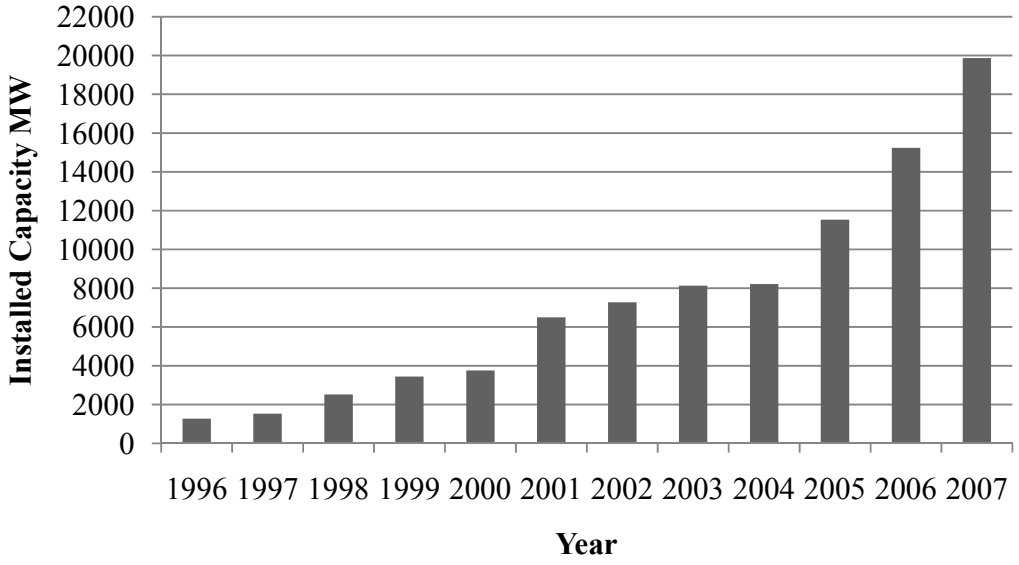

Figure 1.1. Yearly Wind Energy Installation

1.2 Proliferation of Wind Energy

The Kyoto protocol has set in motion a series of incentive programs oriented towards aiding and encouraging investors in renewable energies. In Europe, the Feed-in tariff is the most widespread renewable energy promotion policy. The feed-in tariffs set the price to be paid for renewable energy generated along with an obligation to purchase that energy. Europe's objective is to reach 300GW of wind energy by the year 2030. The United States put forth a production tax credit policy, recently extended to 2012, and renewable portfolio standard to aid in the integration of renewable generation. These incentive programs aided the United States to surpass a record high of 20,000MW of installed wind capacity with a 20% target set for the year 2030. Canada surpassed the 2GW installed wind capacity in 2008 and is aiming at 20% wind penetration by 2025.

1.2.1 Wind Turbine Generator Technologies

The first commercial wind turbines used fixed speed generators to convert the wind power into electrical power. With fixed speed technology, the rotational speed is defined by the grid operating conditions and independent of wind speed. Fixed speed wind turbine generators are designed to achieve maximum efficiency at a predefined wind speed. This type of technology increases the stress on the mechanical components of the system due to the presence of periodic pulsations [3].

As the capital cost of wind farms is usually large [4], there is interest in maximizing the energy produced and the life expectancy of Wind Turbine Generators (WTG) for a wide range of wind speeds and grid operations. Popular solutions include the use of power electronics converters, Figure 1.2, in order to asynchronously couple the WTGs from the grid thus allowing operation at different rotational speed in order to maximize energy capture.

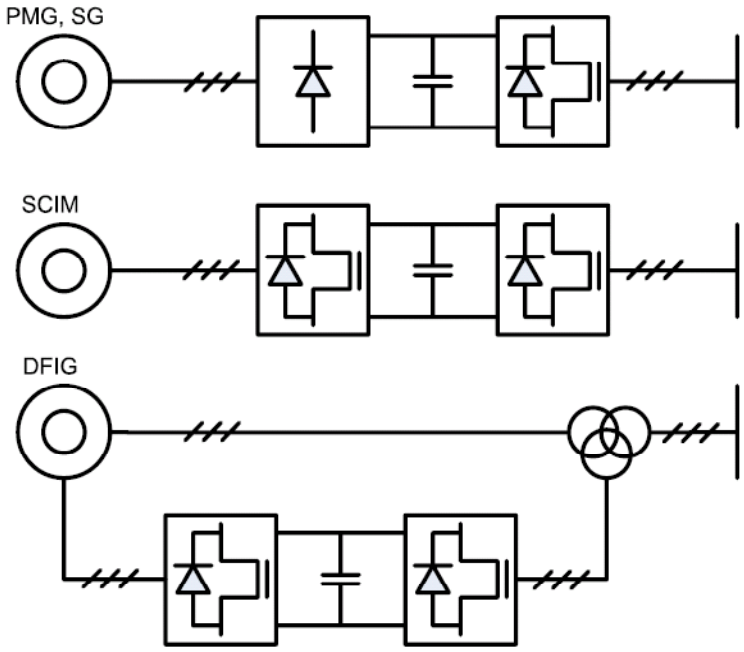

Figure 1.2. Topologies of Converter Based Variable Speed Wind Turbine Technologies

1.2.2 Variable Speed Wind Turbine

Variable Speed Wind Turbine Generators (VSWTG) solutions include direct drive, where the generator shaft is directly coupled to the wind turbine, and the geared drive, where the generator shaft is coupled to the wind turbine via one or more gears.
Available VSWTG technologies include:

- Squirrel Cage Induction Machine (SCIM)
- Doubly Fed Induction Generator with three-stage Gearbox (DFIG3G)
- Direct-Drive Synchronous Generator (DDSG)
- Direct-Drive Permanent Magnet Generator (DDPMG)
- Permanent Magnet Generator with single stage Gearbox (PMG1G)
- Doubly fed induction generator with single-stage gearbox (DFIG1G)
- Synchronous Machine equipped with Hydro-Dynamically Controlled Gearbox and directly connected to the grid (HGSG)

Table 1.1. Variable speed wind turbine technologies

Drive Type	**Geared Dive**				**Direct Drive**	
Technology	**DFIG3G**	**PMG1G**	**DFIG1G**	**HGSG**	**DDSG**	**DDPMG**
Converter Rating	20-50%	100%	20-50%	0%	100%	100%
Gearboxes	3	1	1	1	0	0

The DFIG3G and PMG1G are most suitable for offshore installations due to their relatively lower weight. Currently, the most widespread technologies are the DFIG3G, having the highest yearly energy yield per cost [5], followed by the DDSG.

1.2.3 Technical Benefits of Variable Speed Wind Turbines

It is feared that the presence of large wind penetration will reduce the system inertia and thus affect the overall frequency regulation and power system robustness. Hydro dominated power systems are particularly vulnerable to frequency incursions. In the event of frequency drop, governor control sends a command to open the valve in order to increase the flow of water. However, as the valve opens, pressure decreases while the flow of water is kept constant due to its inertia, thus leading to a decrease in the power output followed by an increase when the pressure builds back up. Asynchronous coupling

and fast current control dynamics allow converter based VSWTGs to tap into the stored kinetic energy in order to provide fast frequency support to limit frequency excursions [6-9]. Horns Rev offshore wind farm is equipped with controls to provide balancing and frequency support for the power grid [10].

VSWTGs may contribute to the short term voltage stability and transient stability of distribution networks by modulation of active and reactive power [11]. Both voltage flicker and harmonic levels are lower with VSWTGs than fixed speed wind turbine generators [12].

1.2.4 Wind Integration and Grid Codes

System operators are more inclined to operate wind parks similar to synchronous generators as the experience in dealing with conventional plants is well established. Typical wind farm operation requirements were imposed in the form of grid codes for wind farms in order to ensure safe operation to the power system. Requirements include [13,14]:

- Real and reactive power control, including ramp rates
- Power factor must remain above 0.95(leading or lagging)
- Terminal voltage control
- Low voltage ride through capabilities
- Operational monitoring and communication data
- Frequency regulation and power system stabilizers (optional)

One of the main concerns to power system operators is the variability of the wind generation and the complication it may cause in terms of line congestion, market prices and power system stability. Today's power systems are capable of reaching 20% wind penetration [15]. But, in order to reach higher penetrations, further advancements are suggested [16,17]:

- Improvements in wind plant modeling
- Improvement in wind plant operation (frequency regulation, voltage control, PSS)
- Load following, quick start
- Improved global wind generation forecasting (hour and day ahead)

- Transmission planning
- Wide area control
- Energy storage

1.2.5 Compliance of Wind Farm with Grid Code Requirements

Wind integration grid codes require control of power factor, terminal voltage and low voltage ride through technologies. Therefore, wind farms must be equipped with local reactive power control technologies. Converter based reactive compensation technologies, shown in Figure 1.3, include Thyristor Controlled Reactors (TCRS), Thyristor Switched Capacitors (TSC) and Static Compensators (STATCOM). Power electronics solutions are favored due to their control flexibility, response time and relatively lower cost than traditional synchronous condensers [18-20].

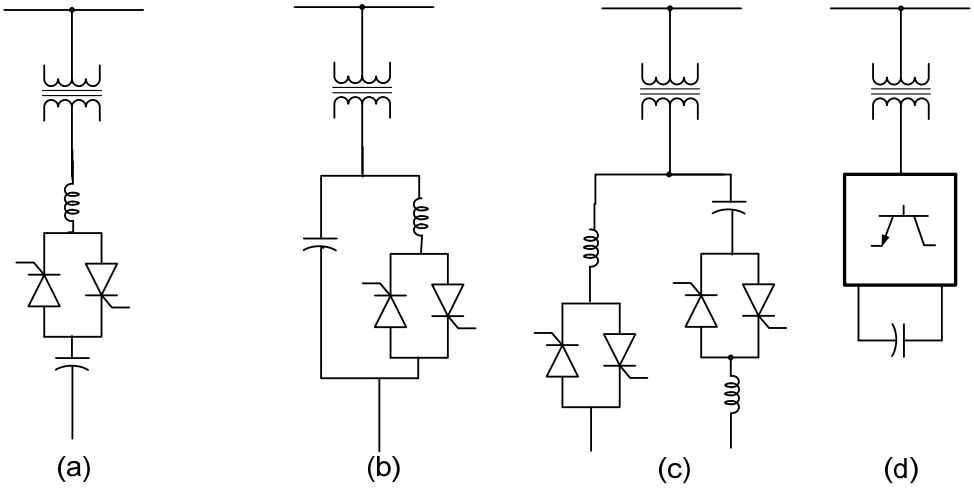

Figure 1.3. Power Electronics Based Reactive Power Compensation. (a)TSC configuration; (b) TCR configuration; (c) Combined TCR and TSR; (d) STATCOM

Table 1.2. Overview of Reactive Power Compensation Solutions

	Synchronous Condenser	TCR & TSC	STATCOM
Compensation Accuracy	Good	Very Good	Excellent
Control Flexibility	Good	Very Good	Excellent
Response Time	Slow	Fast	Very Fast
Cost	High	Moderate	Low

1.3 Power System Stabilizers

Small-signal analysis of power systems shows that large interconnected power systems exhibit power oscillations between coherent groups of generators within the order of 0.1-0.8Hz [21-25], known as interarea oscillations. Synchronous units also exhibit local oscillatory modes between generators within the same plant (*also known as intraplant modes)*, in the range of 1-4Hz, and torsional modes associated with the shaft system, in the range of 10-46Hz [26]. These power swings causes the rotor speed of conventional machines to oscillate, with the same frequency, around their nominal synchronous speed.

Stressed operation of power system reduces damping of interarea modes [26-28]. Stability of swing modes is essential to maintain synchronous operation of generating plants in a power system. PSS were designed to produce a controllable damping torque by modulating the field excitation winding of synchronous machines. Typical conventional PSS design, Figure 1.4. Figure 1.5 displays a block diagram of a single synchronous machine infinite bus model.

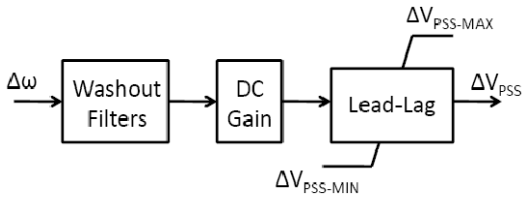

Figure 1.4. Conventional Power System Stabilizer Design

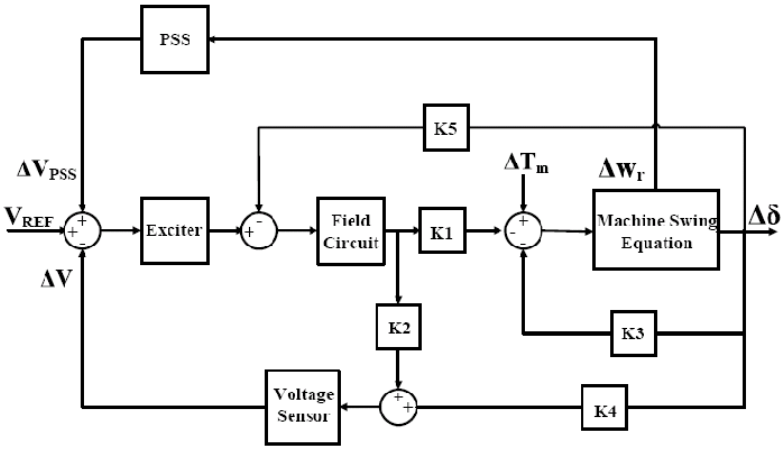

Figure 1.5. Synchronous Machine Infinite Bus Comprehensive Model

1.3.1 Synchronous Machine Based Power System Stabilizers: State of The Art

A modal performance measure was introduced as a cost function in an optimization approach to tune [29]. The method consists of specifying an envelope for a given oscillating mode and then optimizes PSS parameters to minimize the weighed area enclosed in the envelope and thus reducing the amplitude of oscillations. Kamwa *et. Al* defined a new modal performance measure in order to ensure and enhance modal selectivity [30]. Stability and robustness optimization constraints were introduced to improve the overall performance of the PSS design [31].

Recent work shows that conventional PSS have limited capabilities when it comes to damping the common low frequency. In [32], the capabilities of conventional PSS are enhanced using instantaneous measurements from Phase Measurement Units (PMU). PSS optimization methods and coordination of multiple PSS in a large system consists of [32]:

- Having 2 separate control loops (Local and Global)
- Tune the local channel first
- Tune global channel and coordinate channels

Multiband PSS (PSS4B) design, shown in Figure 1.6, has enhanced performance for interarea, islanding and steady state dynamics [21]. PSS4B uses rotational speed deviation, derived from electrical measurement at the machine terminal, and the electric power output as feedback signals. The low and intermediate frequency control loops are used respectively for interarea and local modes of oscillations while the high frequency control loop is used for torsional modes. PSS4B was found to have superior damping capability of the low frequency mode, compared to conventional PSS, without compromising the damping of local and torsional modes.

In [33], wide area control scheme for conventional generators is designed to increase damping of pre-selected interarea mode(s) of oscillation. The approach requires monitoring of synchronous machines and communication to send and receive control commands. Communication and processing delays are not expected to impact the performance of the damping controller since the oscillating modes in question are in the order of 0.1-0.8Hz.

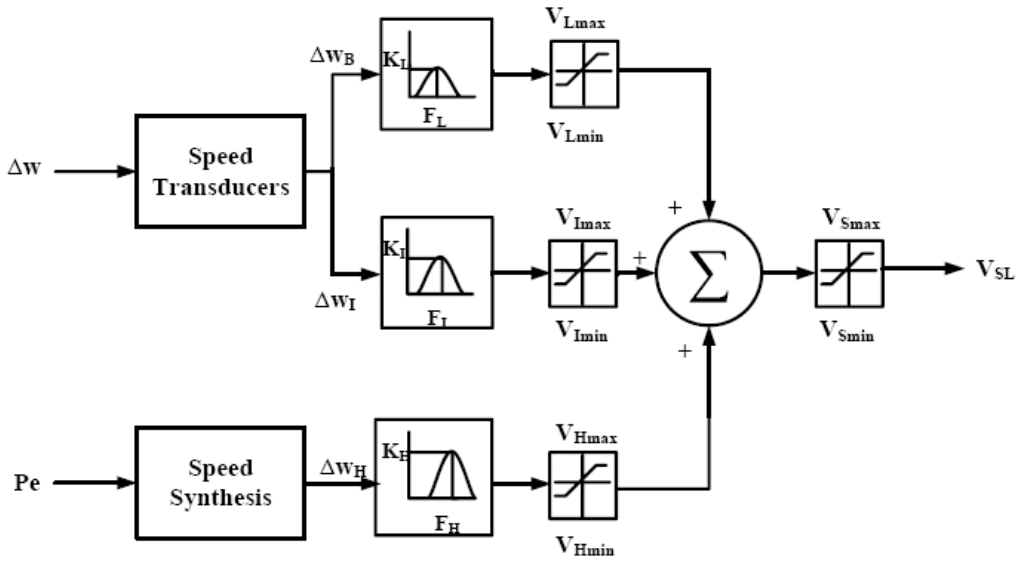

Figure 1.6. Multiband Power System Stabilizer

1.3.2 Experience with FACTS, HVDC and Load Modulation

VSWTGs are comparable to shunt FACTs and VSC-HVDC in their control of real and/or reactive power. It is demonstrated that FACTS and VSC-HVDC can contribute to damping of interarea oscillations. This section reviews research on FACTS, HVDC and load modulation that could be extended to VSWTG based PSS controllers.

In [34-36], it is proven that, in order to damp the rotor oscillation of a synchronous generator, P injection is most effective near the generator and Q injection is most effective at the middle of a line. The frequency deviation at the point of connection was found to be a good stabilizing signal. The study concludes that a combination of P and Q injection is ideal to damp oscillation along a line.

In [37], HVDC based PSS have proven to enhance the damping of power swings in the Chinese Southern power grid. It is found that the frequency deviation, between the rectifier and inverter point of connection, is a sufficient input signal and does not need phase compensation. In [37], a coordinate controller tuning method, focusing on maximizing damping through an optimization formulation, is presented.

In [38,39], a Lyapunov based approach is used to derive control laws for series FACTS or Controllable Series Devices to damp interarea mode of oscillation. In [40-42], the damping potential of FACTS devices is investigated through development of a linearized state space model of a power system. SVCs have good damping capabilities;

however precautions must be taken, since at very low loads, SVCs could provide negative damping. A mathematical measure for selection and placement of FACTS damping controllers is proposed [40-42].

In [43], interarea oscillation damping is done using active load modulation. It is worth mentioning that only a small percentage of a total bus load needs to be modulated. In [44], super magnetic energy storage systems proved to be capable of damping interarea oscillations.

1.3.3 Wind Machine Based Power System Stabilizers

It was argued that VSWTGs could add damping of interarea oscillations as they reduce the electric loading of conventional plants, thus reducing the stress in the system [45,46]. The studies do not take into consideration any increase in load or the retirement of fossil fuel plants. On the other hand, recent studies have shown that DFIG based WTGs may potentially degrade the angle stability of the system [47]. In [48], it is observed that an increase in penetration of DFIG may have a beneficial or detrimental impact on the damping of interarea modes. In light of conflicting arguments, it is safe to assume that damping contribution of DFIG based wind farms under standard operating modes is not guaranteed.

Hughes *et al.* designed a Power System Stabilizer (PSS) for DFIG based VSWTGs. The stabilizer uses the slip as a feedback signal and modulates the real power output of the wind farm [49,50]. However, the test system used does not exhibit interarea oscillations, in which case, conventional power system stabilizers are capable of damping such modes. The observability of interarea mode(s) may not be guaranteed, thus potentially degrading the damping capability of the DFIG based PSS.

1.4 Research Motivation

One of the motivations behind this work is to continue the line of research done by the McGill Power Engineering Research Laboratory (PERL) on grid integration of wind energy resources [7,51-58]. Research objectives are to investigate the potential of a wind farm to damp interarea oscillations and to develop a control algorithm in order to allow a wind farm to actively contribute to damping of critical interarea modes of oscillations.

1.4.1 Problem Definition

Wind energy is intended to replace fossil fuel based generation. As conventional plants are curtailed, their corresponding PSS are taken offline thus potentially reducing angular stability in a power system. Reported angular instability incidents include disabling of conventional power system stabilizers due to under/over excitation current limiters, transducer failures and/or scheduled maintenance [59]. The problem is further aggravated during periods of high demand or if the range of interarea oscillations falls outside the bandwidth of available power system stabilizers following a severe disturbance [21-25].

Marginally damped or undamped interarea oscillations often lead to excessive power swings across inter-tie connections, forcing relays to trip the lines and separate a power system into a number of islands. Each island will have to balance its real and reactive power generation and demand in order to ensure voltage and transient stability and maintain continuous operation. An unbalance between generation and load often leads to generator tripping and/or load shedding. In worst case scenarios, the unbalance is not met and the cascading events lead to a blackout.

Several reports show that angular instability either caused or contributed to a series of cascading events leading to separation of a power system [60], and blackouts [61,26].

1.4.2 Research Goals

Wind energy is increasing its penetration into the generation mix. Variable speed wind generators have the added capability of fast control of real and reactive power generation. The purpose of this research is to take advantage of the flexible control of real and reactive power to enhance damping of critical interarea oscillations. Earlier research showed that the location and the type of modulated power directly impact the damping potential of the wind farm. This research is primarily focused on assessing the damping potential of a wind farm in a predefined location. It is worth emphasizing that the research does not deal with placing the wind farms where there is high damping potential but to assess the damping potential given a wind farm location.

Research objectives include:

- Investigate the damping potential of wind generation

- Develop a methodology to select the type of power modulation
- Design supplementary control loops in order to modulate the active and/or reactive power output of wind turbines
- Make use of wide area measurements to maximize the overall performance of the proposed stabilizer
- Integrate a robust wind based power system stabilizer, with discontinuous damping action, into global wind farm controller
- Coordinate individual wind generator operation
- Test the proposed controller

1.4.3 Contributions

To the best of the author's knowledge, the thesis provides new ideas in the field of power system stabilizers by:

- Design of supplementary active power modulation loop
- Develop a methodology to assess and compare the damping potential of the active and/or reactive power modulation given the location of a wind farm
- Provide recommendation to install wind based power system stabilizers given the location of a wind park
- Tuning a wind based power system stabilizer via H∞ constraint optimization

1.5 Thesis Outline

The thesis covers the following topics:

Chapter 2 gives a background on doubly fed induction wind generator, and introduces the model and controls of a commercial doubly fed induction generator. Chapter 2 also covers modeling of a wind farm used in this thesis.

Modal analysis on a power system benchmark is highlighted in Chapter 3. In addition, Chapter 3 describes the method used to assess and quantify the damping potential of active and reactive power modulation, and to select feedback signals for the wind based power system stabilizer.

Chapter 4 presents a methodology to design robust wind based power system stabilizer. An interarea oscillation detection scheme is incorporated into the controls of

individual wind turbine generators. Time domain simulation results, displaying the wind based power system stabilizer performance and robustness, are included in Chapter 4.

Chapter 5 summarizes the performance of the proposed solution as well as potential applications and future work.

Chapter 2: Wind Plant Modeling and Control

2.1 Introduction

Fixed speed generators were the most popular choice in the early stages of development of the wind industry. However, fixed speed wind turbine generators faced serious deficiencies when it came to grid integration, mechanical fatigue and energy conversion. Fixed speed wind turbine generators suffer from periodic pulsation, leading to increased stress on the mechanical component of machine, nacelle and drive train [3]. Due to the lack of control, only a portion of the power may be harnessed thus limiting the revenues from energy sold. Squirrel cage induction machine, one of the most widespread, exhibits a drop in power factor when operating below nominal point due to the increase in reactive power consumption.

Although the cost of fuel of wind generators is practically zero, capital costs of wind farms can reach 80% of the total project cost over its lifetime and a developer is often required to cover this cost at the initial stages of building [4]. It is within the wind farm owner's best interest to maximize the life of the wind turbine generators and the energy sold to the grid while complying with evolving grid codes. Modern wind generators make use of power electronics solutions to allow the wind turbine to maximize energy capture [62,63], reduce stress on the shaft and gearbox and improve power quality of the wind park [12].

The DFIG is the most economical as its performance is comparable to that of full converter WTGs but uses a back to back VSC converter rated at 20-50% of its nominal power. In light of the technical and economical aspects of variable speed turbine solutions, the thesis considers the control and modeling of DFIG based wind parks. The published 1.5MW DFIG model and controls schematics are considered [64,65]. However, the proposed wind based power system stabilizer can be customized to operate with other types of converter based wind generators.

2.2 Doubly Fed Induction Machine Background

The doubly fed induction machine is, in theory, a transformer with its secondary rotating at a certain speed ω_m when a mechanical torque is applied to the shaft, Figure 2.1. Power is transmitted through the magnetic core. The slip is defined in Eq. (2.1) as the ratio between the rotor circuit electric frequency and the stator electric frequency. *n.s* in Eq. (2.2) represents the transformer ratio between the rotor side and the stator side.

$$s = \frac{\omega_0 - \omega_m}{\omega_0} = \frac{\omega_r}{\omega_0} \tag{2.1}$$

$$|V_{rs}| = n\,s|V_r| \tag{2.2}$$

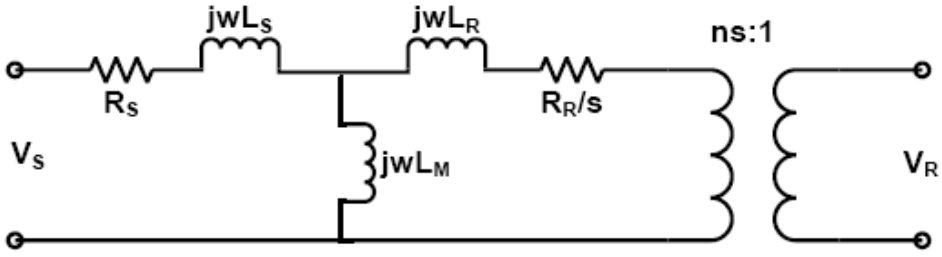

Figure 2.1. Doubly Fed Induction Machine Equivalent Circuit

The mathematical model of the DFIG in the dq frame is shown in Eq. (2.9) (2.5). The machine parameters Ls, Lm, Lr, Rs and Rr are determined a priori by machine field tests.

$$L_{ss} = L_S + L_M \tag{2.3}$$

$$L_{rr} = L_R + L_M \tag{2.4}$$

$$M_1 = \begin{bmatrix} R_s + \dfrac{dL_{ss}}{dt} & -\omega_0 L_{ss} \\ \omega_0 L_{ss} & R_s + \dfrac{dL_{ss}}{dt} \end{bmatrix} \tag{2.5}$$

$$M_2 = \begin{bmatrix} \dfrac{dL_m}{dt} & -\omega_0 L_m \\ \omega_0 L_m & \dfrac{dL_m}{dt} \end{bmatrix} \tag{2.6}$$

$$M_3 = \begin{bmatrix} \dfrac{dL_m}{dt} & -(\omega_0 - \omega_m)L_m \\ (\omega_0 - \omega_m)L_m & \dfrac{dL_m}{dt} \end{bmatrix} \tag{2.7}$$

$$M_4 = \begin{bmatrix} R_r + \dfrac{dL_{rr}}{dt} & (\omega_0 - \omega_m)L_{rr} \\ (\omega_0 - \omega_m)L_{rr} & R_r + \dfrac{dL_{rr}}{dt} \end{bmatrix} \tag{2.8}$$

$$\begin{bmatrix} V_{sd} \\ V_{sq} \\ V_{rd} \\ V_{rq} \end{bmatrix} = \begin{bmatrix} M_1 & M_2 \\ M_3 & M_4 \end{bmatrix} \begin{bmatrix} I_{sd} \\ I_{sq} \\ I_{rd} \\ I_{rq} \end{bmatrix} \tag{2.9}$$

2.3 Wind Turbine Generator

Modern wind turbines use aerodynamic lift to convert the kinetic energy of air into mechanical power. The rotating blades transfer the captured power from wind to the generator where the mechanical power is converted to electrical power and fed to the grid.

The mechanical power captured by the WTG, Figure 2.2, is calculated using Eq. (2.10). The power coefficient, Cp, is the percentage of energy captured by the rotating blade. According to Betz's law, the theoretical maximum power coefficient is of the order of 59%.

$$P_W = 0.5\pi\rho_{air} C_P(\lambda, \beta) R^2 V_W^3 \tag{2.10}$$

Where ρ_{air} is the density of air, λ is the tip speed ratio defined in Eq. (2.11), V_w is the wind speed in m/s, R is the blade radius and β is the pitch blade angle.

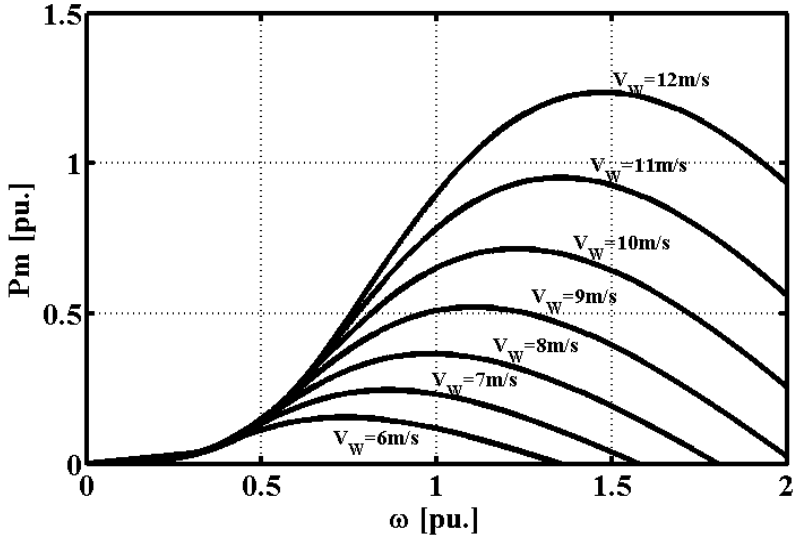

Figure 2.2. Wind Power Versus Rotational Speed

$$\lambda = K_G \frac{\omega_m R}{V_W} \tag{2.11}$$

2.3.1 Grid side converter control

Depending on the rotational speed, the DFIG rotor may absorb or generate power, leading to a reduction or increase in dc-link capacitor voltage. The grid side converter is controlled to maintain the dc voltage to its reference value through continuous exchange of active power between the grid and the converter system. The grid side converter may also be equipped with a reactive power control loop, whose capacity is limited by the converter rating the active power exchange.

2.3.2 Machine side converter control

In steady-state mode of operation, the magnetic shunt inductance, in Figure 2.1, may be neglected due to its relative high impedance and the derivative terms in Eq (2.5) may be set to zero. Thus, reference rotor current may be calculated based on the desired active and reactive power output [66,67]. High current control bandwidth is preferred since slow current control bandwidths render the closed loop system vulnerable to oscillatory modes within the range of line frequency [68].

2.3.3 Variable Pitch Control

Controlling the pitch angle affects the lift forces on the blades thus varying the aerodynamic torque. In other words, pitch control actions modify the power coefficient, Cp, of Eq. (2.10) and directly impacts the mechanical power at the shaft of the generator, Figure 2.3.

During rated WTG power operation, variable pitch control is used to maintain the rotor speed within acceptable limits; while variable pitch control is applied to ensure maximum power capture at low wind and below rated WTG power.

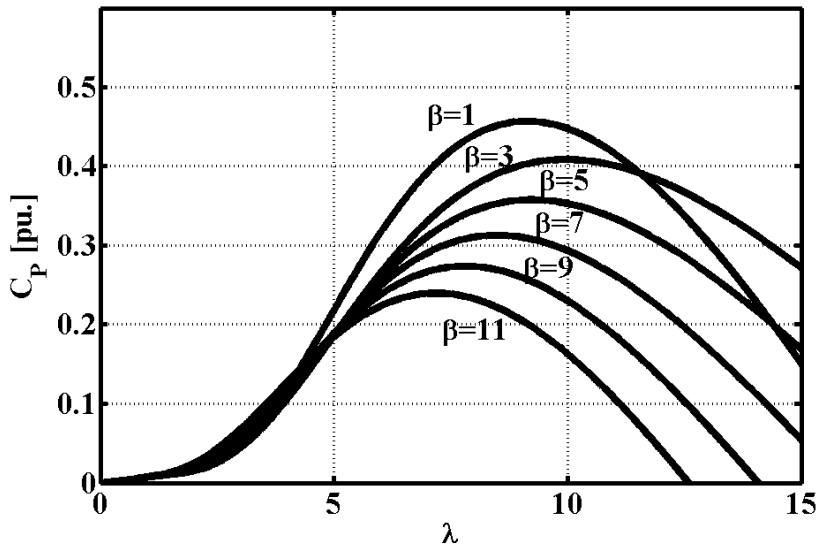

Figure 2.3. Power Coefficient Versus Tip Speed Ratio

2.4 Commercial 1.5MW Wind Turbine Model

This section describes the steady-state standard control of a commercial 1.5MW DFIG based wind turbine.

2.4.1 Active Power Control

Maximum peak power tracking is achieved by regulating the rotational speed based on a predefined lookup table, shown in Figure 2.4, given the measured electric power output of the DFIG. Once the reference speed is derived from Figure 2.4, torque control is used to match the rotational speed to its reference value, Figure 2.5. The control algorithm of the WTG, shown in Figure 2.5 [65], is summarized below:

- When the generated power is below 0.75pu, Eq. (2.12) is used to generate the reference rotational speed, ω_{REF}.
- The reference speed is set to 1.2pu for power levels above 0.75pu and pitch control operates when rotational speed increase above 1.2pu.

$$\omega_{REF} = -0.67P_e^2 + 1.42P_e + 0.51 \tag{2.12}$$

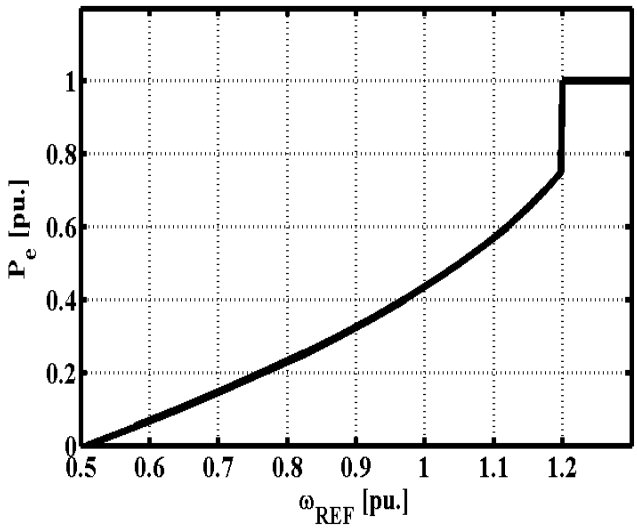

Figure 2.4. Variable Speed Control Range of DFIG

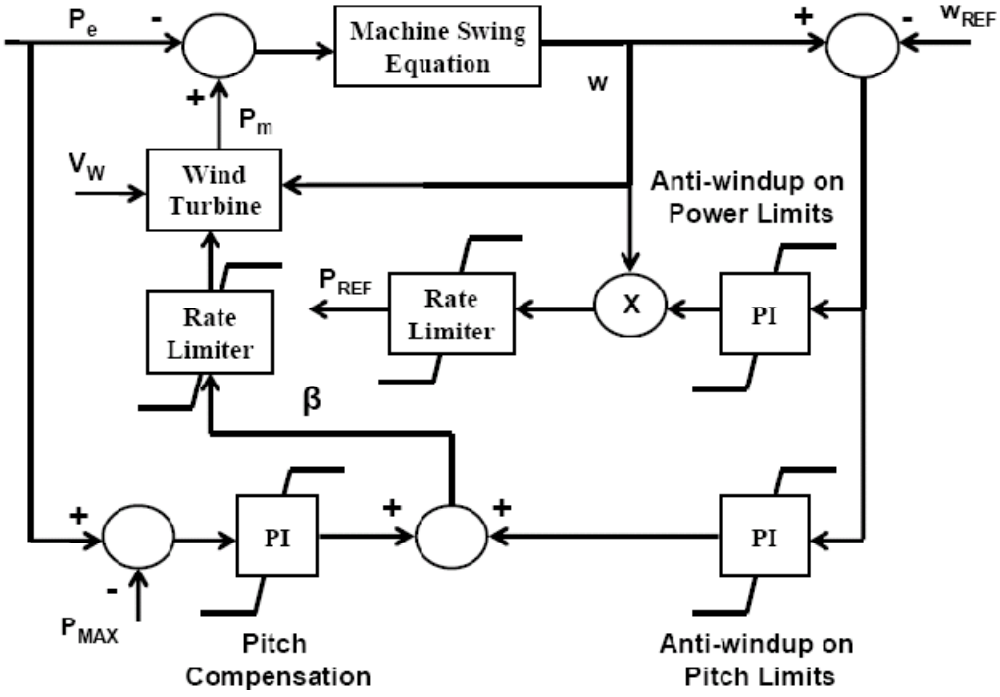

Figure 2.5. Wind Generator Control Model Block Diagram

2.4.2 Reactive Power Control

There are three types of reactive power control in variable speed wind turbine generators:

- Power factor control: reactive power is constantly adjusted, following the active power level, so that the generator power factor remains within a predefined range.
- Voltage control: control reactive power in order to maintain the terminal voltage at reference value
- Reactive power regulation: the DFIG and converter system are set to maintain their reactive power generation at a reference set-point.

2.4.3 Wind Turbine Electric Interface Model

The VSWTG is modeled as a controlled current source with parallel transient impedance, Figure 2.6. The dynamic model and the controls of the VSWTG, modeled in Figure 2.5, generate the reference active power P_{REF} for the controlled current source. Equivalent models are used in software packages such as PSS/E. The IEEE Tutorial on wind generation modeling in PES General Meeting, Pittsburg in 2008 deemed this line of VSWTG models adequate for mimicking the DFIG's dynamic behavior and power system interaction. Other industrial reports [64] make use of identical models in their power system studies. The transfer function, shown in Figure 2.6, represents the current control bandwidth of the converter. The wind turbine and generator parameters, Figure 2.5 and Figure 2.6, are published in [64].

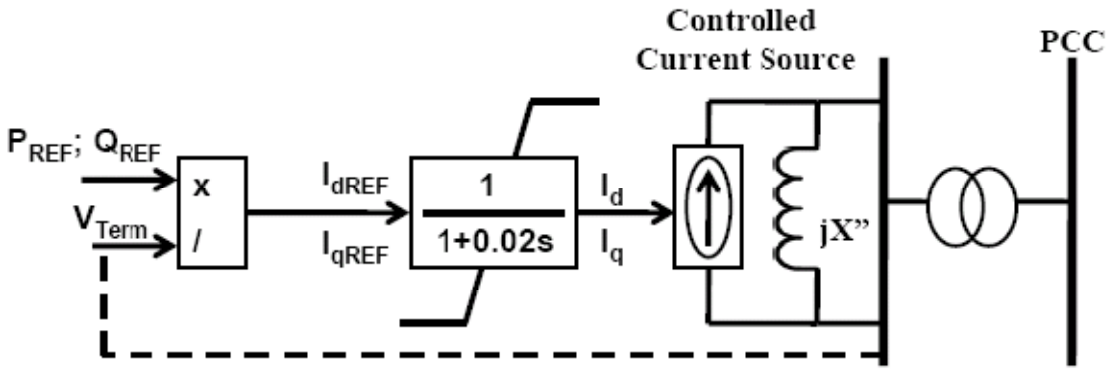

Figure 2.6. Electrical Modeling of the DFIG and its Power Electronics Interface

2.5 Wind Farm Modeling

In this work, the wind farm corresponds to 14 groups of 10 Wind Turbines Generators (WTG), Figure 2.7. The Wind farm rated power is 210MW.

Studies have shown that aggregated electrical models with non-aggregated mechanical models are suitable models for medium to long-term simulations [69].

It is assumed that each group of WTGs exhibits the same wind profile. A wind farm aggregated model is presented in Figure 2.8. Similar models have been used in [45,47,70,71] for stability studies.

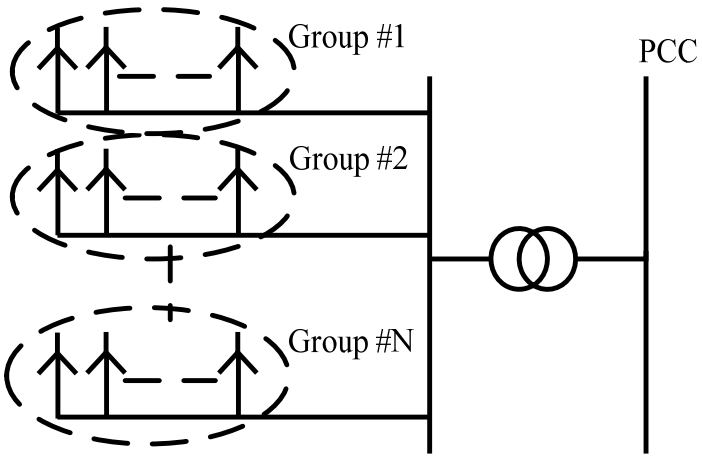

Figure 2.7. Wind Farm Layout

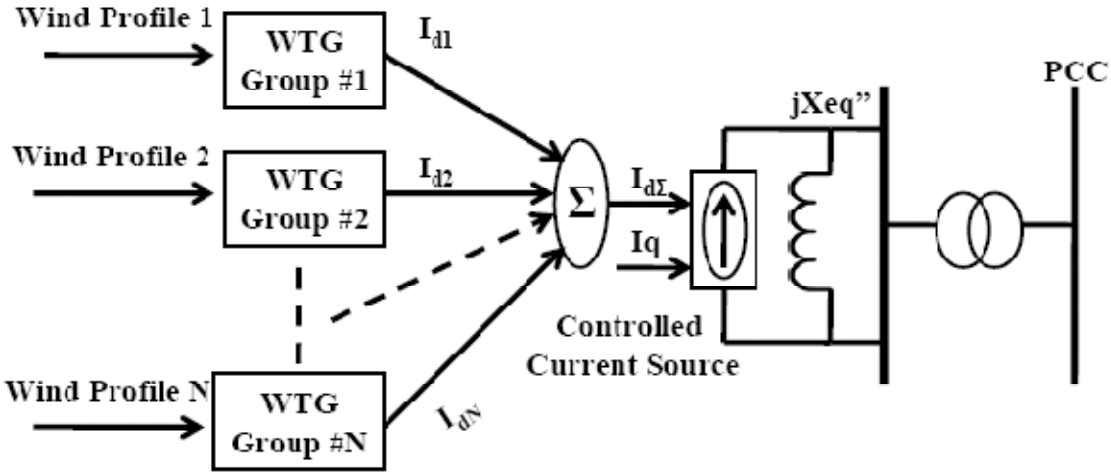

Figure 2.8. Wind Farm Aggregated Model

2.5.1 Supplementary Control Loop

One of the objectives of this thesis is to create a damping torque for the interarea modes of oscillations by modulating the active (P-Loop) and/or reactive power (Q-Loop) outputs of the wind farm. Supplementary control loops are design to operate for a short

time span, within 5 to 15 seconds, following critical angular oscillations in a power system. A trigger is used to enable the operation of both the P-Loop and the Q-Loop. The trigger originates from an interarea oscillation detection scheme that will be presented in Chapter 4.

2.5.1.1 Active Power Modulation Loop

Standard control of active power of the DFIG is discussed in previous sections. The P-Loop is designed to bypass the maximum peak power tracking in order to tap into the stored kinetic energy in the blades. Compared to frequency support kinetic discharge schemes [7,8], where the VSWTG discharges some of its kinetic energy and slowly regains standard control mode, the WPSS modulates its active power by charging/discharging for half an oscillation cycle and then releasing/regaining a portion of its energy in the back swing.

Figure 2.9 displays the structure of the P-Loop. The P-Loop is designed to modulate the active power around a measured mean power output of a WTG. The P-Loop modulation limits are calculated based on the available kinetic energy in the blades. The range of power modulation, for half an interarea oscillation cycle, is calculated based on the following criteria, Eq. (2.13) — (2.16):

- Constant mean wind speed is assumed
- Wind turbine rotational speed deviation is limited to 0.1pu
- Modulation must be maintained for at least one interarea oscillating cycle, f_{OS}

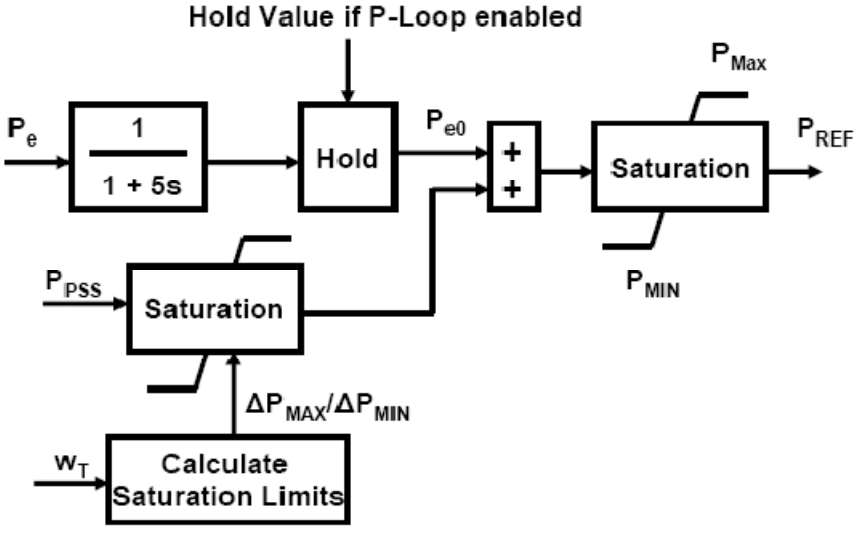

Figure 2.9. Supplementary Active Control Loop

$$2H_T\omega_T\frac{d\omega_T}{dt} = P_m - P_e \tag{2.13}$$

$$\Delta E = H_T\left(\omega_T^2 - \omega_{T0}^2\right) \tag{2.14}$$

$$\Delta P = \Delta E * 0.5 f_{OS} = H_T * 0.5 f_{OS}\left(\omega_T^2 - \omega_{T0}^2\right) \tag{2.15}$$

$$\Delta P_{MAX} = -\Delta P_{MIN} \approx 0.2 * H_T * f_{OS} * \omega_{T0} \tag{2.16}$$

Where ω_{T0} is the turbine rotational speed at the instant of operation of the P-Loop.

The value of the interarea frequency f_{OS} is calculated offline. If more than one interarea mode is present, the smallest interarea frequency for which the WPSS is designed to damp should be used in the calculation of ΔP_{MAX} and ΔP_{MIN}.

The turbine rotational speed is continuously monitored in real time. If at any instant the rotational speed ω_T falls below 0.7pu or above 1.2pu then P-Loop is disabled and the WTG is allowed to return to its standard mode of operation. The rated power of the generators is the absolute upper limit under both supplementary control and standard control modes.

2.5.1.2 Reactive Power Modulation Loop

In this thesis, WTGs will be assumed to operate under constant reactive power control mode since research on reactive power control modes, such as voltage and power factor modes, has been addressed extensively with FACTS based PSS applications and thus very little contribution may be done in this area. One of the objectives, however, is to address the issues regarding the increase in damping capability when combining real and reactive power modulation. Figure 2.10 displays the structure of the Q-Loop.

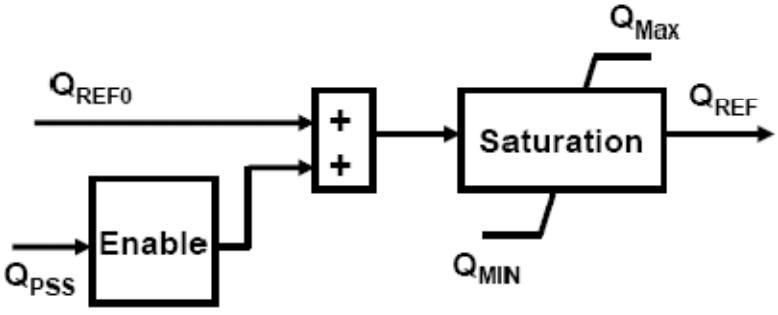

Figure 2.10. Supplementary Reactive Control Loop

2.5.2 Time Domain Simulation

A single WTG infinite bus test system is used to test the operation of the wind farm model and the performance of the supplementary control loops, Figure 2.11. The objective of the wind based power system stabilizer is to contribute to the short term angular stability by creating a damping torque for the interarea oscillation through modulating the active and/or reactive power output of a wind farm.

Figure 2.12. represents the wind profile of the different groups of wind generators [72]. The wind speed is divided or multiplied by a constant gain in order to reduce or increase the active power generation of the wind farm.

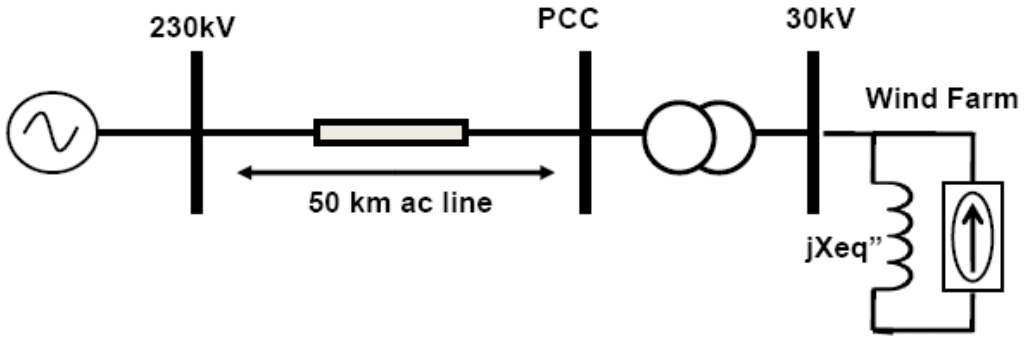

Figure 2.11 Single Line Diagram of the Test System

Table 2.1. Test system parameters

Wind Farm		Transformer		Line Parameters		
Rated Power	**Xeq"**	**Rated Power**	**X_T**	**R**	**X_L**	**B**
210 MW	0.5 pu	252 MW	0.1 pu	0.0000233 pu	0.000233 pu	0.0075 pu

Wind farm rated power is used as based power in Table 2.1

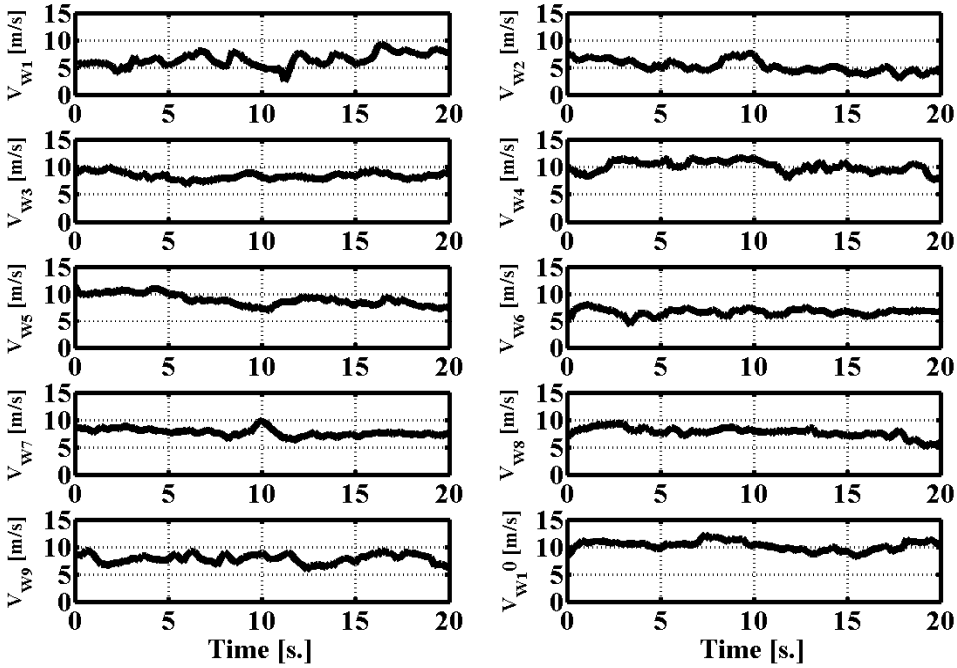

Figure 2.12 Wind profile for different groups of wind turbine generators

A reference modulating signal, with amplitude, 0.2 pu, is used to test the performance of the supplementary control loops. Modulating frequencies of 0.25Hz and 0.5Hz are used. Figure 2.13 and Figure 2.14 display the ability of the P-Loop and Q-Loop to follow a reference signal (Ref.). Figure 2.13 (a) and Figure 2.14 (a) show the capacity of the wind farm to follow a 0.25 Hz reference signal of amplitude 0.2pu. The area in the dotted section represents the operation of the supplementary control loop. Outside of the dotted sections, standard wind turbine control is enabled and the supplementary control loops disabled. Figure 2.13 (n) and Figure 2.14 (b) show the capacity of the wind farm to follow a 0.5 Hz reference signal of amplitude 0.2pu.

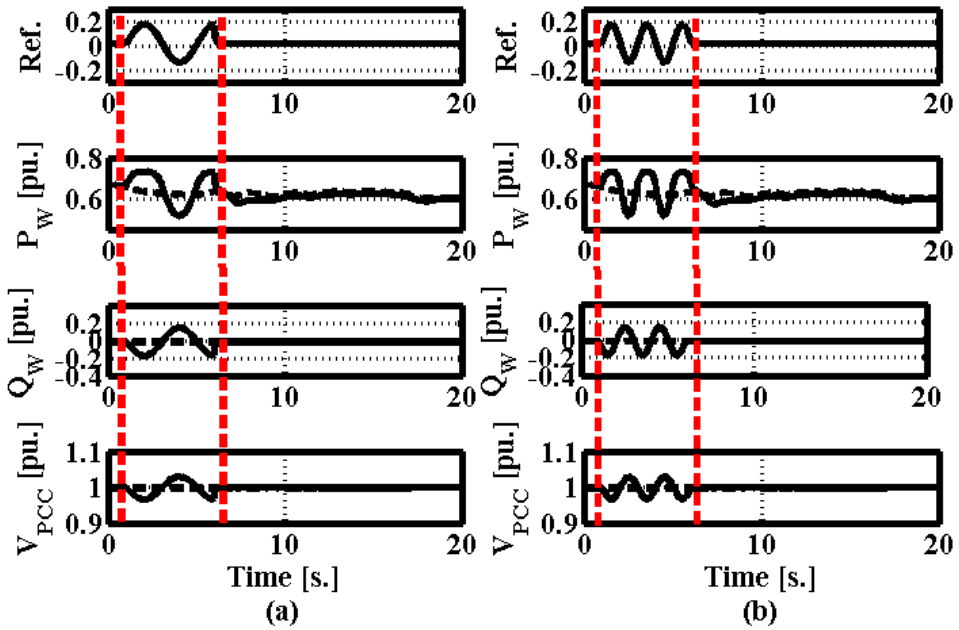

Figure 2.13. Power Matching Capability of the Active and Reactive Supplementary Control Loops. Wind farm generation above 100MW. (a) Modulation at 0.25Hz frequency; (b) Modulation at 0.5Hz frequency

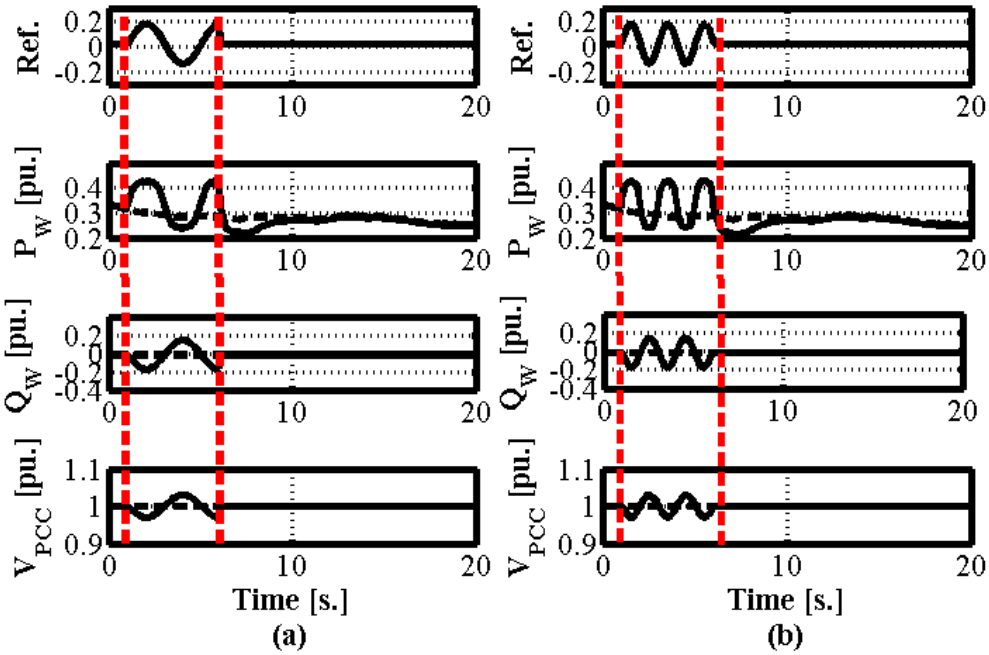

Figure 2.14. Matching Capability of the Active and Reactive Supplementary Control Loops. Wind farm generation below 100MW. (a) Modulation with a 0.25Hz frequency; (b) Modulation with a 0.5Hz frequency

2.6 Summary

This chapter summarized the control principles of DFIG based wind generators. A commercial wind turbine model is presented. An aggregated wind farm electrical model is developed. The model makes use of non-aggregated mechanical models. Supplementary active and reactive control loops are introduced. The supplementary loops are needed to modulate the active or reactive power model of a wind farm in order to generate a damping torque in phase with interarea oscillations. Standard control and supplementary controls are tested on a single wind turbine machine infinite bus system.

Chapter 3: Assessing the Damping Potential of Wind Farms

3.1 Introduction

Wind farm capital cost encompasses of nearly 80% of the total project cost. The major objective to a wind farm owner is to maintain maximum peak power tracking and reduce losses in the wind farm network in order to maximize energy sales and thus revenues. Meanwhile, stable and secure operation of the power system must be maintained in order to sustain the power transfer from generators to loads. It would be within the wind farm operator's best interest to contribute to the short term angular stability of a power system in order to maintain the revenue stream.

The ability of the wind generator to modulate its active and reactive power output impacts the electrical loading of synchronous machines in power systems. Power modulation allows wind generators to affect the electromechanical dynamics of synchronous machines in a power system. However, preliminary studies [73] showed that the effectiveness of active or reactive power modulation of a wind farm in damping interarea modes depends on the location of the wind farm's point of common coupling and the type of power modulation.

A power system benchmark is introduced and used throughout analytical and time domain simulations tests. A small signal linear state space model of the power system including wind generation is developed. The model gives insight on the interaction between the electromechanical dynamics of synchronous machine and wind farm power modulation. Wind farm power system stabilizers controlled variables (i.e. active and reactive power) are introduced to the state model of the power system as an input matrix. This chapter develops an analytical approach that serves as a preliminary step in assessing the damping potential of a wind farm based on its point of common coupling. The author emphasizes that the work does not cover placement of wind farms to damp interarea oscillations but assessing the damping potential and defining the type of power to modulate given a wind farm predefined location since the location of wind generation is

entirely dependent on the wind speeds. The work also covers a feedback selection method that allows, through the use of wide area measurements, high observability of a selected interarea mode. Validation of the modal analysis is presented in section 3.4.

3.2 Power System Benchmark

The thesis used the two areas four generators power system benchmark [27]. All synchronous plants are equipped with automatic voltage regulators and governors. The base case, shown in Figure 3.1, suffers from a lowly damped interarea oscillation in the range of 0.6 Hz. The base case interarea mode shape, showing the coherent groups of generators, is presented in Figure 3.2. Following the tripping of one of the tie lines between buses 7 and 9, the interarea frequency falls to the range of 0.4Hz. The power system also has two local modes above 1Hz.

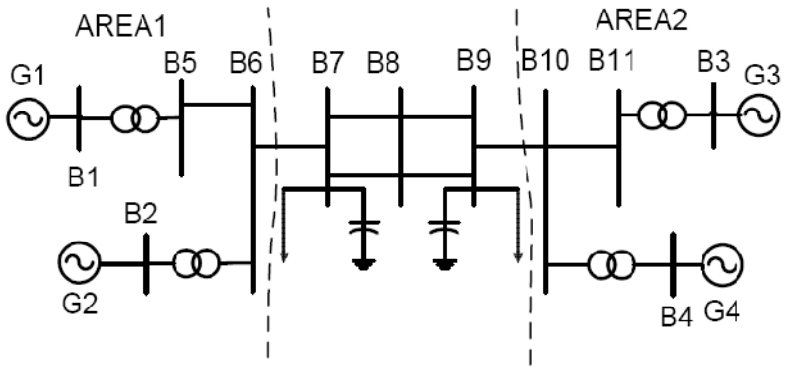

Figure 3.1. Four Generators Two Area Power System Benchmark

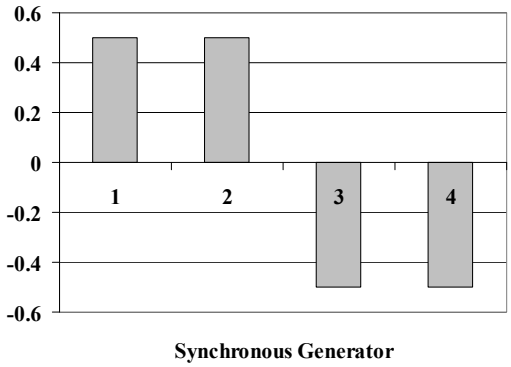

Figure 3.2. Interarea Mode Shape

3.2.1 Small Signal State Space Model of Power System

As discussed in Chapter 2, wind farm output power fluctuations are reduced due to wide geographical distribution of wind turbines, inertia of the blade, and ramp limits [51]. Therefore, the wind farm power output will be assumed constant in the seconds to seconds and seconds to minute time frames.

The wind farm's PCC is considered as a PV bus in the load flow formulation. However, the wind farm is modeled as a constant power negative shunt load in the derivation of the state space model of the power system. Note that the constant power negative load wind farm model used is not valid if the wind farm is providing inertial response.

For interarea modes identification and selection, the classical generator model is used to represent the synchronous machines in the power system. A similar approach has been reported in [33].

The linearization of the swing equations of a synchronous unit 'i' is derived in Eq. (3.1) and Eq. (3.2). There exists an interaction between the swing equation of a synchronous unit and the active and reactive power output of a wind farm, Eq. (3.2). An analytical approach is laid down in order to quantify the changes in synchronous units electric power output with respect to changes in active and reactive power of the wind farm, Eq. (3.3) — (3.9).

$$\Delta \dot{\delta} i = \Delta \omega i \tag{3.1}$$

$$\Delta \dot{\omega} i = -\frac{1}{Mi}\frac{dP_{Gi}}{d\underline{\delta}}\Delta\underline{\delta} - \frac{1}{Mi}\frac{dP_{Gi}}{dP_W}\Delta P_W - \frac{1}{Mi}\frac{dP_{Gi}}{dQ_W}\Delta Q_W - \frac{Di}{Mi}\Delta\omega i \tag{3.2}$$

Figure 3.3 displays the interconnections between generation, loads and wind farms. The transmission network can be described as follows:

$$\begin{bmatrix} I_G \\ I_L \end{bmatrix} = \begin{bmatrix} Y_{GG} & Y_{GL} \\ Y_{LG} & Y_{LL} \end{bmatrix} \begin{bmatrix} V_G \\ V_L \end{bmatrix} \tag{3.3}$$

Where subscript G denotes generator buses and subscript L denotes load buses
The load current injection is described in Eq. (3.4) and Eq. (3.3):

$$I_L = -(Y_L + Y_{WIND})V_L \tag{3.4}$$

Both Y_L and Y_{WIND} are diagonal matrices. The diagonal entries of Y_L are set to zero for buses with no loads. Similarly, the diagonal elements of Y_{WIND} are set to zero for buses with no wind generation. The reduced network admittance matrix becomes:

$$Y_R = Y_{GG} - Y_{GL}\left(Y_L + Y_{WIND} + Y_{LL}\right)^{-1} Y_{LG} \tag{3.5}$$

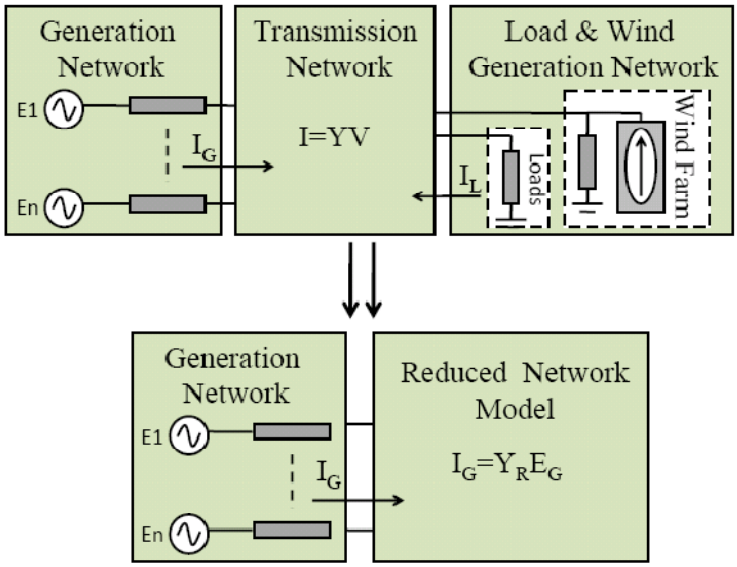

Figure 3.3. Power System Admittance Matrix Reduction

Based on the Eq. (3.6) — (3.9), the elements of the input matrix [B] can be calculated given the following information:

- Admittance matrix
- Load levels/types
- Wind farms power output
- Synchronous machine terminal voltages

$$\frac{dP_G}{dP_W} = real\left\{diag\left(V_G\right)\frac{dY_R^*}{dP_W}V_G^*\right\} \tag{3.6}$$

$$\frac{dP_G}{dQ_W} = imag\left\{diag\left(V_G\right)\frac{dY_R^*}{dQ_W}V_G^*\right\} \tag{3.7}$$

$$\frac{dY_R}{dP_W} = Y_{GL}\left(Y_L + Y_{WIND} + Y_{LL}\right)^{-1}\frac{dY_{WIND}}{dP_W}\left(Y_L + Y_{WIND} + Y_{LL}\right)^{-1}Y_{LG} \tag{3.8}$$

$$\frac{dY_R}{dQ_W} = Y_{GL}\left(Y_L + Y_{WIND} + Y_{LL}\right)^{-1} \frac{dY_{WIND}}{dQ_W}\left(Y_L + Y_{WIND} + Y_{LL}\right)^{-1} Y_{LG} \tag{3.9}$$

The state space model of the power system becomes, Eq. (3.10):

$$\begin{bmatrix} \dot{\Delta\delta} \\ \dot{\Delta\omega} \end{bmatrix} = \begin{bmatrix} 0 & I \\ A_{\omega\delta} & A_{\omega\omega} \end{bmatrix} \begin{bmatrix} \Delta\delta \\ \Delta\omega \end{bmatrix} + \begin{bmatrix} 0_\delta \\ B_\omega \end{bmatrix} \begin{bmatrix} \Delta P_W & \Delta Q_W \end{bmatrix} \tag{3.10}$$

$$A_{\omega\delta} = -\frac{1}{\omega_0} diag\left(M^{-1}\right)\frac{dP_G}{d\delta} \tag{3.11}$$

$$A_{\omega\omega} = -\frac{1}{\omega_0} diag\left(M^{-1}\right)D \tag{3.12}$$

$$B_\omega = -\frac{1}{\omega_0}\left[diag(M^{-1})\frac{dP_G}{dP_W} \quad diag(M^{-1})\frac{dP_G}{dQ_W} \right] \tag{3.13}$$

Where M is the synchronous machines inertia vector, and D is the synchronous units damping vector.

In this text, Eq. (3.14), will be used to refer to the state-space power system presentation.

$$\begin{aligned} \dot{x} &= [A]x + [B]u \\ y &= [C]x \end{aligned} \tag{3.14}$$

3.3 Modal Analysis

Modal analysis is introduced as means to evaluate the potential contribution of the P-Loop and the Q-Loop in damping selected interarea modes. Modal analysis makes use of the left and right matrices, [F] and [U], in order to evaluate respectively the controllability of an input on a system mode, and the observability of a mode given a measured power system quantity.

3.3.1 Modal Controllability

In [74], a comparison between two methods to design power system damping controller on a utility system proved that the geometric approach is ideally suited for wide area measurements based power system stabilizers. Given the power system state equation and the left eigen vector, it is possible to calculate the controllability index, CI, of active or reactive power damping control loop in a wind farm, Eq. (3.15).

$$CI = \frac{\left| b_k^T f_i \right|}{\left\| f_i \right\| \left\| b_k \right\|} \tag{3.15}$$

Where b_k is the *k-th* column of the input vector B and f_i is the *i-th* left eigenvector.
The coefficient $|b_k|$ is replaced with a predefined base value in order to facilitate the comparison between the controllability of different control loops and different wind farm locations, Eq. (3.16).

$$CI = \frac{\left| b_k^T f_i \right|}{\left\| f_i \right\| CI_{BASE}} \tag{3.16}$$

Where CI_{BASE} may be selected as the controllability index of different damping controllers in the system, such as PSS, or, in this case, the controllability index of the active power loop of a wind farm with its PCC coupled directly to bus 5.

Several cases are presented in this section. Different study cases are setup by varying the location of the PCC and the active power output of a wind park, Figure 3.1.

3.3.1.1 Case 1: Connection at Bus 5

The PCC of the wind farm is coupled to bus 5 via an ac transmission line. Both the length and active power output of the wind farm are varied in order to generate and assess the impact of these parameters on the controllability indices.

Figure 3.4. displays the evolution of the CI_P and CI_Q with respect to power generated and ac line length. Keeping in mind the low probability of a wind farm operating at rated power and the small margin for power modulation near rated power, the authors turn their attention to operation within 0.2pu-0.7pu. In this region, the damping contribution of active power modulation should be vastly superior to that of reactive power modulation.

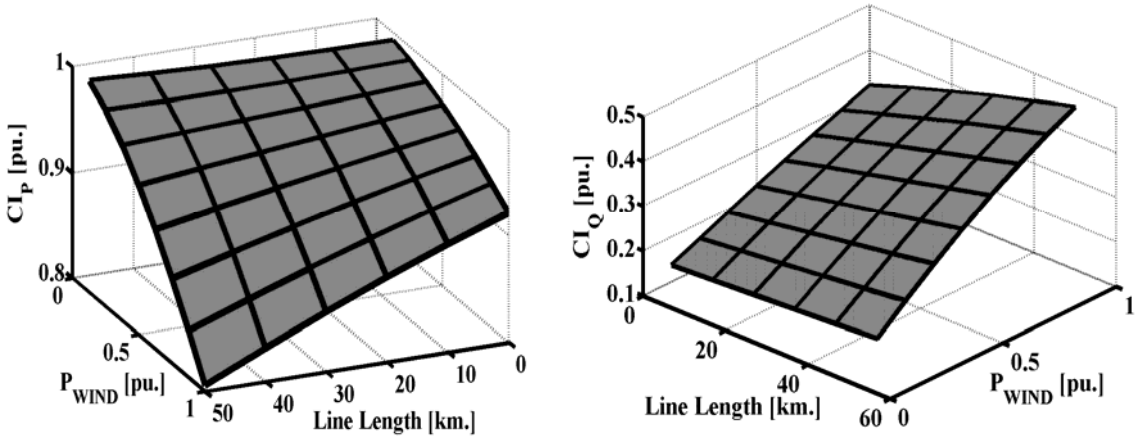

(a) (b)

Figure 3.4. Controllability Assessment of WPSS with PCC connected at Bus 5 via an ac Transmission Line. (a) Controllability index of the active power control loop; (b) Controllability index of the reactive power control loop

3.3.1.2 Case 2: Connection at Bus 6

The PCC of the wind farm is coupled to bus 6 via an ac transmission line. Figure 3.5 shows a reduction in damping capabilities of the active power control loop with respect to that of Case 1. However, CI_P remains higher than CI_Q.

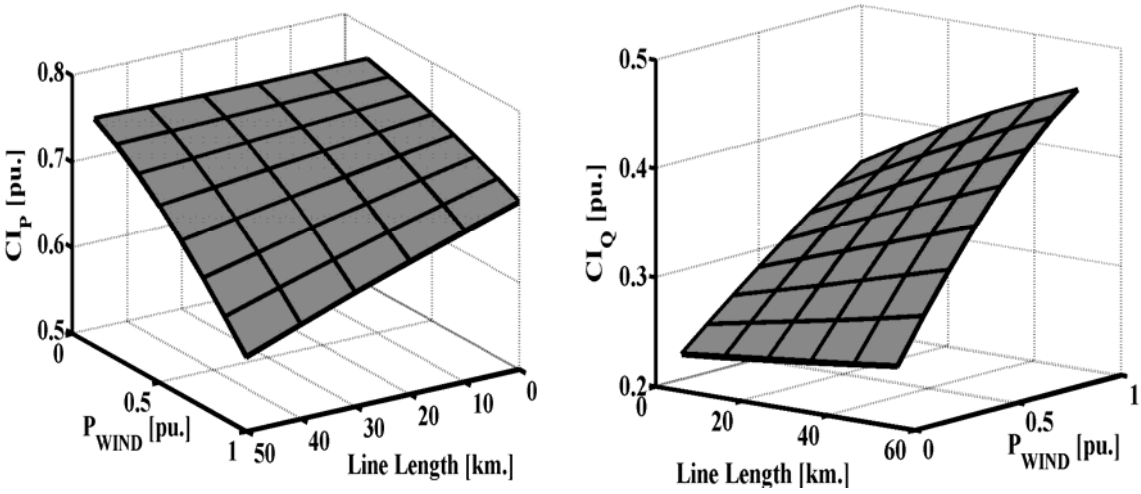

(a) (b)

Figure 3.5. Controllability Assessment of WPSS with PCC connected at Bus 6 via an ac Transmission Line. (a) Controllability index of the active power control loop; (b) Controllability index of the reactive power control loop

3.3.1.3 Case 3: Connection at Bus 7

The PCC of the wind farm is coupled to bus 7 via an ac transmission line Figure 3.6 shows an increase in the damping potential of the reactive power control loop with respect to that of Cases 1 and 2. CI_P is still higher than CI_Q in Case 3, however they are closer in magnitude than in previous cases. It would be worth exploiting the reactive power capabilities in a wind farm in order to assist active power modulation damping controller in contributing to damping of interarea oscillations

3.3.1.4 Case 4: Connection at Bus 8

The PCC of the wind farm is coupled to bus 8 via an ac transmission line. CI_P and CI_Q are roughly 7 to 10 times smaller than the values in Case 1, Figure 3.7. Given the humble controllability indices, installing WPSS in a wind farm connected at B8 is not expected to yield significant contribution to damping. However, Case 4 is interesting since wind farm's active and reactive power variations would have small impact on power system angular stability compared to the other cases.

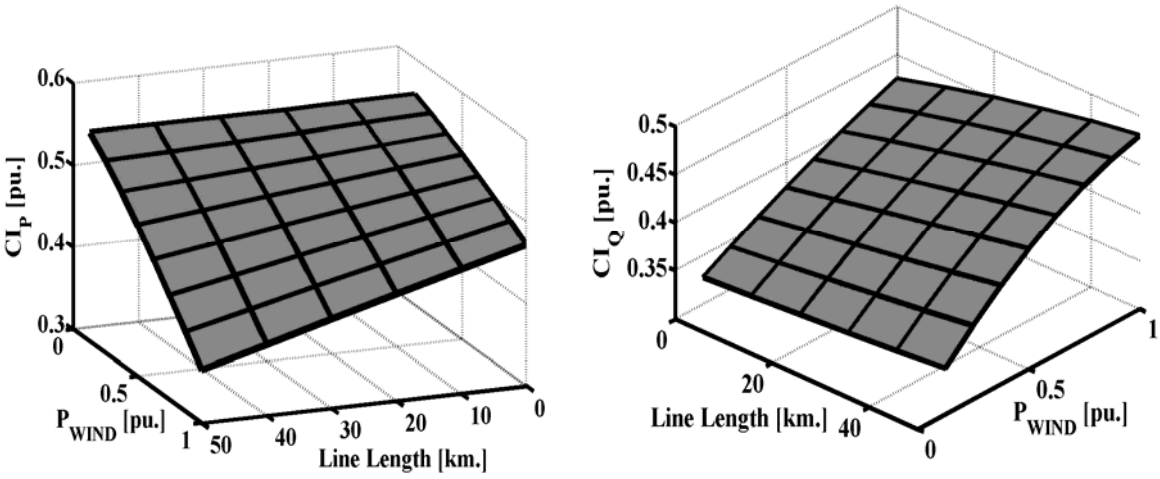

(a) (b)

Figure 3.6. Controllability Assessment of WPSS with PCC connected at Bus 7 via an ac Transmission Line. (a) Controllability index of the active power control loop; (b) Controllability index of the reactive power control loop

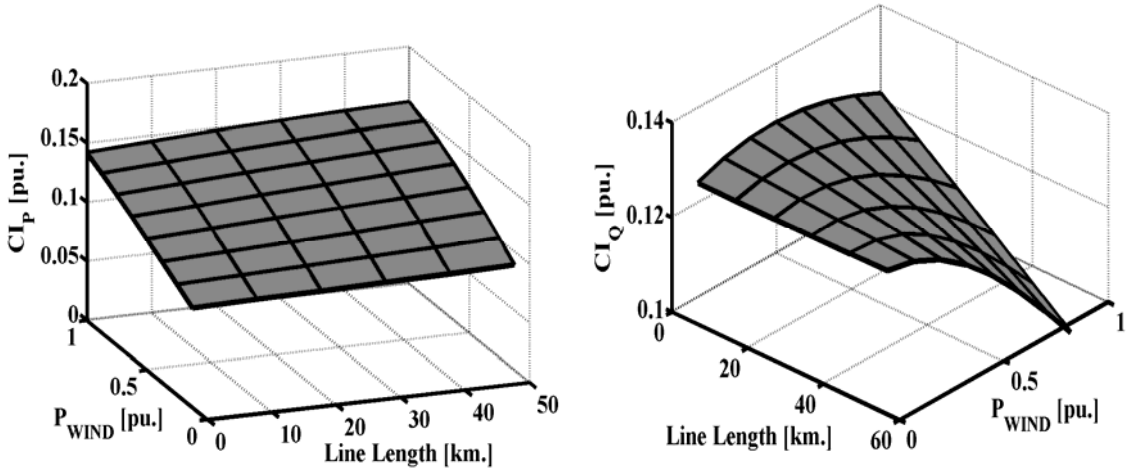

(a) (b)

Figure 3.7. Controllability Assessment of WPSS with PCC connected at Bus 8 via an ac Transmission Line. (a) Controllability index of the active power control loop; (b) Controllability index of the reactive power control loop

An analytical assessment of the controllability across the tie lines is developed in order to shed some light on the sudden drop in damping potential at bus 8. In order to investigate the change in controllability indices across the tie line, the length of the lines connecting bus 8 to buses 7 and 9 respectively were varied such as the total line length connecting bus 7 to bus 9, Figure 3.8, while the wind farm power is kept constant. The evolution of controllability indices versus the line ration *x* is plotted in Figure 3.9.

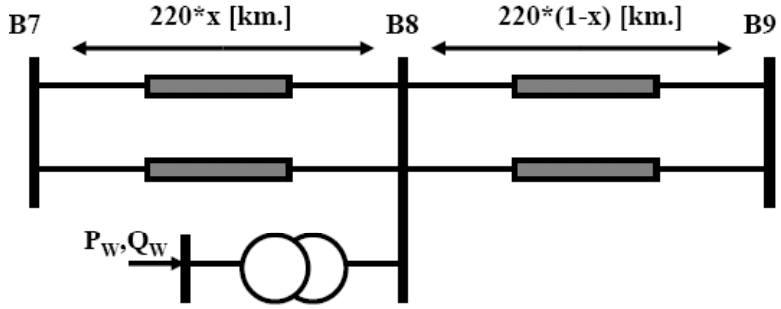

Figure 3.8. Scanning Controllability Indices Evolution by Varying the Length of the Tie Lines.

The point (*x=0)* represent the case when the wind farm is connected at bus 7, the point (*x=0.5)* represent the case when the wind farm is connected to bus 8 and the point (*x=1)* represent the case when the wind farm is connected to bus 9. There is a location for which CI_P drops to zero (*x=0.4)* and another where the CI_Q drops to zero (x=0.65), Figure 3.9.

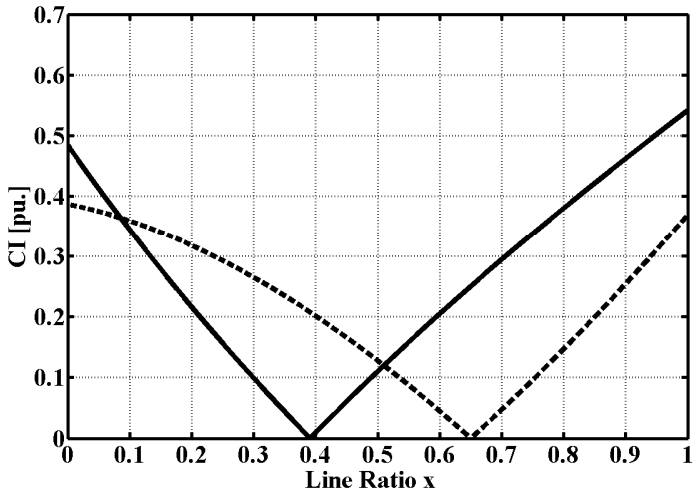

Figure 3.9. Evolution of Controllability Indices Across the Tie Lines.

3.3.1.5 Case 5: Connection at Bus 9

The PCC of the wind farm is coupled to bus 9 via an ac transmission line. Case 5 is comparable to Case 3 where CI_P is higher than CI_Q but reactive power modulation is relatively higher than Cases 1 and 2, Figure 3.10. In fact, looking at the evolution of CI_Q in Figure 3.9, the damping potential of reactive power modulation is highest when the wind farm is coupled directly or via and ac transmission line to bus 7 or bus 9.

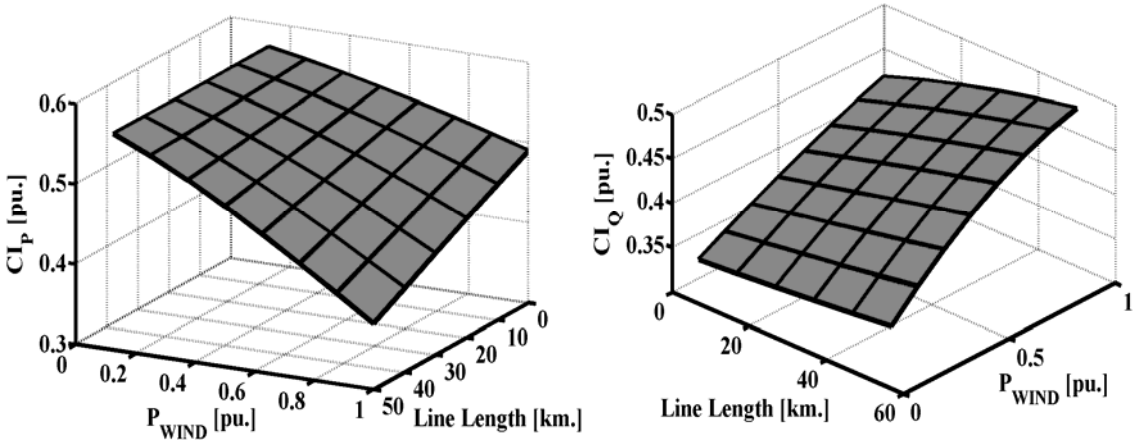

(a) (b)

Figure 3.10. Controllability Assessment of WPSS with PCC connected at Bus 9 via an ac Transmission Line. (a) Controllability index of the active power control loop; (b) Controllability index of the reactive power control loop

3.3.1.6 Case 6: Connection at Bus 10

The PCC of the wind farm is coupled to bus 10 via an ac transmission line. Case 6 shows significant potential for active power modulation with a lower damping capability of the reactive power modulation, Figure 3.11.

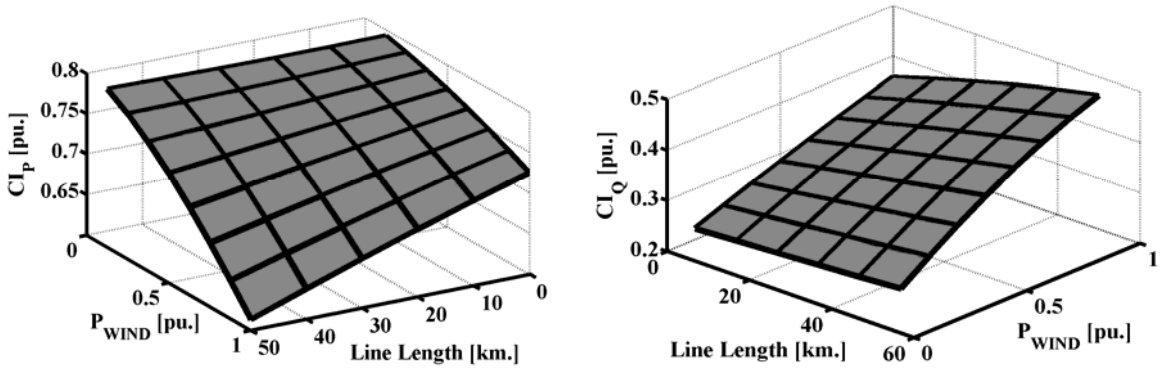

Figure 3.11. Controllability Assessment of WPSS with PCC connected at Bus 10 via an ac Transmission Line. (a) Controllability index of the active power control loop; (b) Controllability index of the reactive power control loop

3.3.1.7 Case 7: Connection at Bus 11

The PCC of the wind farm is coupled to bus 11 via an ac transmission line. Case 6 shows significant potential for active power modulation with a small potential damping contribution of the reactive power modulation, Figure 3.12.

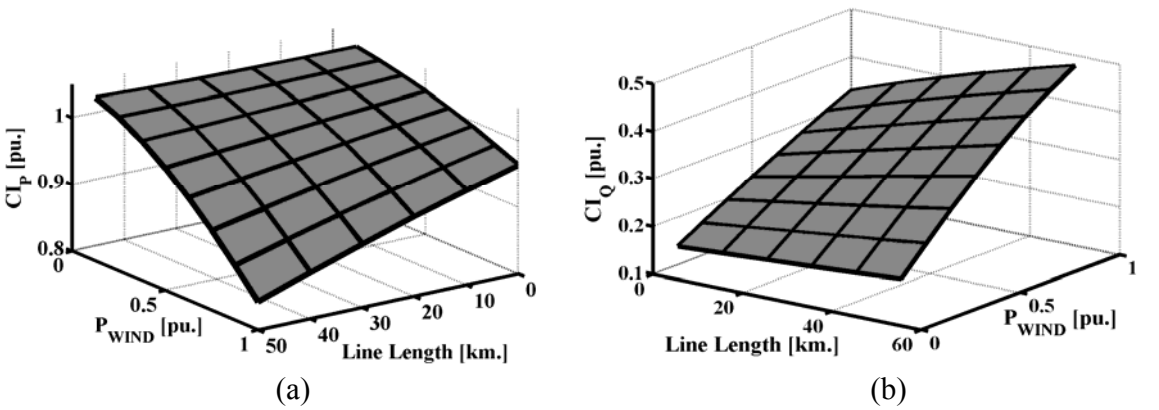

Figure 3.12. Controllability Assessment of WPSS with PCC connected at Bus 11 via an ac Transmission Line. (a) Controllability index of the active power control loop; (b) Controllability index of the reactive power control loop

3.3.1.8 Summary

Analytical results show that damping of the active power loop decrease with the length of the ac transmission line that connects the wind farm to the power system and with the power output of a wind farm. On the other hand, reactive power controllability increases with wind generation and ac transmission line length. Active power modulation is expected to be the most effective.

In [34,73], it was found that reactive power modulation is not effective in damping power swings when the grid connection point of a wind farm is located near a synchronous unit. The relatively high values of controllability indices of reactive power modulation in cases 1, 2, 6 and 7 are a byproduct of the simplifying assumption in the synchronous machine models and controls.

3.3.2 Modal Observability

The geometric measure of observability was deemed ideally suited for wide area measurement feedback selection [74]. High obsevability reduces the need for higher gains thus allowing for a larger gain margin, robust and effective damping control performance. Given the power system state equation and the right eigen vector [U], the observability index, OI, is calculated as shown in (3.17).

$$OI = \frac{\left|c_l e_i\right|}{\left\|c_l\right\|\left\|e_i\right\|} \tag{3.17}$$

Where c_l is the *k-th* column of the input vector B and f_i is the *i-th* left eigenvector.

Ideally, all state variables could be used as feedback for the WPSS. However, the work considers only two wide area measurements as feedback signals for the controller. Table 3.1 displays the observability index of various feedback candidates. The angle deviation between G1 and G4 has the highest observability of the interarea mode and therefore will be used as a feedback signals for the WPSS of Chapter 4.

Table 3.1. Interarea Mode Observability Indices

Feedback Signal	OI [pu.]	Feedback Signal	OI [pu.]
$\delta_1 - \delta_4$	0.72	$\omega_1 - \omega_4$	0.0049
$\delta_1 - \delta_3$	0.69	$\omega_1 - \omega_3$	0.0052
$\delta_2 - \delta_4$	0.55	$\omega_2 - \omega_4$	0.0046
$\delta_2 - \delta_3$	0.52	$\omega_2 - \omega_3$	0.0050

3.4 Validation of Modal Analysis

Preliminary simulation and damping controllers are setup in order to validate the results of the modal analysis. A controllable constant power negative load is used to emulate the wind farm. A full state feedback controller was derived via a constrained optimization. The controller is only used in this section and does not represent the WPSS final design.

3.4.1 Full State Feedback Damping Controller

The power system state equation may take the form of Eq, (3.18) following a change in the coordinates of the state variables of Eq. (3.14).

$$\dot{\underline{z}} = ([\Lambda] + [\Delta\Lambda])\underline{z} \tag{3.18}$$

$$[\Delta\Lambda] = [F]^T [B][K][C][U] \tag{3.19}$$

Where the $[\Lambda]$ is a diagonal matrix containing the poles of the system, [F] and [U] are the right and left eigen matrices, and [K] is a feedback gain.

The real part of the diagonal elements of $[\Delta\Lambda]$ dictate the increase, if real part is negative, or decrease, if real part is positive, of damping of a mode. Negative real part of diagonal elements is enough to ensure stability of a closed loop system [33]. A constrained optimization is used to select the individual gains of the [K] matrix such as:

- Damping of interarea mode increases
- Damping of other modes remain unchanged

It was found that the optimal solution varies based on wind farm location, ac line length. However, all optimal solutions had a structure close to that of Figure 3.13. The

magnitude of the DC gain, PSS, is set to 100. The sign of the DC gain varies with grid coupling point and with the type of power to modulate (i.e active or reactive power).

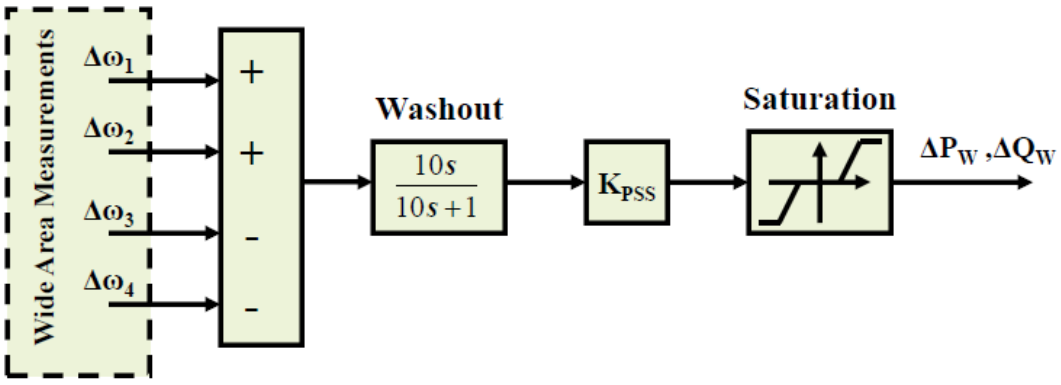

Figure 3.13. Full State Feedback Damping Controller.

3.4.2 Time Domain Simulations

A simplified VSWTG model is used to minimize the number of dynamic variable in order to evaluate the damping assessment methodology. The complete VSWTG model will be used in Chapter 4 for extensive testing the complete prototype (i.e: Complete VSWTG model of Chapter 2, PSS transfer function, and supplementary control loops).

A controllable current source is used to emulate the wind farm, Figure 3.14. The wind machine rotor dynamics are neglected. In these test cases, the wind based damping controller is kept online through the simulation time. All other conventional PSS are disabled in the simulation. A small disturbance in the form of a 12 cycle pulse on the G1 reference voltage, at time equal to 15 seconds, is used to excite the oscillatory modes in the system. The ac line parameters of Table 2.1 are used.

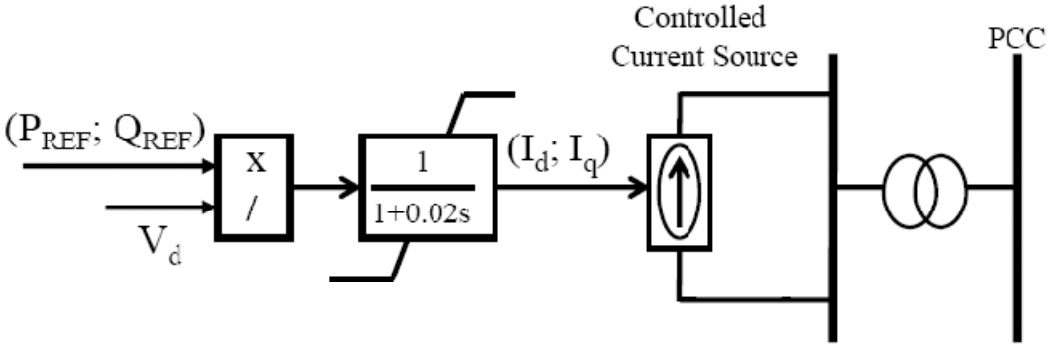

Figure 3.14. Steady State Wind Farm Emulator Model

3.4.2.1 Case 1: Connection at Bus 5

Time domain simulations shows that reactive power modulation has no damping contribution when the grid connection point of the wind farm is at bus 5. 80MVar were allocated for reactive power modulation, however, damping action was not enough as power swings with increasing amplitude were observed across the tie-line. The system looses synchronism few seconds following the disturbance.

On the other hand, real power modulation shows great potential in damping power swings and stabilizing the system. 10MW of active power was allocated for the P-Loop. The active power based damping controller was very efficient in damping power swings within few interarea oscillating cycles, Figure 3.15.

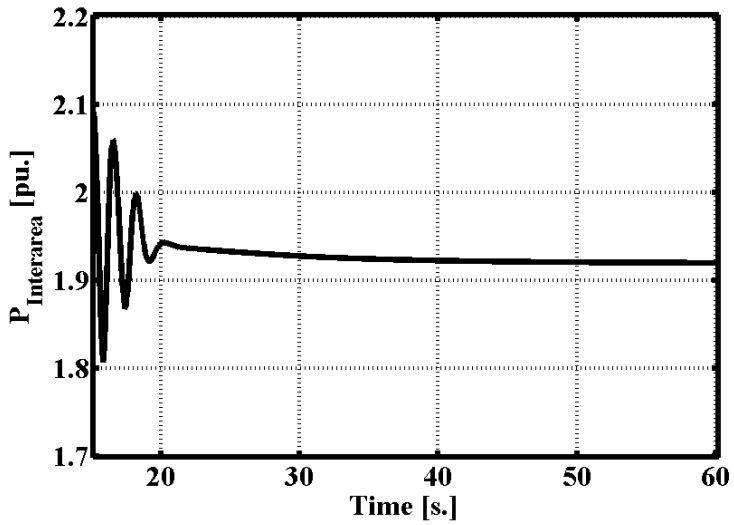

Figure 3.15. Intertie Power Oscillation Following a Pulse in Synchronous Machine G1 Reference Voltage. All power conventional machine power system stabilizers are offline. Wind farm directly coupled to bus 5 and operating at 100MW. 10MW of power is allocated for modulation

3.4.2.2 Case 2: Connection at Bus 6

Similar to Case 1, reactive power modulation did not have significant damping contributions as the power oscillations of increasing amplitude were observed across the tie line. Figure 3.16 shows the damping capability of active power modulation. Similar results were observed for different line length and operating levels.

3.4.2.3 Case 3: Connection at Bus 7

Case 3 represents a grid connection near the load center of Area 1 of the power system benchmark. Figure 3.17 displays the damping potential of both active and reactive power modulation. It is observed that active power modulation is much more effective and efficient as it modulates lower amounts of power than its counterpart, yet possesses a more important contribution to damping. This is due to how each power modulating loop creates their corresponding damping torque. Active power modulation acts directly on the electrical loading of synchronous units while reactive power modulation modulates the power system load active power, by varying the voltage, in order to create a damping torque.

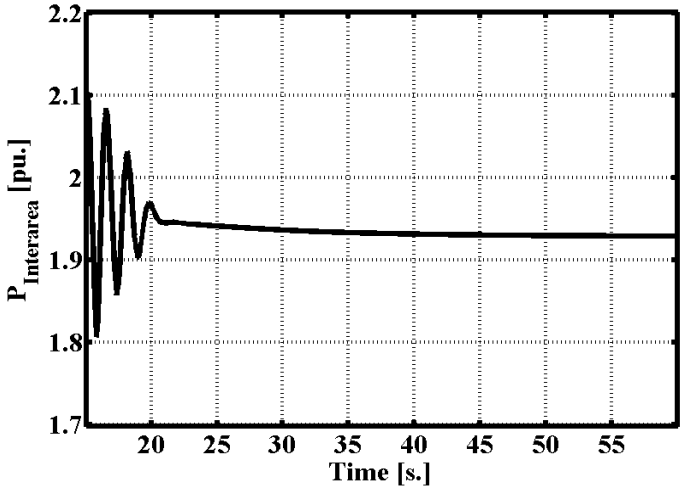

Figure 3.16. Intertie Power Oscillation Following a Pulse in Synchronous Machine G1 Reference Voltage. All power conventional machine power system stabilizers are offline. Wind farm coupled to bus 6 via 25 km ac line and operating at 100MW. 10MW of power is allocated for modulation

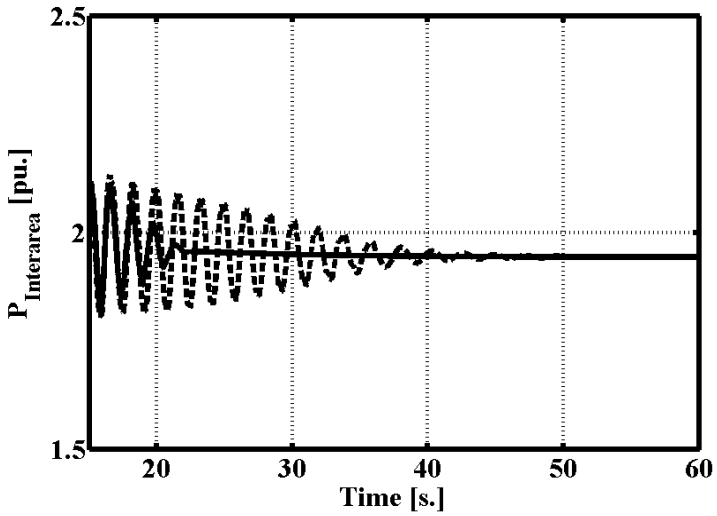

Figure 3.17. Intertie Power Oscillation Following a Pulse in Synchronous Machine G1 Reference Voltage. All power conventional machine power system stabilizers are offline. Wind farm coupled to bus 7 via 25 km ac line and operating at 100MW. — Active power modulation, 10MW; -- Reactive power modulation, 80MVar.

3.4.2.1 Case 4: Connection at Bus 8

According to modal analysis, any type of power modulation will not have a significant damping contribution to the stability of the swing modes in the power system. Angular instability occurred as neither 10 MW of active nor 80MVar of reactive power modulation were capable of generating a significant damping torque. Figure 3.18 displays the instability in the power system.

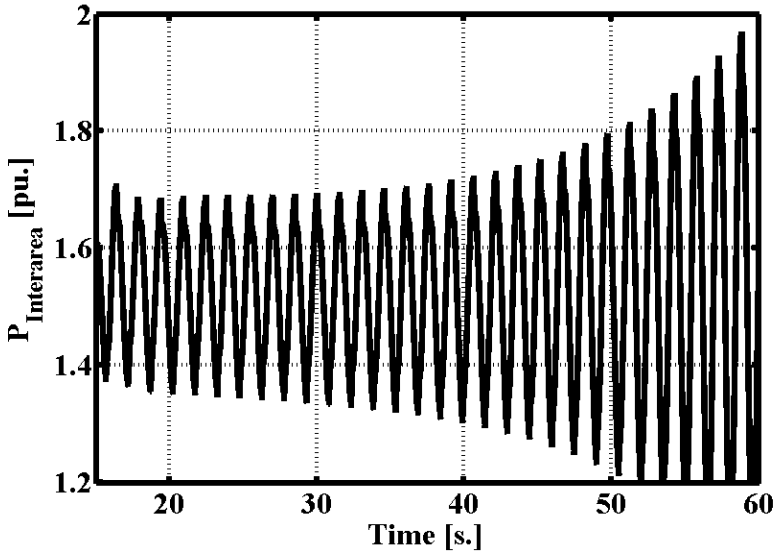

Figure 3.18. Intertie Power Oscillation Following a Pulse in Synchronous Machine G1 Reference Voltage. All power conventional machine power system stabilizers are offline. Wind farm coupled to bus 8 via 25 km ac line and operating at 100MW. Active power modulation (10MW); Reactive power modulation (80MVar).

3.4.2.2 Case 5: Connection at Bus 9

Case 5 is similar to Case 3 as the grid connection point of the wind farm is located near load center. Active power modulation is still more effective than reactive power modulation, but both types of power modulation show significant potential to contribute to power system stability, Figure 3.19.

3.4.2.3 Case 6: Connection at Bus 10

According to modal analysis, active power modulation should have a significant contribution to the stability of the power system. Figure 3.20 displays the performance of active power modulation. Time domain simulations showed no contribution of reactive power modulation to the damping of swing modes.

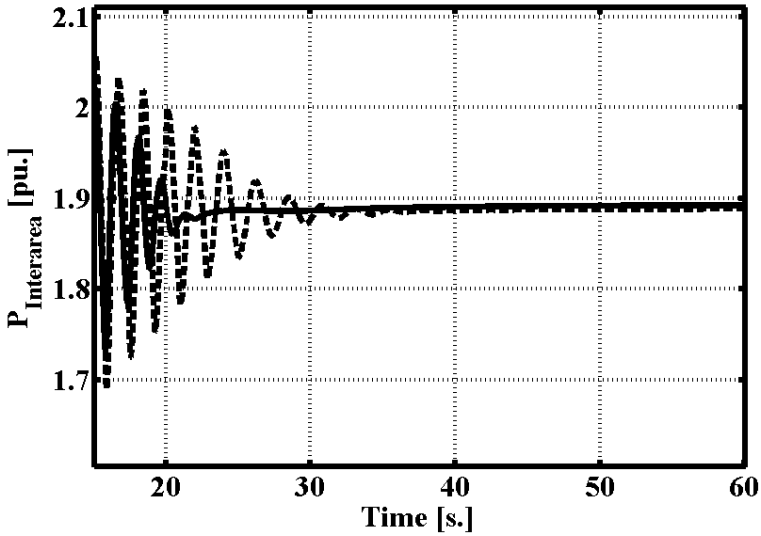

Figure 3.19. Intertie Power Oscillation Following a Pulse in Synchronous Machine G1 Reference Voltage. All power conventional machine power system stabilizers are offline. Wind farm coupled to bus 9 via 25 km ac line and operating at 100MW. — Active power modulation, 10MW; -- Reactive power modulation, 80MVar.

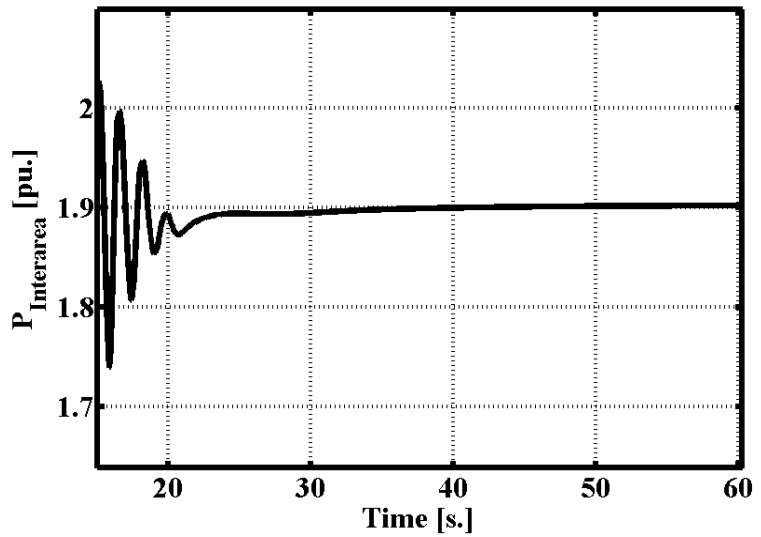

Figure 3.20. Intertie Power Oscillation Following a Pulse in Synchronous Machine G1 Reference Voltage. All power conventional machine power system stabilizers are offline. Wind farm coupled to bus 10 via 25 km ac line and operating at 100MW. Active power modulation, 10MW

3.4.2.4 Case 7: Connection at Bus 11

Similarly to Cases 1,2 and 6, active power modulation proved to be most effective for grid connection points near synchronous plants under all operating conditions and for different ac line lengths. Figure 3.21 shows the damping of the inter-tie power swings following the disturbance.

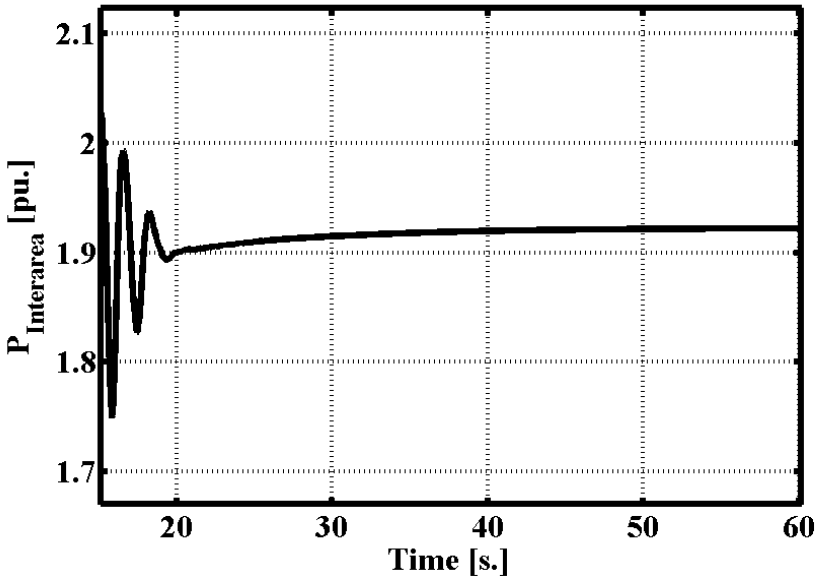

Figure 3.21. Intertie Power Oscillation Following a Pulse in Synchronous Machine G1 Reference Voltage. All power conventional machine power system stabilizers are offline. Wind farm coupled to bus 11 via 25 km ac line and operating at 100MW. Active power modulation, 10MW

3.4.3 Summary

Time domain simulations are coherent with modal analysis. The lowest damping contribution occurs when the wind farm is connected to bus 8. Active power modulation is more effective than reactive power modulation for Cases 1, 2, 3, 5, 6, and 7.Reactive power modulation has no significant contribution when the wind farm is coupled to synchronous plant buses. However, for this benchmark, reactive power modulation is found to be most effective near load centers (i.e: busses 7 and 9).

Table 3.2 provides recommendation for the installation of active and/or reactive power damping controllers.

Table 3.2. Recommendations for the installation of wind farm based power system stabilizers based grid connection point

	WPSS	
Bus	**P-Loop**	**Q-Loop**
5	Effective	Not Effective
6	Effective	Not Effective
7	Effective	Effective
8	Not Effective	Not Effective
9	Effective	Effective
10	Effective	Not Effective
11	Effective	Not Effective

3.5 Quantifying Active and Reactive Power Modulation

The main objective at this stage is to quantify the damping contribution of the wind based power system stabilizer given different modulation levels. The PSS of generating plants 1 and 2, Figure 3.1, are brought online in order to setup a more realistic case study (i.e stable system). The same disturbance as in Section 3.4.2 is applied. Test cases and wind based stabilizers are selected following the recommendations found in

Table 3.2. Time domain simulations are used to quantify the impact of modulation power levels on the damping contribution of wind based PSS. Interarea damping was assessed through modal analysis of the accelerated power of synchronous plant 1.

3.5.1 Active Power Modulation

The damping contribution of different levels of active power modulation is presented in Table 3.3. Active power modulation levels beyond 0.1pu are not justifiable since no significant increase in damping is observed.

Table 3.3. Interarea mode damping contribution of different levels of active power modulation

		Base Case	P-Loop				Base Case	P-Loop	
Bus	**Line [km.]**	**Damping (%)**	**Pmod [pu.]**	**Damping (%)**	**Bus**	**Line [km.]**	**Damping (%)**	**Pmod [pu.]**	**Damping (%)**
5	**0**	19.55	0.05	29.76	**9**	**0**	19.55	0.05	31.47
			0.10	37.89				0.10	36.17
			0.20	31.26				0.20	35.57
	25	19.55	0.05	29.47		**25**	19.55	0.05	31.42
			0.10	37.54				0.10	36.11
			0.20	31.26				0.20	35.44
	50	19.55	0.05	29.01		**50**	19.55	0.05	31.33
			0.10	37.51				0.10	36.03
			0.20	31.15				0.20	35.36
6	**0**	19.55	0.05	36.27	**10**	**0**	19.55	0.05	30.95
			0.10	39.71				0.10	36.34
			0.20	32.58				0.20	35.32
	25	19.55	0.05	35.98		**25**	19.55	0.05	30.95
			0.10	39.68				0.10	36.23
			0.20	33.04				0.20	35.23
	50	19.55	0.05	35.71		**50**	19.55	0.05	30.95
			0.10	39.65				0.10	36.20
			0.20	32.74				0.20	35.15
7	**0**	19.55	0.05	36.41	**11**	**0**	19.55	0.05	31.10
			0.10	40.19				0.10	36.10
			0.20	41.08				0.20	35.54
	25	19.55	0.05	36.37		**25**	19.55	0.05	30.95
			0.10	40.13				0.10	36.08
			0.20	41.08				0.20	35.46
	50	19.55	0.05	36.31		**50**	19.55	0.05	30.95
			0.10	40.10				0.10	36.06
			0.20	41.06				0.20	35.36

3.5.2 Reactive Power Modulation

The damping contribution of different levels of reactive power modulation is presented in Table 3.4. A 0.5pu reactive power modulation level test case is added in order to display the superiority of active power modulation over reactive power modulation. Reactive power modulation within the range of 0.15pu provides adequate interarea damping contribution.

Table 3.4. Interarea mode damping contribution of different levels of reactive power modulation

		Base Case	Q-Loop				Base Case	Q-Loop	
Bus	**Line [km.]**	**Damping (%)**	**Qmod [pu.]**	**Damping**	**Bus**	**Line [km.]**	**Damping (%)**	**Qmod [pu.]**	**Damping (%)**
7	**0**	19.55	0.05	24.43	**9**	**0**	19.55	0.05	22.10
			0.10	26.72				0.10	24.43
			0.15	30.42				0.15	26.48
			0.20	34.90				0.20	23.81
			0.50	34.60				0.50	30.95
	25	19.55	0.05	21.14		**25**	19.55	0.05	22.26
			0.10	26.74				0.10	24.43
			0.15	30.45				0.15	26.53
			0.20	34.90				0.20	23.81
			0.50	34.60				0.50	30.95
	50	19.55	0.05	21.16		**50**	19.55	0.05	22.10
			0.10	26.79				0.10	24.43
			0.15	30.45				0.15	27.44
			0.20	35.06				0.20	23.81
			0.50	34.60				0.50	30.95

3.5.3 Summary

Results show that 0.1pu of active power modulation is sufficient to create a significant damping torque; while 0.15pu of reactive power modulation at buses 7 and 9 is enough to boost damping of interarea oscillations. Table 3.5 summarizes the recommendations for active power and reactive power modulation limits.

Table 3.5. Recommendations for active and reactive power modulation limits

	Modulation Limits	
Bus	**P-Loop**	**Q-Loop**
5	0.1pu	0
6	0.1pu	0
7	0.1pu	0.15pu
9	0.1pu	0.15pu
10	0.1pu	0
11	0.1pu	0

3.6 Conclusions and Recommendations

In this chapter, a pre-feasibility analysis of the wind based power system stabilizer is introduced. The method makes use of geometric approach to assess the modal controllability index of a wind farm given its location in the power system and its generated power. A two area four generator benchmark system is used to illustrate and test the proposed method.

Modal analysis shows that reactive power controllability index increases with the length of the ac line connecting the wind farm's point of common coupling to a bus in the power system while active power controllability index reduces. Time domain simulation using full state feedback damping controller is used to validate the results of modal analysis.

It was found that damping contribution is highest when the wind farm is located in either one of the two areas. In other words, damping contribution is reduced when the wind farm's power system coupling point is located across the inter-tie line. Results indicate that 10MW of active power modulation is more effective than 80MVar of reactive power modulation. The highest active power controllability indices were achieved when the wind farm was connected near conventional generation. Reactive power modulation is not technically justifiable near conventional plants due to the very low damping contribution. This is partly due to the interaction between the automatic voltage regulators of synchronous plants and reactive power modulation control of the wind farm.

Table 3.2 and Table 3.5 provide respectively recommendations for the installation of damping controllers and allocation of active and/or reactive power modulation. Table 3.3 and Table 3.4 display the damping contribution of active and reactive power control loops for different modulating levels. It is important to note that:

- Results, recommendations and conclusions are specific to the benchmark system under study and in no way represent a universal solution for wind based power system stabilizer applications.
- The work does not involve placing of wind farms but assessing the damping potential given a wind farm location in a power system.

- Parametric studies are applied in order to shed some light on the evolution of controllability indices with respect to a wind farm's point of common coupling. Parametric studies do not imply moving a wind farm from one location to another.

Wide area measurement feedback selection method, based on geometric measure of observability, is presented. It is found that angular deviation has higher observability of the interarea mode than the synchronous units speed deviation. The use of angular deviation as feedback signal reduces the need for high dc gain, and can potentially improves the robustness of the wind based damping controller compared to the conventional power system stabilizer that uses speed deviation as an input.

Chapter 4: Robust Design and Testing of Wind Based Power System Stabilizer

4.1 Introduction

Historically, power system stabilizers were used to damp electromechanical swing modes by modulating the field of synchronous machines to create a damping torque. A synchronous machine based power system stabilizer must ensure a phase lead, for the swing modes frequency range, between its input and its controlled signal in order to compensate for the phase lag in the excitation system. As power systems grew in complexity and interconnectivity, low frequency oscillations became more common. Meanwhile, it was observed that conventional power system stabilizers exhibit a reduction in damping potential of low interarea swing modes mainly due to inadequate phase compensation in the low frequency range.

Converter based variable speed wind generators are capable of fast active and reactive power control. This inherent feature of variable speed wind turbine reduces the requirements for phase compensation compared to conventional synchronous units and, due to its asynchronous operation with the grid, enables the use of both active and reactive power to produce a damping torque.

In Chapter 3, a full state feedback controller is used to validate the modal analysis. Even though the controller proved to be effective in damping swing modes, such control structure is very sensitive to all kinds of power system, transducers and communications disturbances. In addition, there are power system stabilizers gain and phase margin requirements that must be respected. In this chapter, a robust wind based power system stabilizer design is derived based on H_∞ constrained optimization. Weighting function selection methods is described. The proposed power system stabilizer makes use of angle deviation as input signals due to their high modal observability. Frequency response, sensitivity, gain and phase margin for each power system stabilizer are presented.

4.2 H_∞ Optimal Design of Wind Based Power System Stabilizer

The main objective in tuning the PSS parameters is to improve stability in the system by moving the modes to the left half of the imaginary axis. The PSS must also deal with a broad range of power system operation and contingencies. Wind based PSS (WPSS) is intended to damp critical interarea oscillations since conventional PSS are very effective in damping local modes.

H_∞ optimal control is used in order to achieve a good tradeoff between the different objectives and constraints of the design [26,75]. Weighing functions are introduced at different levels of the closed loop system, shown in Figure 4.1, to enforce closed loop performance specifications.

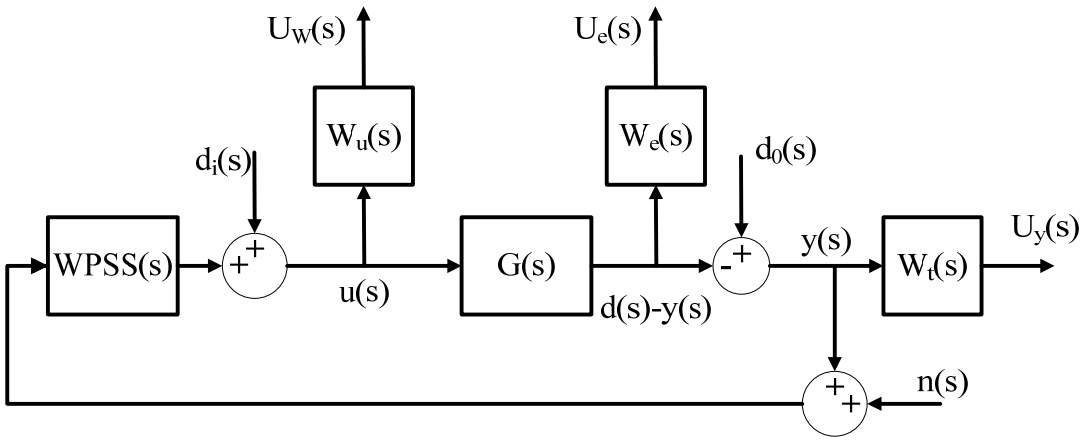

Figure 4.1. Closed-Loop Power System Frequency Domain Model

4.2.1 Background

The infinity norm, also known as L_∞, is the maximum gain of the frequency response of a system. The infinity norm of a system is defined as, Eq. (3.1):

$$\|G\|_\infty = \max_{\omega \in \Re} \|G(j\omega)\| \tag{4.1}$$

Where ||G(jω)|| is the spectral norm of the system G. In this case, G(s) is the transfer function of the power system, Eq. (4.2).

$$G(s) = B * (sI - A) * C^{-1} \tag{4.2}$$

Where A, B and C are state matrices and I is an identity matrix.

The output sensitivity S_0 of the closed loop system described in Figure 4.1 is defined in Eq. (4.3) as:

$$S_0(s) = (I + G(s)WPSS(s))^{-1} \tag{4.3}$$

$$M_S = \|S_0\|_\infty \tag{4.4}$$

The output complementary sensitivity T_0, also known as transmission, is defined in Eq. (4.5) as:

$$T_0(s) = G(s)WPSS(s)S_0(s) \tag{4.5}$$

$$M_T = \|T_0\|_\infty \tag{4.6}$$

Through algebraic manipulations, the system of Figure 4.1 can be described as:

$$\begin{bmatrix} y(s) \\ u(s) \end{bmatrix} = \begin{bmatrix} S_0(s)G(s) \\ -WPSS(s)S_0(s) \end{bmatrix} d_0(s) \tag{4.7}$$

Where y is the output of the system, u is the controlled output of the WPSS, which consist of active and reactive power modulation, and d_0 is an output disturbance function.

Thus, following the closed loop structure of Figure 4.1 and Eq. (4.7), the output variables of the weighting functions, *Wu, We* and *Wt*, become, Eq. (4.8):

$$\begin{bmatrix} U_u(s) \\ U_t(s) \\ U_e(s) \end{bmatrix} = -\begin{bmatrix} W_u(s)WPSS(s)S_0(s) \\ W_t(s)T_0(s) \\ W_e(s)S_0(s) \end{bmatrix} d_0(s) \tag{4.8}$$

A robust controller is derived by minimizing the infinity norm of the staked matrix of Eq. (4.9). According to robust theory [75], Eq. (4.9) implies Eq. (4.10) and Eq. (4.11).

$$\left\| \begin{bmatrix} W_u(s)WPSS(s)S_0(s) \\ W_t(s)T_0(s) \\ W_e(s)S_0(s) \end{bmatrix} \right\|_\infty < 1 \tag{4.9}$$

$$\|W_t(s)\|_\infty < M_T^{-1} \tag{4.10}$$

$$\|W_e(s)\|_\infty < M_S^{-1} \tag{4.11}$$

4.2.2 Problem Formulation

According to [31], the infinity norms of the output sensitivity and output transmission, namely M_S and M_T, are associated with the Gain Margin (GM) and Phase Margin (PM) of a closed loop system, Eq. (4.12) — (4.13).

$$GM \geq \begin{cases} 1+\left(M_S-1\right)^{-1} \\ 1+M_T^{-1} \end{cases} \tag{4.12}$$

$$PM \geq \begin{cases} M_S^{-1} \\ M_T^{-1} \end{cases} \tag{4.13}$$

Robustness criteria imposes that GM ≥ 2 and PM $\geq 30^{\circ}$. Combining these conditions with Eq. (4.12) — (4.13) gives the following robustness constraint, Eq. (4.14):

$$\begin{aligned} M_S &\leq 2 \\ M_T &\geq 1.5 \end{aligned} \tag{4.14}$$

The constraints described in Eq. (4.14) form the basis for selecting weighting functions.

4.2.3 Controller Design

This section describes the reasoning and the approach for selection of suitable weighting functions for deriving the transfer function of the WPSS controller. Weighting function selection was achieved by combining the design philosophies of [26,31,76]. The author makes use of the μ-synthesis toolbox in Matlab in order to derive the WPSS transfer function.

4.2.3.1 Input Weighting Function Wu(s)

The input weighting function design objectives are:

- Eliminate DC component in the input signal (i.e Washout)
- Attenuate input signal component beyond interarea frequency range
- Amplify the interarea frequency component
- Minimize the control energy

Keeping in mind that angular deviation between G1 and G4 is the input signal to the WPSS, a washout element in the form of an integral was introduced to the transfer

function of *Wu*. The derivative component serves as a washout element. The transfer function of *Wu* consists of a high pass filter with a cut-off frequency at 1Hz and combined with an integrator, Eq. (4.15).

$$Wu(s) = \frac{s^2 + (2\pi)s + 4*\pi^2}{10^{-6}s^2 + 0.01s + 10^{-6}} \tag{4.15}$$

The DC gain of *Wu* is intentionally kept high because it was observed that, regardless of the gain, the H_∞ solution is more robust than conventional requirements defined Eq. (4.14). Thus, following the derivation of the WPSS' transfer function, the gain is fine tuned in order to achieve best damping performance while abiding by the conventional robustness constraints of Eq. (4.14).

4.2.3.2 Output Weighting Function We(s)

We is used to minimize sensitivity within the operating bandwidth of operation of the WPSS frequencies. In [26], *We* is defined as a low pass filter, Eq. (4.16). The dc gain is calculated such as the conditions of Eq. (4.10) and Eq. (4.14) are respected.

$$We(s) = 0.5*\frac{s+300}{s+30} \tag{4.16}$$

4.2.3.3 Transmission Weighting Function Wt(s)

According to [76], the transmission weighting function is necessary in order to ensure acceptable performance of the closed loop system at high frequencies, especially since the power system model is an approximation of the actual one. *Wt* is chosen to be a 2nd order high pass filter with cut off frequency of 40Hz, Eq. (4.17). Similar to section 4.2.3.2, a dc gain is introduced in order to ensure conventional robustness conditions.

$$Wt(s) = 11.5*\left(\frac{s+2*pi*8}{s+2*pi*40}\right)^2 \tag{4.17}$$

4.2.3.4 Summary

A weighting function selection methodology suitable for designing wind based power system stabilizers is introduced. The wind based stabilizer uses angular deviation as an input signal, and thus the input weighting function was selected accordingly.

Transmission and sensitivity weighting function selection is discussed. Figure 4.2 displays the bode plot of the weighting functions. Note that the input weighting function was scaled down in order to observe detailed magnitude response of all weighting functions.

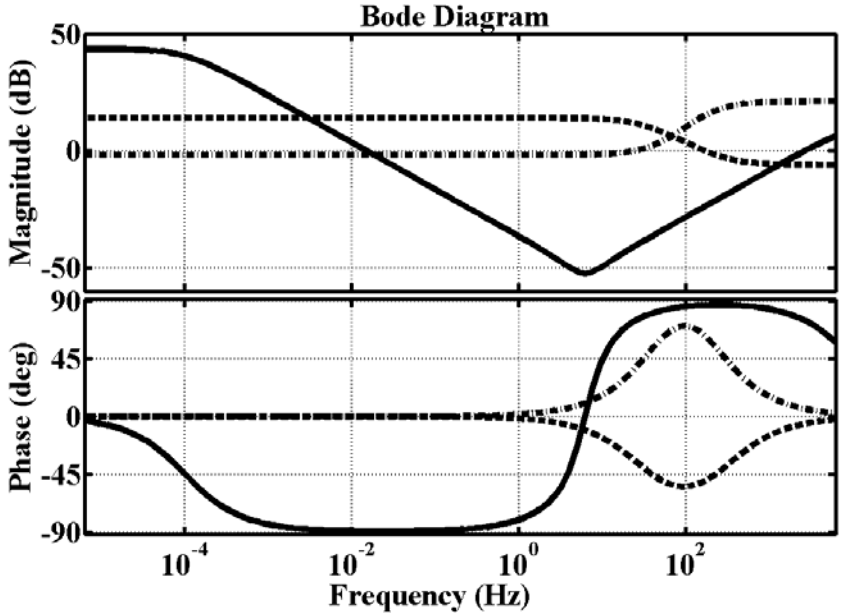

Figure 4.2. Magnitude Response of Weighting Functions. — Input Weighting Function Wu; -- Sensitivity Weighting Function We; -.Transmission Weighting Function

4.3 Wind Based Power System Stabilizer

This section presents the different WPSS controllers that were designed. Detailed sensitivity plots will be presented for connection points at buses 7 and 9. Note that the changes in the controller's frequency response with respect to line length is not observable which is why only one bode plot per connection point is presented. Section 4.2.3.4 contains details about phase and gain margins of the closed loop system for different connections points and ac line lengths. The order of the derived WPSS function is 13.

4.3.1 Grid Connection Point at Bus 7

In Chapter 3, it was observed that both active and reactive power modulation can be effective in damping interarea power swings. This section presents the proposed WPSS

controller, Figure 4.3, for both the real and reactive power loops as well as the sensitivity plots of the closed loop system, Figure 4.4 and Figure 4.5.

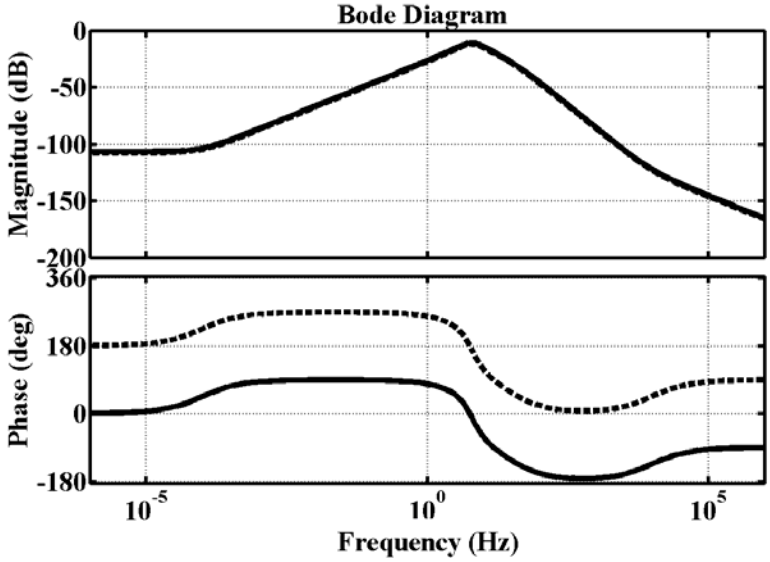

Figure 4.3. Bode Plot of the WPSS. Wind farm connected at bus 7. — Real power control loop; -- Reactive power control loop

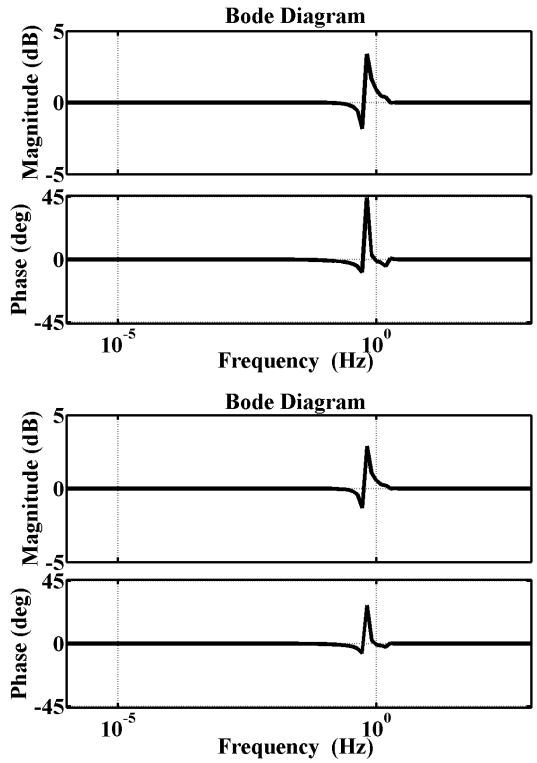

(a) **(b)**

Figure 4.4. Output Sensitivity Plots of the WPSS. Wind farm connected at bus 7. (a) Real power control loop;(b) Reactive power control loop

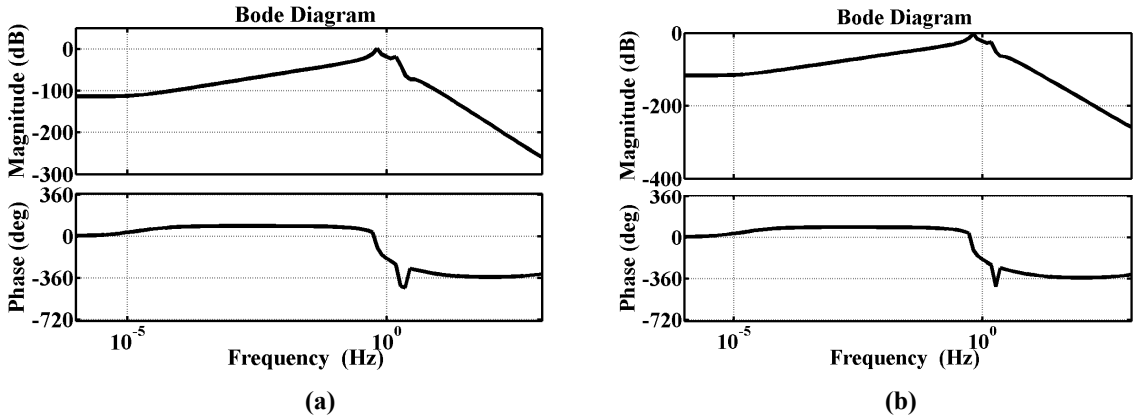

Figure 4.5. Output Transmission Plots of the WPSS. Wind farm connected at bus 7. (a) Real power control loop;(b) Reactive power control loop

Figure 4.4 displays the small magnitude of output sensitivity of the closed loop system in the low frequency range.

4.3.2 Grid Connection Point at Bus 9

Figure 4.6 displays the bode plot of the WPSS controller for a grid connection point located at bus 9. The magnitude response of the WPSS is roughly the same for the real and reactive power control loop while a 180 degrees phase shift is observed in the phase diagram.

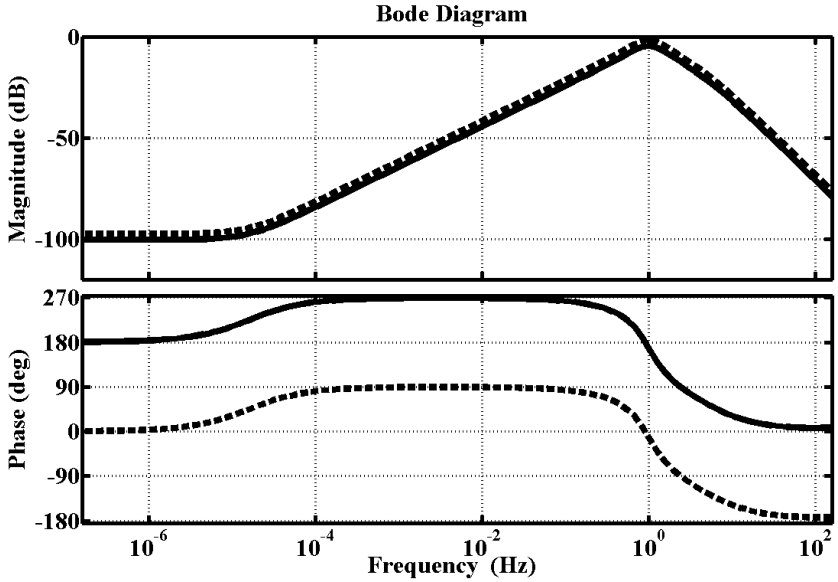

Figure 4.6. Bode Plot of the WPSS. Wind farm connected at bus 9— Real power control loop; -- Reactive power control loop

Figure 4.7 and Figure 4.8 present respectively the output sensitivity plot and the transmission plot of the closed loop system.

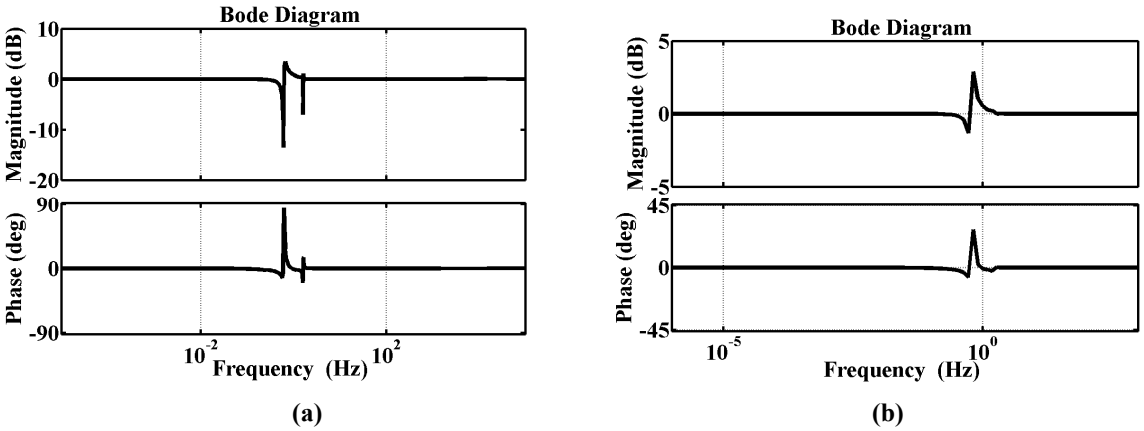

Figure 4.7. Output Sensitivity Plots of the WPSS. (a) Real power control loop;(b) Reactive power control loop

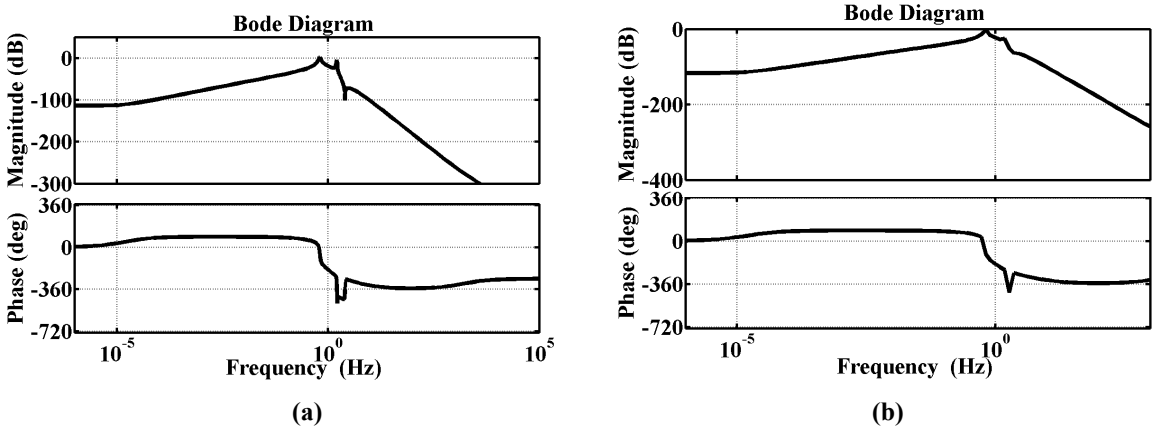

Figure 4.8. Output Transmission Plots of the WPSS. (a) Real power control loop;(b) Reactive power control loop

4.3.3 Grid Connection Points at Bus 5, 6, 10 and 11

As presented in the previous chapter, only real power modulation control is effective near synchronous units. In this section, bode plots of the real power modulation WPSS is presented, Figure 4.9 — Figure 4.12.

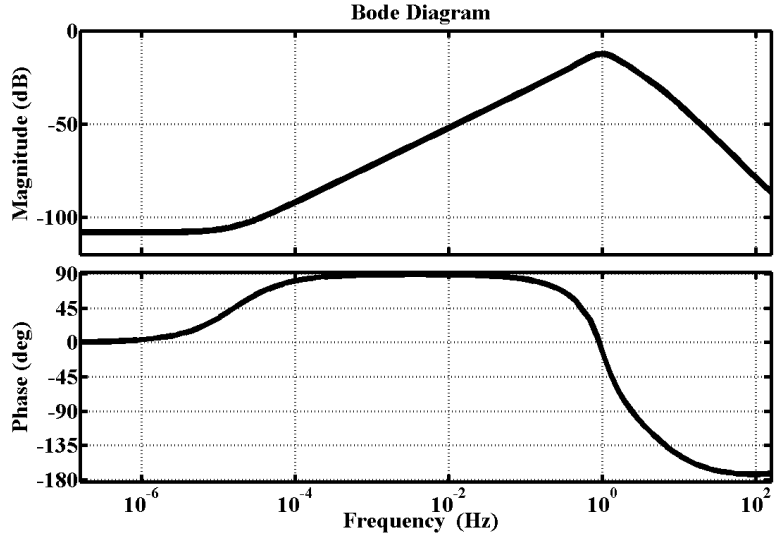

Figure 4.9. Bode Plot of the WPSS. Wind farm connected at bus 5

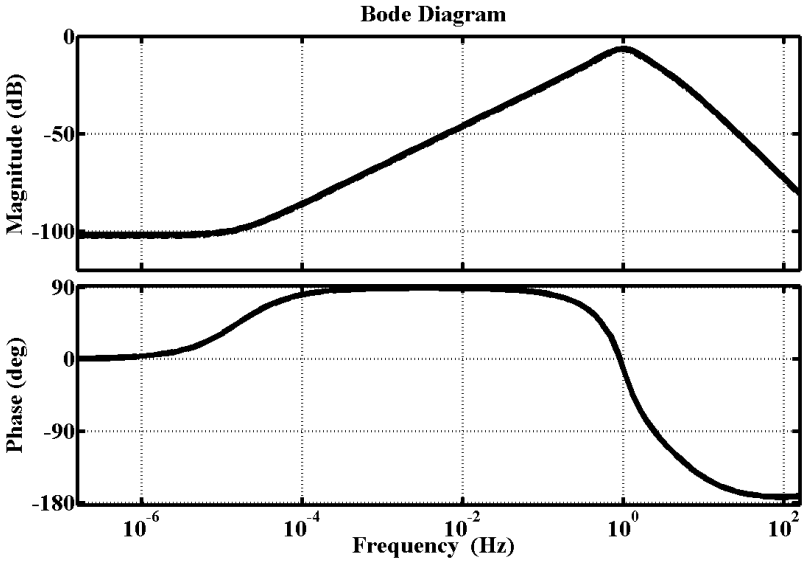

Figure 4.10. Bode Plot of the WPSS. Wind farm connected at bus 6

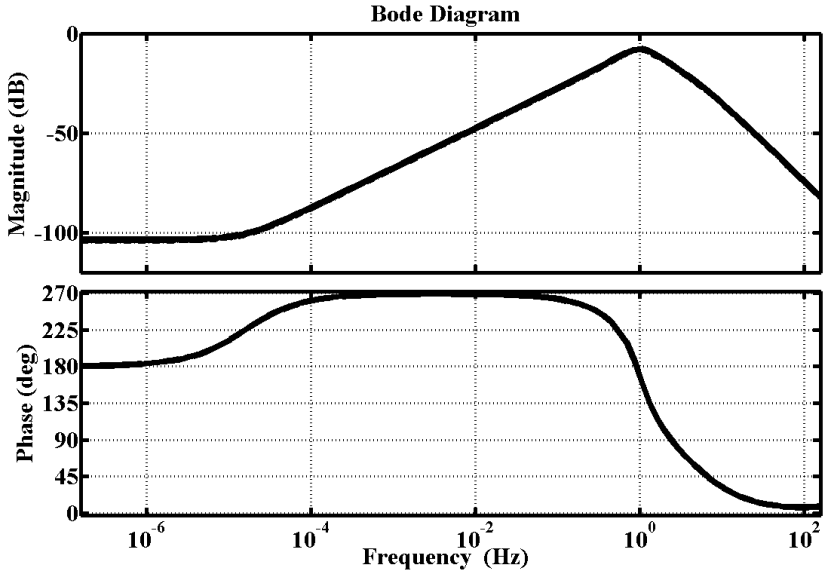

Figure 4.11. Bode Plot of the WPSS. Wind farm connected at bus 10

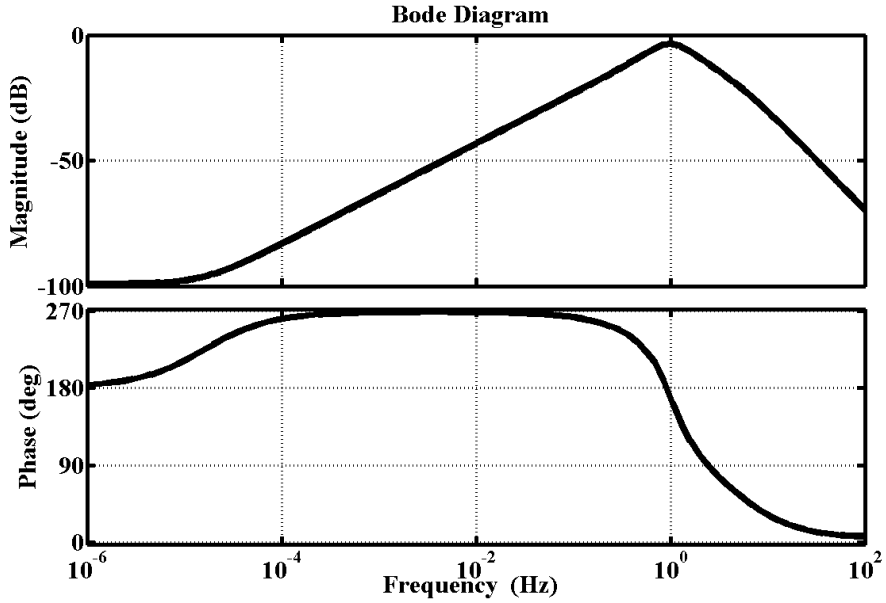

Figure 4.12. Bode Plot of the WPSS. Wind farm connected at bus 11

4.3.4 Controllers Performance Summary

An interesting feature of the WPSS design is that constant phase compensation is maintained for a wide range of low frequencies. The fast control dynamics of the real and reactive power of the wind turbines enable such phase response.

Table 4.1 presents the robustness of different WPSS for multiple wind farm locations. Note that for each wind farm location, a specific WPSS design is derived following the method described in this chapter.

Table 4.1. Summary of controller performance and robustness

		P-Loop Control			Q-Loop Control		
Bus	**ac Line Length [km.]**	**DC Gain (10-5)**	**Gain Margin**	**Phase Margin [deg.]**	**DC Gain (10-5)**	**Gain Margin**	**Phase Margin [deg.]**
5	**0**	0.40	3.20	78.27	N/A	N/A	N/A
	25	0.39	3.32	79.35	N/A	N/A	N/A
	50	0.38	3.45	80.57	N/A	N/A	N/A
6	**0**	0.78	4.05	60.07	N/A	N/A	N/A
	25	0.77	4.14	61.19	N/A	N/A	N/A
	50	0.75	4.25	62.47	N/A	N/A	N/A
7	**0**	2.06	2.89	45.51	-1.66	3.73	55.44
	25	1.97	3.00	46.72	-1.75	3.51	52.95
	50	1.88	3.14	48.14	-1.85	3.33	50.73
9	**0**	-0.95	2.98	62.67	1.32	3.39	62.83
	25	-0.91	3.21	64.66	1.41	2.95	59.43
	50	-0.87	3.47	67.05	1.50	2.59	56.47
10	**0**	-0.66	3.20	65.03	N/A	N/A	N/A
	25	-0.65	3.32	66.20	N/A	N/A	N/A
	50	-0.63	3.46	67.54	N/A	N/A	N/A
11	**0**	-1.10	3.03	48.07	N/A	N/A	N/A
	25	-1.08	3.06	48.46	N/A	N/A	N/A
	50	-1.07	3.10	48.90	N/A	N/A	N/A

4.4 Oscillation Detection Scheme

The output of the WPSS, given its robust design, is used as a trigger to initiate the operation of WPSS supplementary control loop, Figure 4.13. The controller then checks the angular oscillation levels at a pre-specified time intervals in order to maintain or disable the supplementary loop. Real power modulation is maintained as long as the wind turbine speed remains within acceptable operating range (0.7-1.2pu) or until the interarea

power swings are eliminated. Reactive power modulation is allowed to operate until the elimination of power swings.

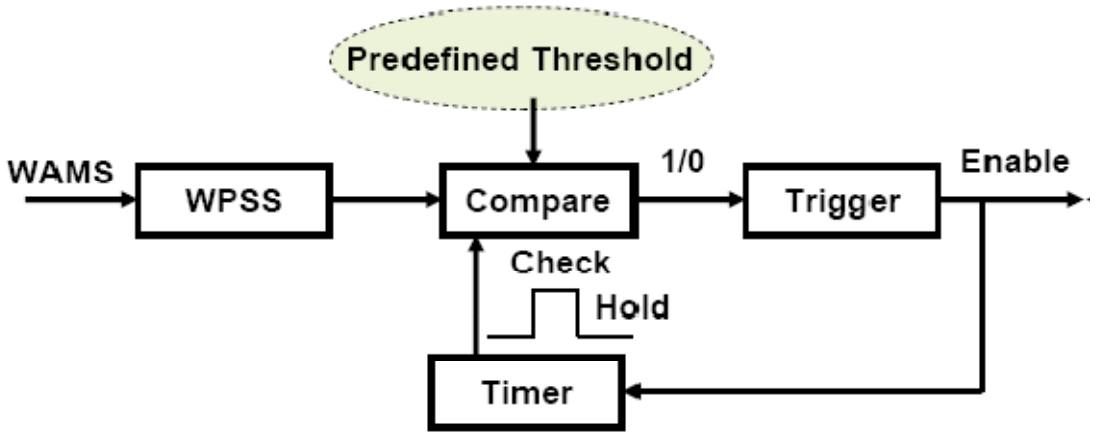

Figure 4.13. Power Swings Detection Scheme

4.5 Multi-Scenario Testing

Testing was done on the two area four generator benchmark, Figure 3.1. Time domain simulations are performed on the Matlab/Simulink platform. Testing scenarios include power transfer from Area 1 to Area 2 and vice versa in order to assess the performance of the WPSS under various operating conditions and interarea frequencies. Different wind farm coupling points and operating power levels are considered. Angle deviation between G1 and G4 is used as a feedback for the WPSS. The wind farm rated power (210MW) is used as base power.

The base case for every gird connection point consists of disabling the PSS of G2 and G4 and the WPSS while keeping the PSS of G1 and G3 online.

4.5.1 Large Disturbance Simulation

This test case is also setup such as around 400MW is transferred from Area 1 to Area 2. The large disturbance consists of a three phase to ground fault at bus 8. The fault is cleared in 8-cycles by tripping one of the tie line. The interarea frequency, following the disturbance, falls to the range of 0.4Hz. The designed WPSS must be capable of handling such power system events.

4.5.1.1 Test Case 1: Grid Connection at Bus 7 — Detailed Results

Figure 4.14 and Figure 4.15 show a significant improvement to power system angular stability compared to the base case *(i.e. only 2 synchronous machine PSS in service. G1 and G2)*. In fact, looking at Figure 4.14, the damping contribution of the WPSS is comparable to the addition of the PSS of G2 and G4. These results display how the proposed WPSS can compensate for the absence of conventional PSS. Figure 4.16 display the effectiveness of the action of the active and reactive power WPSS, during a short period following the disturbance.

It is observed in Figure 4.15 that the post-disturbance power angles are different from the pre-disturbance ones. Tripping of one of the interarea tie lines to clear the fault changed the admittance in between the Area 1 and Area 2 yet the power exchange did not change significantly. The larger impedance between the areas leads to higher angular separation and thus triggering a change in the power angles in the system.

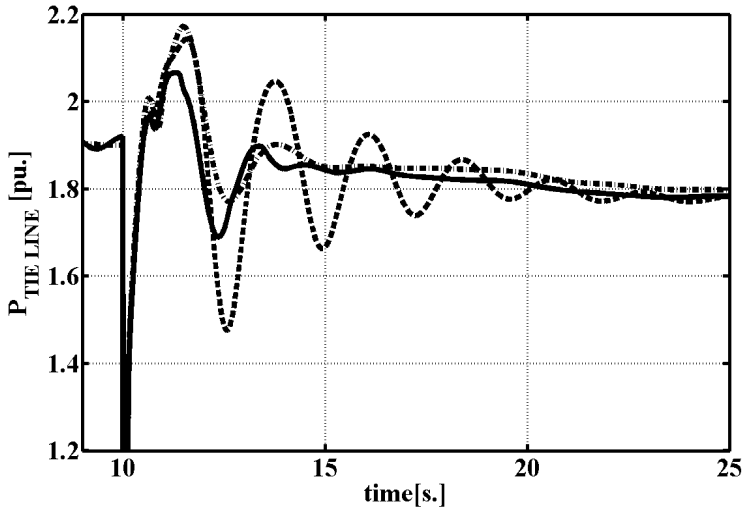

Figure 4.14. Inter-Tie Power Swings Following a 3 Phase Fault to Ground at Bus 8 Cleared in 8 Cycles. Wind Farm PCC connected at bus 7 via 25km ac line — WPSS online with G1 and G2 equipped with PSS; -- WPSS offline with G1 and G2 equipped with PSS; -. G1, G2, G3 and G4 equipped with PSS and WPSS disabled.

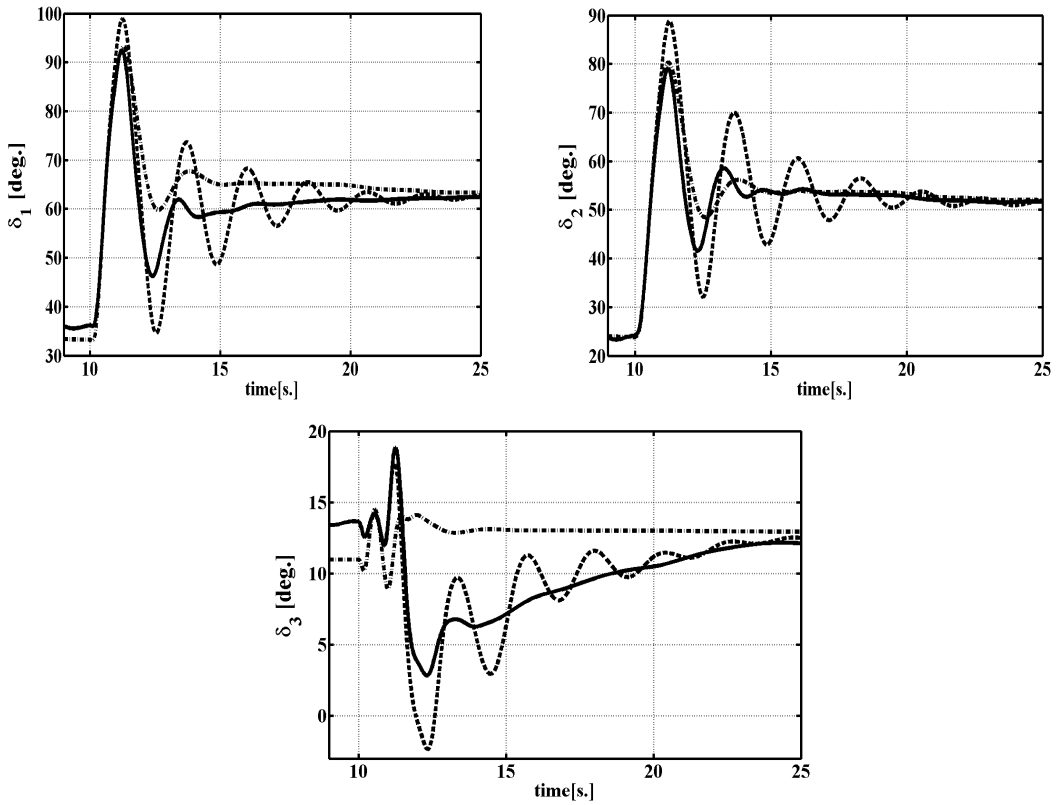

Figure 4.15. Synchronous Machines G1, G2 and G3 Angular Oscillations with Respect to G4. Wind Farm PCC connected at bus 7 via 25km ac line. — WPSS online with G1 and G2 equipped with PSS; -- WPSS offline with G1 and G2 equipped with PSS; -. G1, G2, G3 and G4 equipped with PSS and WPSS disabled.

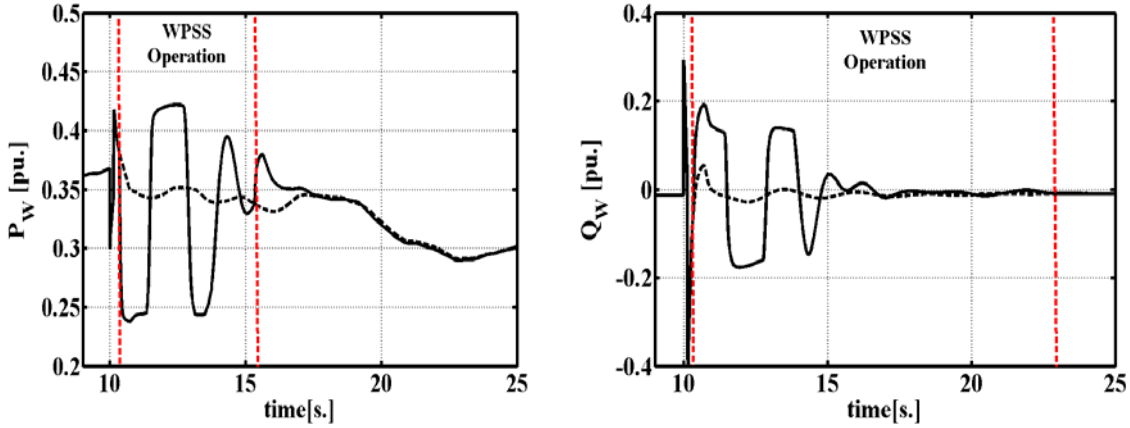

Figure 4.16. Wind Farm Power Output after Disturbance. Wind Farm PCC connected at bus 7 via 25km ac line. (a) Real power output of the wind farm; (b) reactive power output of the wind farm— WPSS online; -- WPSS offline;

Figure 4.17 display the WPSS performance for different operating powers of the wind farm. Figure 4.18 shows that a lower threshold on the upper saturation limit of the active

power modulation loop is present. However, the combined action of the active and reactive power modulation created a large damping torque sufficient to stabilize the power swings within 1 to 2 interarea cycles.

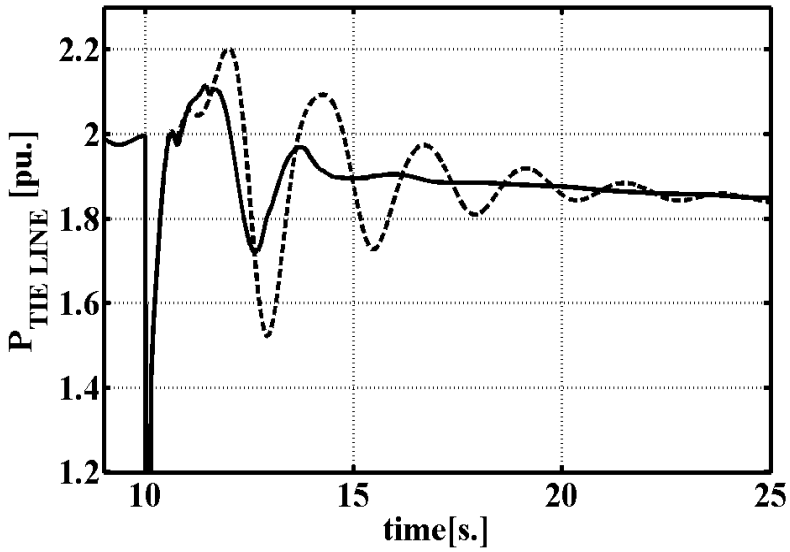

Figure 4.17. Inter-Tie Power Swings Following a 3 Phase Fault to Ground at Bus 8 Cleared in 8 Cycles. Wind Farm PCC connected at bus 7 via 25km ac line. Wind farm operating power above 0.5pu — WPSS online with G1 and G2 equipped with PSS; -- WPSS offline with G1 and G2 equipped with PSS;

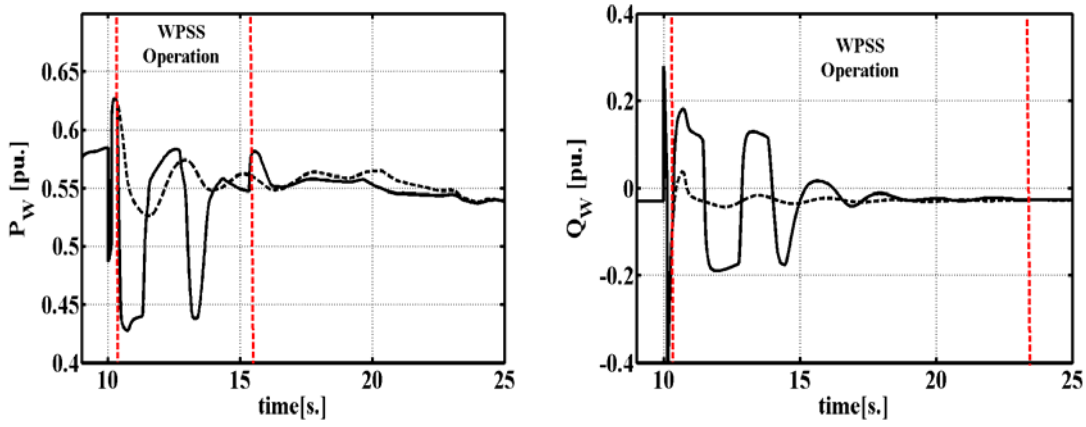

Figure 4.18. Wind Farm Power Output after Disturbance. Wind Farm PCC connected at bus 7 via 25km ac line. Wind farm operating power above 0.5pu(a) Real power output of the wind farm; (b) reactive power output of the wind farm— WPSS online; -- WPSS offline;

4.5.1.2 Test Case 2: Grid Connection at Bus 5 — Snapshot

Marginal contribution to damping of power swings is achieved when the grid connection point of the wind farm is coupled to bus 5. Figure 4.19 displays the power

swings between Area 1 and Area 2 following the tripping of one of the tie lines. Figure 4.20 shows the active power modulation of the wind farm.

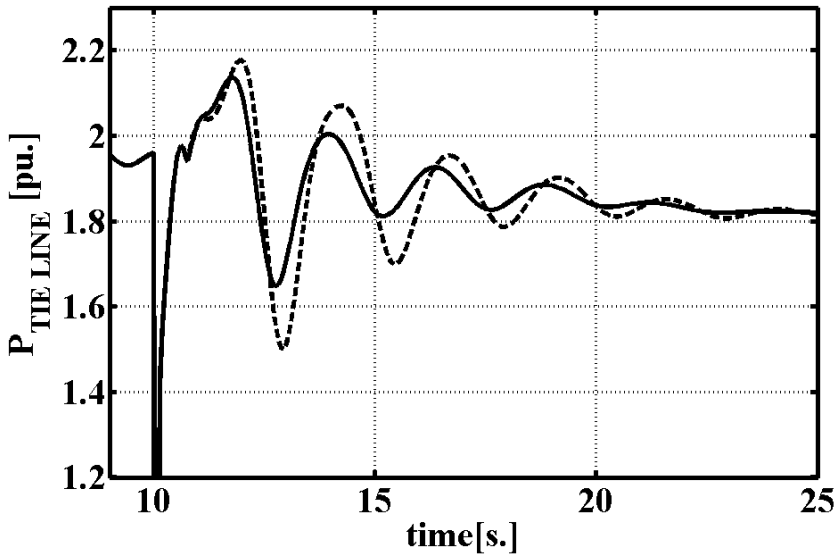

Figure 4.19. Inter-Tie Power Swings Following a 3-phase to Ground Fault at Bus 8 Cleared in 8 Cycles. Wind Farm PCC connected at bus 5 via 25km ac line — WPSS online with G1 and G2 equipped with PSS; -- WPSS offline with G1 and G2 equipped with PSS;

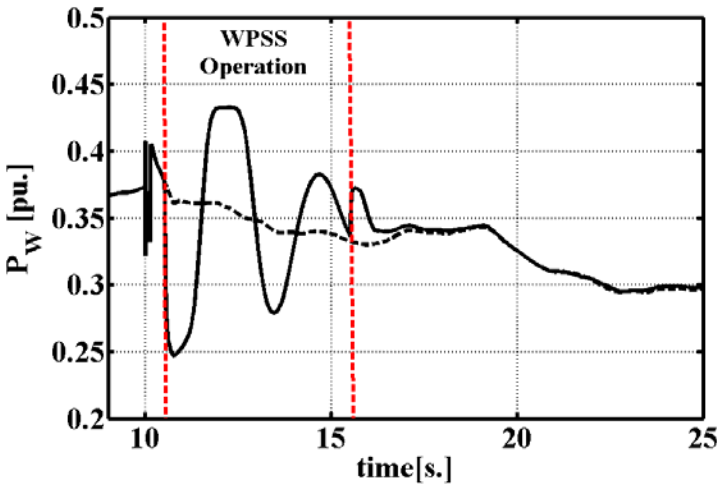

Figure 4.20. Wind Based Power System Stabilizer Operation. Wind Farm PCC connected at bus 5 via 25km ac line. — WPSS online; -- WPSS offline

4.5.1.3 Test Case 3: Grid Connection at Bus 6— Snapshot

Figure 4.21 shows the effectiveness of the active power based WPSS in damping power swings following a severe disturbance. Figure 4.22 demonstrates that few seconds of active power modulation is sufficient to stabilize angular swings in power system.

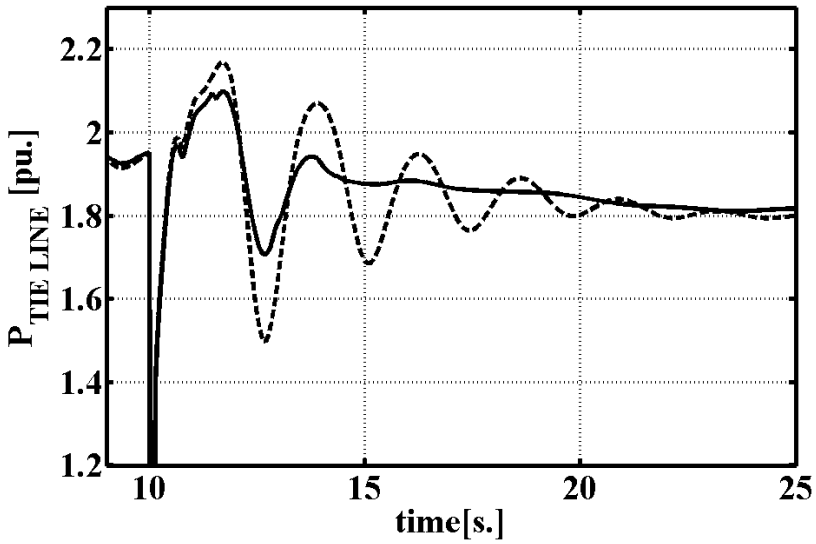

Figure 4.21. Inter-Tie Power Swings Following a 3-phase to Ground Fault at Bus 8 Cleared in 8 cycles. Wind Farm PCC connected at bus 6 via 25km ac line — WPSS online with G1 and G2 equipped with PSS; -- WPSS offline with G1 and G2 equipped with PSS;

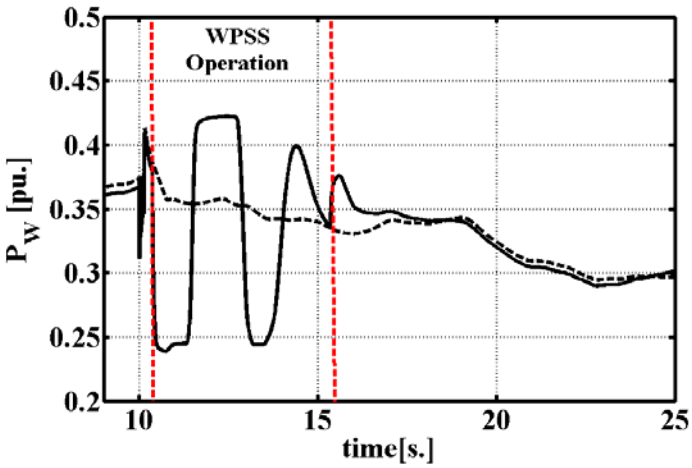

Figure 4.22. Wind Based Power System Stabilizer Operation. Wind Farm PCC connected at bus 6 via 25km ac line. — WPSS online; -- WPSS offline

4.5.1.4 Test Case 4: Grid Connection at Bus 9— Detailed Results

The power system lost synchronism following the fault at bus 8 in the base case of Test Case 4 (i.e. WPSS offline). This is partly due to the relatively high level of power transfer between areas. Figure 4.23 demonstrates the capability of the WPSS in enforcing angular stability and maintaining a high level of interarea power transfer. Figure 4.24 displays the evolution of the synchronous machine angles for the base case and the case

with WPSS online. Figure 4.25 shows the wind farm's active and reactive power modulation.

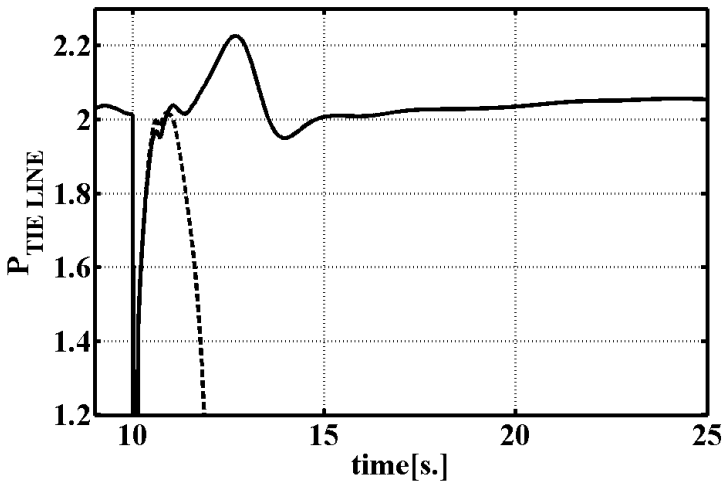

Figure 4.23. Inter-Tie Power Swings Following a 3-phase to Ground Fault at Bus 8 Cleared in 8 cycles. Wind Farm PCC connected at bus 9 via 25km ac line — WPSS online with G1 and G2 equipped with PSS; -- WPSS offline with G1 and G2 equipped with PSS;

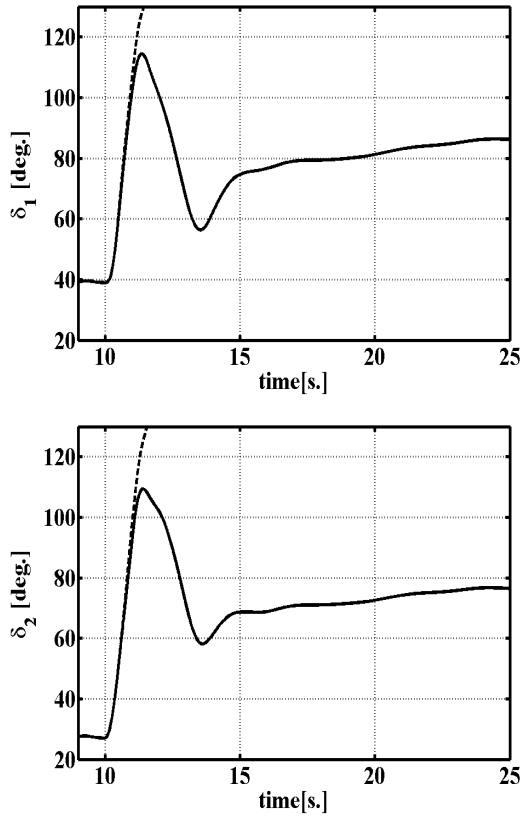

Figure 4.24. Synchronous Machines G1 and G2 Angular Oscillations with Respect to G4. Wind Farm PCC connected at bus 9 via 25km ac line. — WPSS online with G1 and G2 equipped with PSS; -- WPSS offline with G1 and G2 equipped with PSS; -. G1, G2, G3 and G4 equipped with PSS and WPSS disabled.

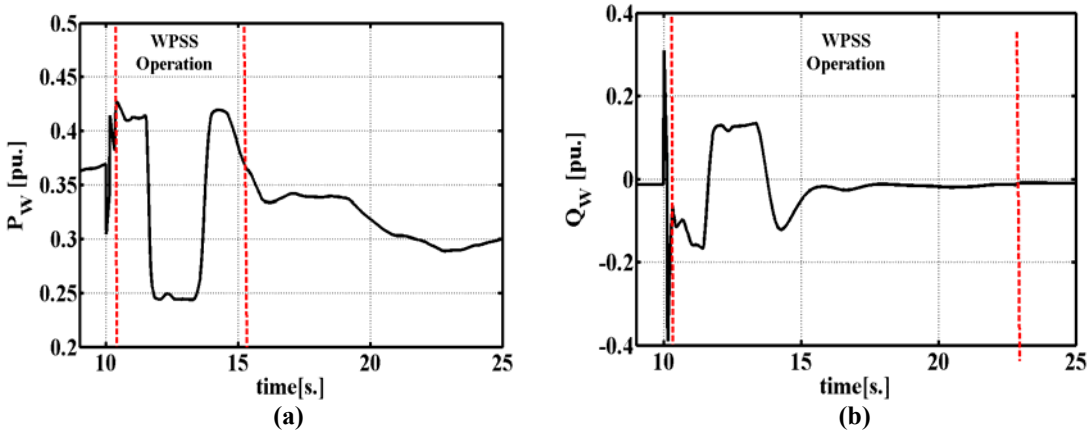

Figure 4.25. Wind Based Power System Stabilizer Operation. Wind Farm PCC connected at bus 9 via 25km ac line. — WPSS online; -- WPSS offline

4.5.1.5 Test Case 5: Grid Connection at Bus 10— Snapshot

In this Test Case, the damping action of the WPSS enabled the synchronous plants to maintain synchronous following a severe disturbance, Figure 4.26. Furthermore, the power transfer between the two areas is maintained above 400MW. Figure 4.27 displays the operation of the active power modulation supplementary control loop.

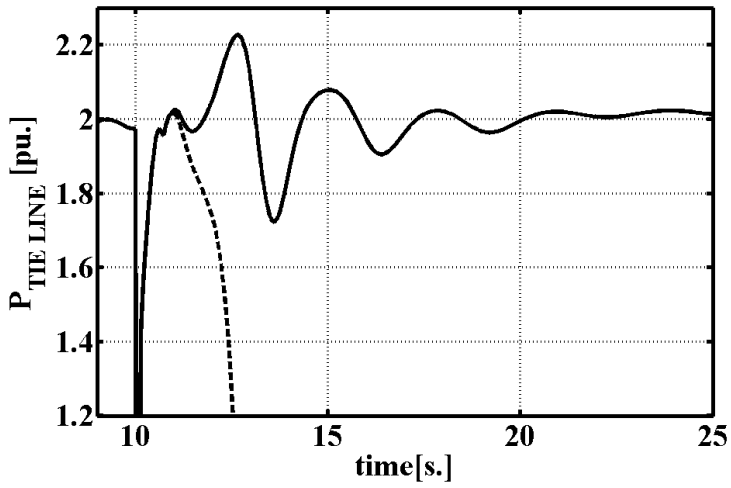

Figure 4.26. Inter-Tie Power Swings Following a 3-phase to Ground Fault at Bus 8 Cleared in 8 cycles. Wind Farm PCC connected at bus 10 via 25km ac line — WPSS online with G1 and G2 equipped with PSS; -- WPSS offline with G1 and G2 equipped with PSS;

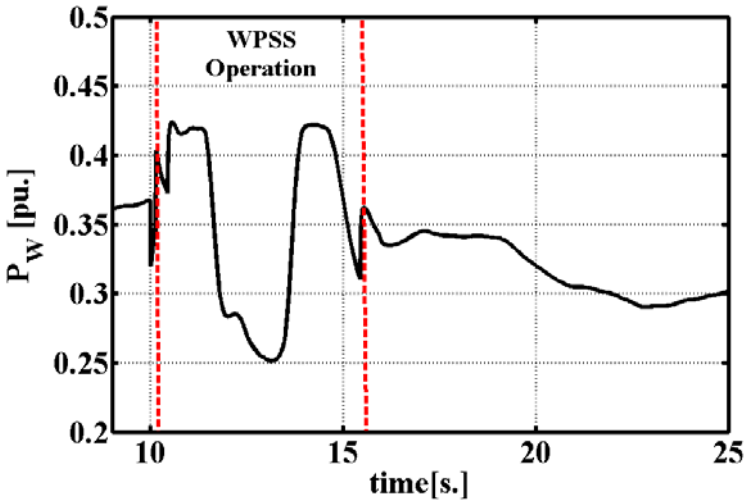

Figure 4.27. Wind Based Power System Stabilizer Operation. Wind Farm PCC connected at bus 10 via 25km ac line. — WPSS online; -- WPSS offline

4.5.1.6 Test Case 6: Grid Connection at Bus 11— Detailed Results

Similarly to Test Case 4 and Test Case 6, the synchronous machines lost synchronism following the severe disturbance. The WPSS was able to enforce stability by modulating the active power output of the wind farm, Figure 4.28. An extended operation of the WPSS is observed in Figure 4.29. The extended operation is possible under these conditions, Figure 4.30:

- Presence of angular oscillations with enough amplitude to trigger the WPSS action
- The supplementary control loop detects that the wind turbine rotational speed is within the predefined acceptable range (i.e 0.7-1.2pu).

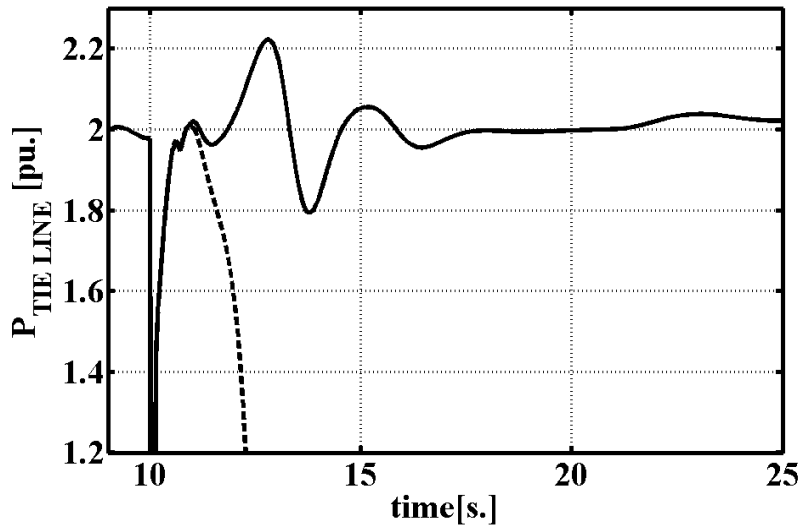

Figure 4.28. Inter-Tie Power Swings Following a 3-phase to Ground Fault at Bus 8 Cleared in 8 cycles. Wind Farm PCC connected at bus 11 via 25km ac line — WPSS online with G1 and G2 equipped with PSS; -- WPSS offline with G1 and G2 equipped with PSS;

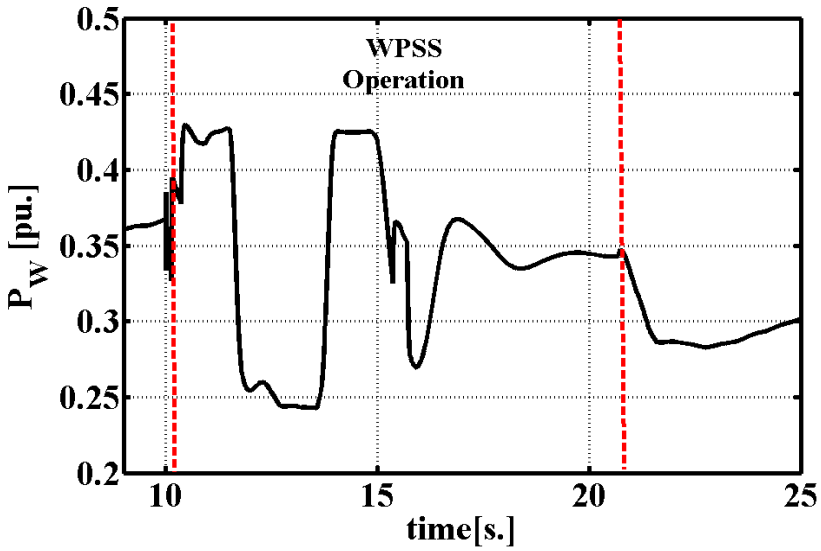

Figure 4.29. Wind Based Power System Stabilizer Operation. Wind Farm PCC connected at bus 11 via 25km ac line. — WPSS online; -- WPSS offline

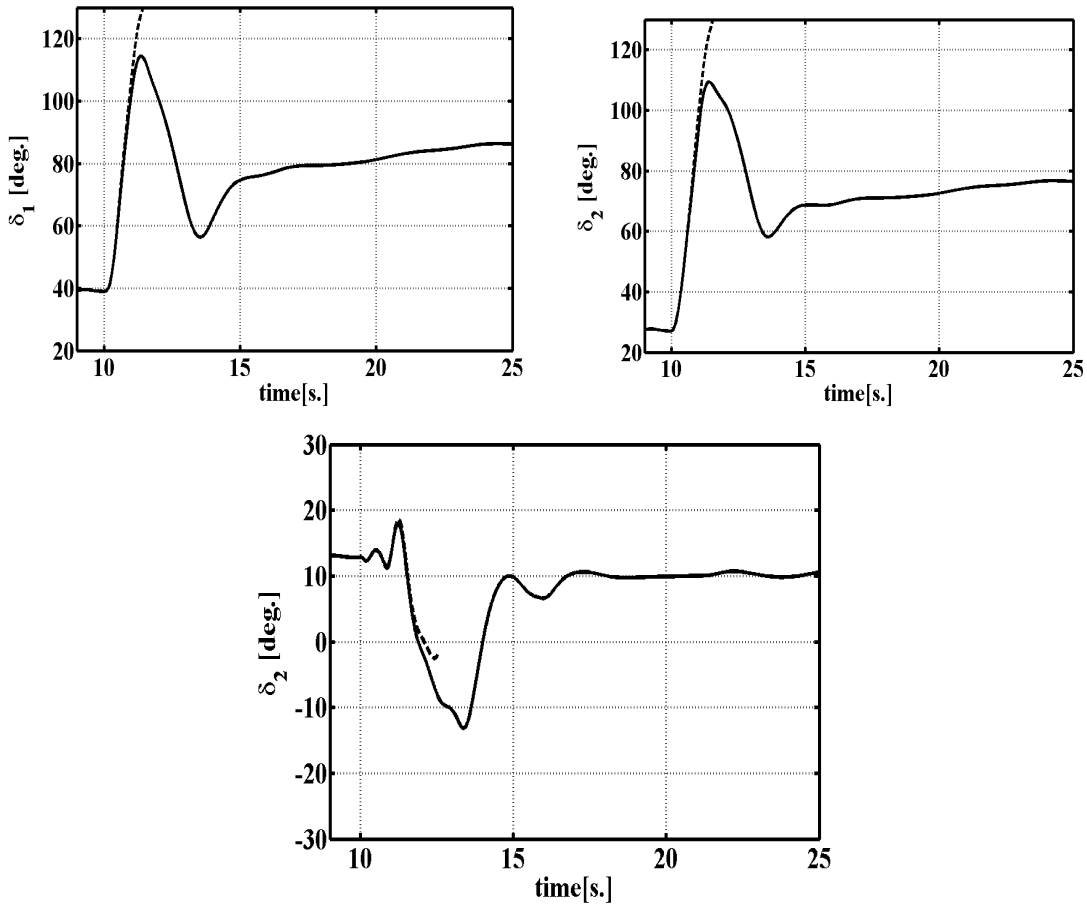

Figure 4.30. Synchronous Machines G1, G2 and G3 Angular Oscillations with Respect to G4. Wind Farm PCC connected at bus 11 via 25km ac line. — WPSS online with G1 and G2 equipped with PSS; -- WPSS offline with G1 and G2 equipped with PSS; -. G1, G2, G3 and G4 equipped with PSS and WPSS disabled.

4.5.2 Reverse Power: 400MW Exported From Area 2 to Area 1

The reverse power test case is setup in order to assess the performance of the WPSS with varying power system operations. Now, around 400MW is being exported from Area 2 to Area 1. Test Case 1 (i.e grid connection point at bus 7) is considered. The large disturbance, described in section 4.5.1, is used in order to trigger angular oscillations.

The WPSS proved its robustness and effectiveness in damping interarea oscillations under varying power system operation, Figure 4.31 — Figure 4.34. Wide area measurements are a major role player in maintaining good obsevability of the interarea mode and allowing the WPSS to create a damping torque in phase with the oscillations.

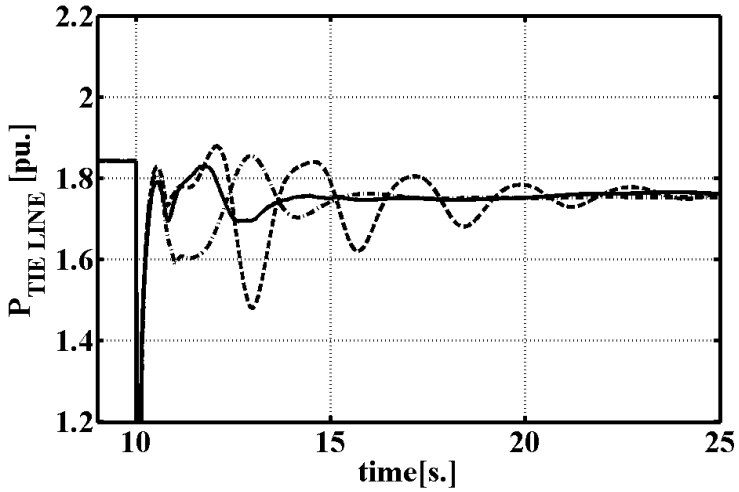

Figure 4.31. Inter-Tie Power Swings Following a 12 Cycle Pulse Change in the Reference Voltage of G1. Wind Farm PCC connected at bus 7 via 25km ac line — WPSS online with G1 and G2 equipped with PSS; -- WPSS offline with G1 and G2 equipped with PSS; -. G1, G2, G3 and G4 equipped with PSS and WPSS disabled.

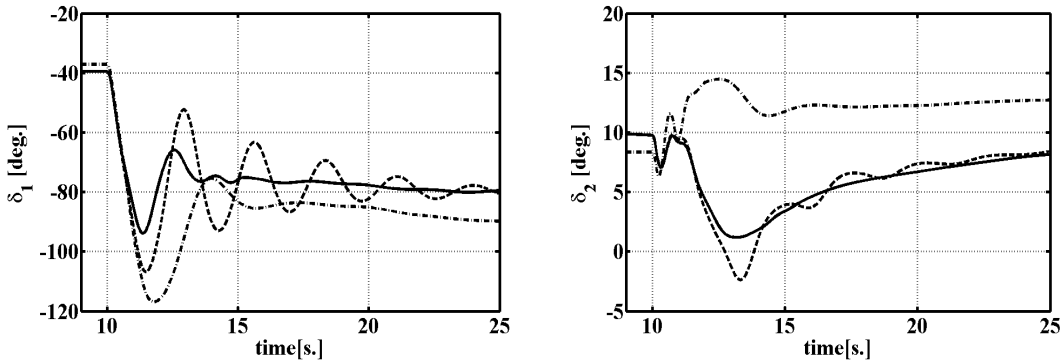

Figure 4.32. Synchronous Machines G1, G2 and G3 Angular Oscillations with Respect to G4. Wind Farm PCC connected at bus 7 via 25km ac line. — WPSS online with G1 and G2 equipped with PSS; -- WPSS offline with G1 and G2 equipped with PSS; -. G1, G2, G3 and G4 equipped with PSS and WPSS disabled.

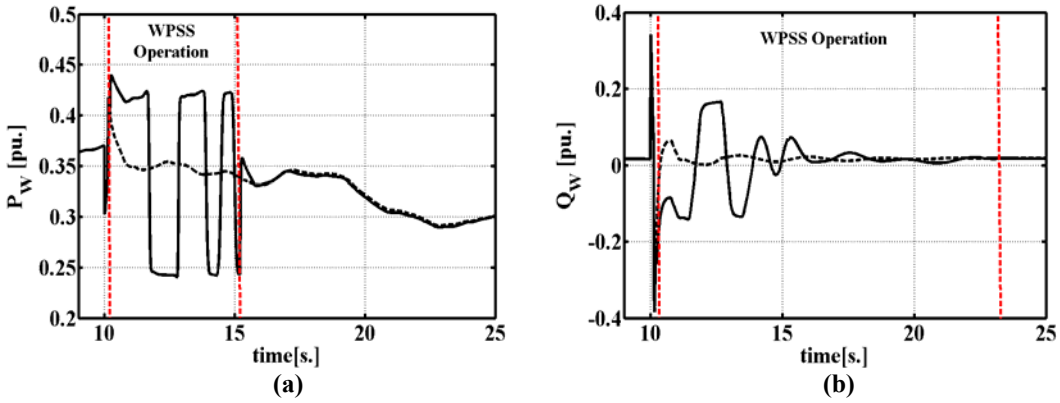

Figure 4.33. Wind Based Power System Stabilizer Operation. Wind Farm PCC connected at bus 7 via 25km ac line. — WPSS online; -- WPSS offline

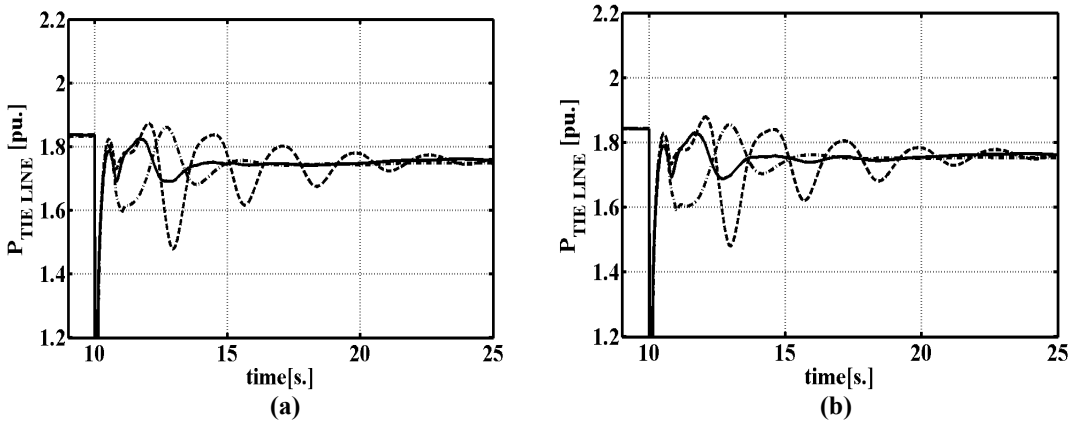

Figure 4.34. Inter-Tie Power Swings Following a 12 Cycle Pulse Change in the Reference Voltage of G1. (a) Wind Farm PCC directly connected at bus 7; (b) Wind Farm PCC connected at bus 7 via 50km ac line— WPSS online with G1 and G2 equipped with PSS; -- WPSS offline with G1 and G2 equipped with PSS; -. G1, G2, G3 and G4 equipped with PSS and WPSS disabled.

4.6 Summary

This chapter describes an H_∞ optimization technique for the design of wind farm based power system stabilizers. The proposed approach combines different design philosophies in order to achieve maximum damping capability while abiding to robustness requirements. Typical wind based power system stabilizer designs, suitable for the proposed benchmark, are presented. Gain and phase margin of designed controller is presented.

An oscillation trigger mechanism is introduced to initiate the operation of the wind based power system stabilizer as power modulation is intended to contribute to angular stability by providing a strong discontinuous damping action in the presence excessive angular oscillations in a power system.

The proposed wind based power system stabilizer, summarized in Figure 4.35 and Figure 4.36, is tested under different disturbances, power transfer scenarios, power system operations, wind farm location and operating power levels. Results indicate the resiliency and robustness of the proposed stabilizer in dealing with various power system events.

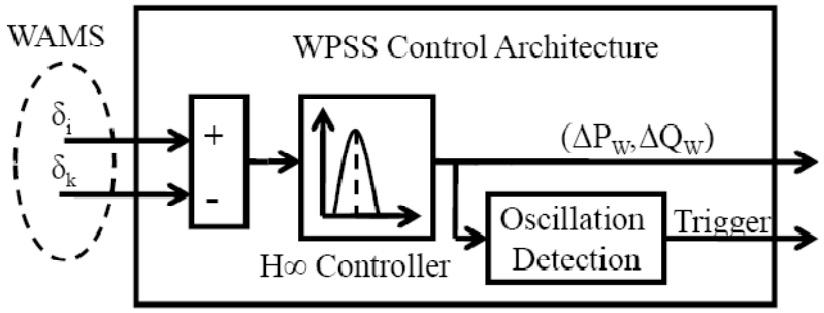

Figure 4.35. Wind Farm Base Power System Stabilizer Control Architecture

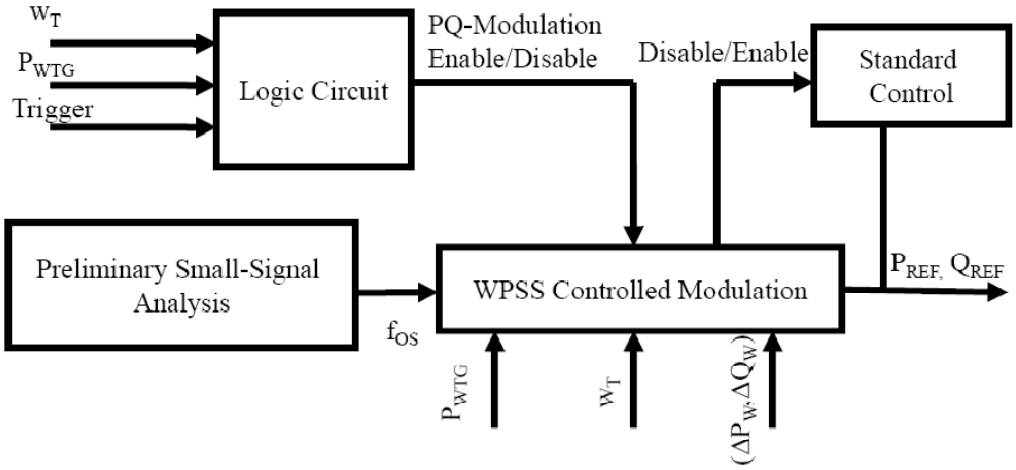

Figure 4.36. Comprehensive Overview of WPSS Supplementary Control Scheme

Chapter 5: Conclusion and Future Work

5.1 Summary

Wind industry is growing rapidly and is expected to take over a significant portion of generation away from polluting plants. As polluting synchronous plants are curtailed, their corresponding power system stabilizers will be taken offline, therefore potentially reducing the angular stability of the system. Reported angular instability incidents include disabling of conventional power system stabilizers due to under excitation field current limiters, transducers failures and/or scheduled maintenance.

This work introduces wind farm based power system stabilizers in order to help the power system cope with potential angular instability and cascading outages. A methodology is developed in order to justify the use of wind based power system stabilizers, identify ideal feedback signals and tune the stabilizer controller. Supplementary control loops are added to the standard control of a commercial model of a doubly fed induction machine to enable real and reactive power modulation. The methodology does not deal with placing the wind farm in order to damp power swings but it is mainly used as a tool to assess, given a wind farm point of common coupling, the damping potential and the type of power to modulate. Wide area measurements enable the wind based power system stabilizer to select feedback signal with high observability of a targeted mode. An H∞ constraint optimization is used to derive the transfer function of the wind based power system stabilizer.

The design criteria of the proposed power system stabilizer are:

- Allow variable speed wind turbines to operate under maximum peak power tracking when no or low oscillation levels are present
- Provide discontinuous strong damping action in the presence of large interarea power swings
- Effective for a wide range of power system operation
- Robust against disturbances
- Maintain the wind turbine rotational speed within acceptable range

The final product is tested on a 4 synchronous plants 2 area power system benchmark.

5.2 Conclusions

The damping contribution of active and reactive power modulation is highly dependent on the point of common coupling bus of the wind farm. Time domain simulations results are coherent with modal analysis. Results show that active power modulation is generally much more effective than reactive power modulation. A small portion of active power modulation, 5 to 10%, is needed for a short period of time. Higher levels of reactive power modulation, typically above 15%, are required to provide comparable damping contribution to active power modulation. Conclusions concerning active and reactive power modulation allocation are specific to the power system benchmark used. The different scenarios demonstrate the resiliency of the power system stabilizer to deal with various operations of a power system. Converter based wind generators show significant capabilities in damping interarea oscillations.

5.3 Future Work

The work presented in this thesis is only at its initial stages. Even though, wind based power system stabilizer design and integration philosophies are presented, there are significant opportunities towards extending the scope of the work to cover different interconnection issues, requirements and impact on power system stability of large wind penetration levels.

5.3.1 Online Assessment of Wind Farm Damping Potential

In [77], a low order power system model is developed by probing the network in open-loop with low-energy pulses. In [78], a method for assessing the controllability and the contribution of synchronous machines to selected mode is presented.

Since real power systems are very large, it would be beneficiary to avoid extensive analytical procedure for assessing controllability of a wind farm. Low energy pulse probing, using the active and reactive power output of a wind farm, would be beneficiary in assessing the damping potential of a wind farm in a fast and accurate way.

5.3.2 Coordination of Stabilizing Control in a Power System

This thesis considers the use of one wind farm. In [31], coordinated robust design of multiple synchronous machine based power system stabilizer is presented. The work makes use of a modal performance measure as an objective function to minimize in a constrained non-linear optimization problem. The approach can be extended to cover wind based power system stabilizer in an effort to coordinate the damping action of both synchronous and wind machine based power system stabilizers.

References

[1] G. Trudel, J. Gingras, and J. Pierre, "Designing a Reliable Power System: Hydro-Quebec's Integrated Approach" *Proc. of the IEEE*, vol. 93, pp. 907-917, 2005.

[2] Global Wind Energy Council, "Global Wind Energy Outlook 2008" www.gwec.org.

[3] T. Thiringer and J. Dahlberg, "Periodic Pulsations from a Three-Bladed Wind Turbine", *IEEE Trans. Energy Convers.*, vol. 16, 2001, pp. 128-133.

[4] M.I. Blanco, "The economics of wind energy" *Renewable and Sustainable Energy Reviews Elsevier*, vol. 13, pp. 1372-1382, 2009.

[5] H. Polinder, F. van der Pijl, G. de Vilder, and P. Tavner, "Comparison of Direct-Drive and Geared Generator Concepts for Wind Turbines" *IEEE Trans. Energy Convers.*, vol. 21, pp. 725-733, 2006.

[6] N. Ullah, T. Thiringer, and D. Karlsson, "Temporary Primary Frequency Control Support by Variable Speed Wind Turbines— Potential and Applications" *IEEE Trans. Power Syst.*, vol. 23, pp. 601-612, 2008.

[7] Ping-Kwan Keung, Pei Li, H. Banakar, and Boon Teck Ooi, "Kinetic Energy of Wind-Turbine Generators for System Frequency Support" *IEEE Trans. Power Syst.*, vol. 24, pp. 279-287, 2009.

[8] J. Mauricio, A. Marano, A. Gomez-Exposito, and J. Martinez Ramos, "Frequency Regulation Contribution Through Variable-Speed Wind Energy Conversion Systems" *IEEE Trans. Power Syst.*, vol. 24, pp. 173-180, 2009.

[9] R. de Almeida and J. Lopes, "Participation of Doubly Fed Induction Wind Generators in System Frequency Regulation" *IEEE Trans. Power Syst.*, vol. 22, pp. 944-950, 2007.

[10] J. Smith, R. Thresher, R. Zavadil, E. DeMeo, R. Piwko, B. Ernst, and T. Ackermann, "A mighty wind" *Power and Energy Magazine, IEEE*, vol. 7, pp. 41-51, 2009.

[11] Nayeem Rahmat Ullah and Torbjrn Thiringer, "Variable Speed Wind Turbines for Power System Stability Enhancement" *IEEE Trans. Energy Convers.*, vol. 22, pp. 52-60, 2007.

[12] Z. Chen and E. Spooner, "Grid Power Quality with Variable Speed Wind turbines" *IEEE Trans. Energy Convers.*, vol. 16, pp. 148-154, 2008.

[13] M. Leblanc, L. Evans, P. Gardner, N. Scott and S. Wittaker, "Canadian Grid Code for Wind Development Review and Recommendation", Garrad Hassan and CanWEA, Ottawa, ON, Oct. 2005.

[14] ___,"Technical Requirements For The Connection of Generating Facilities To The Hydro Quebec Transmission System - Supplementary Requirements For Wind Generation", Hydro Quebec TransEnergie, Quebec, Oct. 2005.

[15] H. Banakar, Changling Luo, and Boon Teck Ooi, "Impacts of Wind Power Minute-to-Minute Variations on Power System Operation" *IEEE Trans. Power Syst.*, vol. 23, pp. 150-160, 2008.

[16] J. Smith, M. Milligan, E. De Meo, and B. Parsons, "Utility Wind Integration and Operating Impact State of the Art" *IEEE Trans. Power Syst.*, vol. 22, pp. 900-908, 2007.

[17] G. Joos, “Workshop Summary: Wind Delivery and Reiability”, CanWEA, Toronto, ON, Mar. 2005.
[18] J. Dixon, L. Moran, E. Rodriguez, and R. Domke, “Reactive Power Compensation Technologies: State-of-the-Art Review” *Proc. of the IEEE*, vol. 93, pp. 2144-2164, 2005.
[19] S. Bozhko, G. Asher, Risheng Li, J. Clare, and Liangzhong Yao, “Large Offshore DFIG-Based Wind Farm With Line-Commutated HVDC Connection to the Main Grid: Engineering Studies” *IEEE Trans. Energy Convers.*, vol. 23, pp. 119-127, 2008.
[20] P. Bresesti, W. Kling, R. Hendriks, and R. Vailati, “HVDC Connection of Offshore Wind Farms to the Transmission System” *IEEE Trans. Energy Convers.*, vol. 22, pp. 37-43, 2007.
[21] I. Kamwa, R. Grondin, and G. Trudel, “IEEE PSS2B versus PSS4B: the limits of performance of modern power system stabilizers” *IEEE Trans. Power Syst.*, vol. 20, pp. 903-915, 2005.
[22] C. Taylor, D. Erickson, K. Martin, R. Wilson, and V. Venkatasubramanian, “WACS-Wide-Area Stability and Voltage Control System: R&D and Online Demonstration” *Proc. of the IEEE*, vol. 93, pp. 892-906, 2005,.
[23] N. Martins, A. Barbosa, J. Ferraz, M. dos Santos, A. Bergamo, C. Yung, V. Oliveira, and N. Macedo, “Retuning stabilizers for the north-south Brazilian interconnection”, Power Engineering Society Summer Meeting, 1999, IEEE, vol. 1, pp. 58-67, 1999.
[24] A. Fischer and I. Erlich, “Impact of long-distance power transits on the dynamic security of large interconnected power systems” *Power Tech Proceedings, 2001 IEEE Porto*, vol. 2 pp. 1-6, 2001.
[25] Z. Xiaoxin, Y. Jun, S. Ruihua, Y. Xiaoyu, L. Yan, and T. Haiyan, “An overview of power transmission systems in China” *Energy Elsevier*, vol. In Press, Corrected Proof, 2009.
[26] B. Pal and B. Chaudhuri, *Robust Control in Power Systems*, Springer, 1st Edition, London, Jun. 2005.
[27] P. Kundur, *Power System Stability and Control*, McGraw-Hill Professional, 1st Edition, 1994.
[28] B. Archer, U. Annakkage, B. Jayasekara, and P. Wijetunge, “Accurate Prediction of Damping in Large Interconnected Power Systems With the Aid of Regression Analysis” *IEEE Trans. Power Syst.*, vol. 23, pp. 1170-1178, 2008.
[29] M. Khaldi, A. Sarkar, K. Lee, and Y. Park, “The modal performance measure for parameter optimization of power system stabilizers", IEEE Trans. Power Syst., vol. 8, pp. 660-666, 1993.
[30] J. Simo, I. Kamwa, G. Trudel, and S. Tahan, “Validation of a new modal performance measure for flexible controllers design” *IEEE Trans. Power Syst.*, vol. 11, pp. 819-826, 1996.
[31] I. Kamwa, G. Trudel, and L. Gerin-Lajoie, “Robust design and coordination of multiple damping controllers using nonlinear constrained optimization” *IEEE Trans. Power Syst.*, vol. 15, pp. 1084-1092, 2000.
[32] I. Kamwa, R. Grondin, and Y. Hebert, “Wide-area measurement based stabilizing control of large power systems-a decentralized/hierarchical approach” *IEEE Trans. Power Syst.*, vol. 16, pp. 136-153, 2001.

[33] H. Golestani Far, H. Banakar, P. Li, C. Luo, and B. Ooi, "Damping Interarea Oscillations by Multiple Modal Selectivity Method" *IEEE Trans. Power Syst.*, vol. 24, pp. 766-755, 2009.
[34] S. Ruan, G. Li, B. Ooi, and Y. Sun, "Power System Damping from Energy Function Analysis Implemented by Voltage-Source-Converter Stations", *Electric Power Systems Research,* vol. 78, pp. 1353-1360, Aug. 2008.
[35] L. Zhang, L. Harnefors, and R. Pablo, "Power System Reliability and Transfer Capability Improvement by VSC-HVDC" *CIGRÉ Regional Meeting, Security and Reliability of Electric Power Systems*, Jun. 2007.
[36] T. Smed and G. Andersson, "Utilizing HVDC to Damp Power Oscillations" *IEEE Trans. Power Del.*, vol. 8, pp. 620-627, 1993.
[37] Li Licheng, Wu Xiaochen, and Li Peng, "Coordinated Control of Multiple HVDC Systems for Damping Interarea Oscillations in CSG" Power Engineering Society Conference and Exposition in Africa 2007, IEEE, pp. 1-7, July 2007.
[38] M. Chandhari, G. Andersson, and I. Hiskens, "Control Lyapunov Functions for Controllable Series Devices" Power Engineering Society Winter Meeting, 2002, IEEE, vol. 2, p. 753.
[39] J. Gronquist, W. Sethares, F. Alvarado, and R. Lasseter, "Power oscillation damping control strategies for FACTS devices using locally measurable quantities" *IEEE Trans. Power Syst.*, vol. 10, pp. 1598-1605, 1995.
[40] H. Wang and F. Swift, "A unified model for the analysis of FACTS devices in damping power system oscillations. I. Single-machine infinite-bus power systems" *IEEE Trans. Power Del.*, vol. 12, 1997, pp. 941-946.
[41] H. Wang, F. Swift, and M. Li, "A unified model for the analysis of FACTS devices in damping power system oscillations. II. Multi-machine power systems" *IEEE Trans. Power Del.*, vol. 13, pp. 1355-1362, 1998.
[42] HaiFeng Wang, "A unified model for the analysis of FACTS devices in damping power system oscillations. III. Unified power flow controller" *IEEE Trans. Power Del.*, vol. 15, pp. 978-983, 2000.
[43] I. Kamwa, R. Grondin, D. Asber, J. Gingras, and G. Trudel, "Active-power stabilizers for multimachine power systems: challenges and prospects" *IEEE Trans. Power Syst.*, vol. 13, pp. 1352-1358, 1998.
[44] A. Heniche and I. Kamwa, "Using global control and SMES to damp inter-area oscillations: an exploratory assessment" *Power Engineering Society Summer Meeting, IEEE*, vol. 3, pp. 1872-1876, 2000.
[45] J. Sanchez-Gasca, N. Miller, and W. Price, "A modal analysis of a two-area system with significant wind power penetration" *Power Systems Conference and Exposition, IEEE PES*, 2004, vol.2, pp. 1148-1152, *2004*.
[46] Lingling Fan, Zhixin Miao, and D. Osborn, "Impact of doubly fed wind turbine generation on inter-area oscillation damping" *Power and Energy Society General Meeting 2008, IEEE*, pp. 1-8, 2008.
[47] E. Muljadi, C. Butterfield, B. Parsons, and A. Ellis, "Effect of Variable Speed Wind Turbine Generator on Stability of a Weak Grid" *IEEE Trans. Energy Convers.*, vol. 22, pp. 29-36, 2007.
[48] D. Gautam, V. Vittal, and T. Harbour, "Impact of Increased Penetration of DFIG-Based Wind Turbine Generators on Transient and Small Signal Stability of Power Systems" *IEEE Trans. Power Syst.*, vol. 24, pp. 1426-1434, 2009.

[49] F. Hughes, O. Anaya-Lara, N. Jenkins, and G. Strbac, "A power system stabilizer for DFIG-based wind generation" *IEEE Trans. Power Syst.*, vol. 21, pp. 763-772, 2006.
[50] F. Hughes, O. Anaya-Lara, G. Ramtharan, N. Jenkins, and G. Strbac, "Influence of Tower Shadow and Wind Turbulence on the Performance of Power System Stabilizers for DFIG-Based Wind Farms" *IEEE Trans. Energy Convers.*, vol. 23, pp. 519-528, 2008.
[51] Pei Li, Hadi Banakar, Ping-Kwan Keung, Hamed Golestani Far, and Boon-Teck Ooi, "Macromodel of Spatial Smoothing in Wind Farms" *IEEE Trans. Energy Convers.*, vol. 22, 2007, pp. 119-128.
[52] P. Li, P. Keung, and B. Ooi, "Development and simulation of dynamic control strategies for wind farms" *Renewable Power Generation, IET*, vol. 3, pp. 180-189, 2009.
[53] M. El Moursi, G. Joos, and C. Abbey, "A Secondary Voltage Control Strategy for Transmission Level Interconnection of Wind Generation" *IEEE Trans. Power Electron.*, vol. 23, pp. 1178-1190, 2008.
[54] J. Morneau, C. Abbey, and G. Joos, "Effect of Low Voltage Ride Through Technologies on Wind Farm" *Electrical Power Conference EPC 2007, IEEE*, pp. 56-61, 2007.
[55] H. Gil and G. Joos, "Generalized Estimation of Average Displaced Emissions by Wind Generation" *IEEE Trans. Power Syst.*, vol. 22, pp. 1035-1043, 2007.
[56] H. Gil and G. Joos, "Models for Quantifying the Economic Benefits of Distributed Generation" *IEEE Trans. Power Syst.*, vol. 23, pp. 327-335, 2008.
[57] Changling Luo and Boon-Teck Ooi, "Frequency deviation of thermal power plants due to wind farms" *IEEE Trans. Energy Convers.*, vol. 21, pp. 708-716, 2006.
[58] C. Abbey and G. Joos, "Supercapacitor Energy Storage for Wind Energy Applications" *IEEE Trans. Ind. Appl.*, vol. 43, pp. 769-776, 2007.
[59] IEEE Task Force on Blackout Experience, Mitigation, and the Role of New Technologies, "Blackout Experiences and Lessons, Best Practices for System Dynamic Performance, and the Role of New Technologies" *Special Publication 07TP190, Power System Dynamic Performance Committee*, 2007.
[60] C. Taylor, T. Van Cutsem, V. Vittal, P. Kundur, J. Paserba, V. Ajjarapu, G. Andersson, A. Bose, C. Canizares, N. Hatziargyriou, D. Hill, and A. Stankovic, "Definition and classification of power system stability IEEE/CIGRE joint task force on stability terms and definitions" *IEEE Trans. Power Syst.,* vol. 19, pp. 1387-1401, 2004.
[61] Y. Makarov, V. Reshetov, A. Stroev, and I. Voropai, "Blackout Prevention in the United States, Europe, and Russia" *Proc. of the IEEE*, vol. 93, pp. 1942-1955, 2005.
[62] E. Koutroulis and K. Kalaitzakis, "Design of a maximum power tracking system for wind-energy-conversion applications" *IEEE Trans. Ind. Electron.*, vol. 53, pp. 486-494, 2006.
[63] R. Datta and V.T. Ranganathan, "A Method of Tracking the Peak Power Points for a Variable Speed Wind Energy Conversion System", *IEEE Trans. Energy Convers., vol. 18, p. 163-168, Mar. 2003*.
[64] R. Piwko, X. Bai, K. Clark, G. Jordan, N. Miller, J. Zimberlin, "The Effects of Integrating Wind Power on Transmission System Planning, Reliability, and

Operations: Report on Phase 2, Prepared for The New York State Energy Research and Development Authority, City, State", General Elec., Albany, NY, Mar. 2005.
[65] N. Miller, J. Sanchez-Gasca, W. Price, and R. Delmerico, "Dynamic modeling of GE 1.5 and 3.6 MW wind turbine-generators for stability simulations" *Power Engineering Society General Meeting, 2003, IEEE*, Vol. 3., pp. 1977-1983, 2003.
[66] Baike Shen and Boon Teck Ooi, "Parameter-Insensitive Sensorless Decoupled P-Q Controller for Doubly-Fed Induction Machine" *Electrical Power Conference EPC 2007, IEEE*, pp. 2102-2107, 2007.
[67] K. Gogas, G. Joos, B. Ooi, Y. Zhang, and B. Mwinyiwiwa, "Design of a Robust Speed and Position Sensorless Decoupled P-Q Controlled Doubly-Fed Induction Generator for Variable-Speed Wind Energy Applications" *Electrical Power Conference EPC 2007, IEEE*, pp. 62-67, 2007.
[68] A. Petersson, L. Harnefors, and T. Thiringer, "Evaluation of current control methods for wind turbines using doubly-fed induction machines" *IEEE Trans. Power Electron.*, vol. 20, 2005, pp. 227-235.
[69] R.J. Konopinski, P. Vijayan, and V. Ajjarapu, "Extended Reactive Capability of DFIG Wind Parks for Enhanced System Performance" *IEEE Trans. Power Syst.*, vol. 24, pp. 1346-1355, 2009.
[70] G. Tsourakis, B. Nomikos, and C. Vournas, "Effect of wind parks with doubly fed asynchronous generators on small-signal stability" *Electric Power Systems Research*, vol. 79, pp. 190-200, Jan. 2009.
[71] Espen Hagstrom, Ian Norheim, and Kjetil Uhlen, "Large-scale wind power integration in Norway and impact on damping in the Nordic grid", *Wind Energy*, John Wiley & Sons, vol. 8, 2005.
[72] website: www.winddata.com.
[73] C. Martinez, G. Joos, and B.T. Ooi, "Power System Stabilizers in Variable Speed Wind Farms" *Power and Energy Society General Meeting, IEEE PES 2009,* pp 1-7, Jul. 2009.
[74] A. Heniche and I. Kamwa, "Assessment of Two Methods to Select Wide-Area Signals for Power System Damping Control" *IEEE Trans. Power Syst.*, vol. 23, pp. 572-581, 2008.
[75] K. Zhou and J.C. Doyle, *Essentials of Robust Control*, Prentice-Hall, Englewood Cliffs, NJ, 1998.
[76] M. Klein, L. Le, G. Rogers, S. Farrokhpay, and N. Balu, "H∞ damping controller design in large power systems" *IEEE Trans. Power Syst.*, vol. 10, pp. 158-166, 1995.
[77] I. Kamwa, G. Trudel, and L. Gerin-Lajoie, "Low-order black-box models for control system design in large power systems" *Power Industry Computer Application Conference, IEEE*, pp. 190-198, 1995.
[78] L. Gerin-Lajoie, D. Lefebvre, M. Racine, L. Soulieres, and I. Kamwa, "Hydro-Quebec Experience with PSS Tuning" *Power Engineering Society Summer Meeting, 1999. IEEE*, vol. 1, pp. 88-95, 1999.

Appendix A: Wind Based Stabilizer Transfer Functions

This appendix is intended to present the parameters of the transfer functions of the wind based power system stabilizer. Eq. (A.1) shows the convention used for the coefficient of a transfer function. In this appendix, Num designate the numerator and Den the denominator.

$$T = a_0 s^{13} + a_1 s^{12} + ... + a_{11} s + a_{12} \tag{A.1}$$

A.1 Grid Connection Point Bus 5

Table A.1. Wind stabilizer active power loop transfer function parameters, bus 5

	P-Loop WPSS					
	0 km. ac line		25 km. ac line		50 km. ac line	
Index	Num	Den	Num	Den	Num	Den
0	0	1E-11	0	1E-11	0	1E-11
1	1.09E-14	4.14E-09	1.08E-14	4.14E-09	1.06E-14	4.14E-09
2	1.13E-10	4.98E-07	1.12E-10	4.98E-07	1.1E-10	4.98E-07
3	4.16E-08	1.49E-05	4.1E-08	1.49E-05	4.03E-08	1.49E-05
4	3.92E-06	0.000203	3.86E-06	0.000203	3.8E-06	0.000203
5	1.07E-05	0.00367	1.05E-05	0.003672	1.04E-05	0.003673
6	0.000888	0.027567	0.000875	0.027581	0.00086	0.027592
7	0.000812	0.301892	0.0008	0.302116	0.000787	0.302283
8	0.056323	1.380226	0.055506	1.381408	0.054604	1.382279
9	0.015907	8.640419	0.01568	8.648961	0.015427	8.65552
10	0.657267	15.70685	0.647993	15.72472	0.6377	15.73859
11	0.051594	72.2748	0.050866	72.37234	0.050058	72.45237
12	5.15E-06	5.581316	5.08E-06	5.588865	5E-06	5.59508

A.2 Grid Connection Point Bus 6

Table A.2. Wind stabilizer active power loop transfer function parameters, bus 6

	P-Loop WPSS					
	0 km. ac line		25 km. ac line		50 km. ac line	
Index	Num	Den	Num	Den	Num	Den
0	0	1E-11	0	1E-11	0	1E-11
1	2.17E-14	4.14E-09	2.12E-14	4.14E-09	2.06E-14	4.14E-09
2	2.25E-10	4.98E-07	2.19E-10	4.98E-07	2.14E-10	4.98E-07
3	8.25E-08	1.49E-05	8.06E-08	1.49E-05	7.85E-08	1.49E-05
4	7.78E-06	0.000203	7.59E-06	0.000203	7.39E-06	0.000203
5	2.12E-05	0.003675	2.07E-05	0.003676	2.02E-05	0.003677
6	0.001763	0.027601	0.001721	0.027615	0.001677	0.027626
7	0.001614	0.302619	0.001577	0.302851	0.001536	0.303026
8	0.112036	1.383246	0.109471	1.384491	0.106697	1.38542
9	0.031666	8.667733	0.030948	8.676994	0.030171	8.684196
10	1.309529	15.74461	1.280285	15.76567	1.24851	15.78242
11	0.1028	72.66334	0.100504	72.77636	0.098009	72.86996
12	1.03E-05	5.611852	1E-05	5.620552	9.79E-06	5.62779

A.3 Grid Connection Point Bus 7

Table A.3. Wind stabilizer active power loop transfer function parameters, bus 7

	P-Loop WPSS					
	0 km. ac line		25 km. ac line		50 km. ac line	
Index	Num	Den	Num	Den	Num	Den
0	0	1E-11	0	1E-11	0	1E-11
1	5.68E-14	4.14E-09	5.44E-14	4.14E-09	5.19E-14	4.14E-09
2	5.9E-10	4.98E-07	5.65E-10	4.98E-07	5.39E-10	4.98E-07
3	2.16E-07	1.49E-05	2.07E-07	1.49E-05	1.98E-07	1.49E-05
4	2.04E-05	0.000203	1.95E-05	0.000203	1.86E-05	0.000203
5	5.57E-05	0.003674	5.34E-05	0.003675	5.09E-05	0.003676
6	0.004625	0.027586	0.004431	0.027594	0.004226	0.027601
7	0.004235	0.302595	0.004059	0.302722	0.003872	0.30284
8	0.294047	1.382311	0.281827	1.382998	0.268864	1.383637
9	0.083114	8.666102	0.079681	8.671889	0.076036	8.677364
10	3.437399	15.72177	3.296576	15.73702	3.146839	15.75159
11	0.269851	72.71291	0.258795	72.79845	0.247041	72.88113
12	2.7E-05	5.616079	2.58E-05	5.622701	2.47E-05	5.629116

Table A.4. Wind stabilizer reactive power loop transfer function parameters, bus 7

	Q-Loop WPSS					
	0 km. ac line		25 km. ac line		50 km. ac line	
Index	Num	Den	Num	Den	Num	Den
0	0	1E-11	0	1E-11	0	1E-11
1	-4.579E-14	4.136E-09	-4.837E-14	4.136E-09	-5.103E-14	4.136E-09
2	-4.752E-10	4.98E-07	-5.019E-10	4.98E-07	-5.295E-10	4.98E-07
3	-1.744E-07	1.486E-05	-1.842E-07	1.486E-05	-1.944E-07	1.487E-05
4	-1.643E-05	0.000203	-1.736E-05	0.000203	-1.831E-05	0.000203
5	-4.49E-05	0.0036736	-4.744E-05	0.0036746	-5.005E-05	0.0036755
6	-0.0037262	0.027573	-0.0039368	0.0275842	-0.0041542	0.0275949
7	-0.003412	0.3025005	-0.0036056	0.3026541	-0.0038056	0.3028006
8	-0.2369084	1.3813649	-0.2503746	1.3823213	-0.2642806	1.3832449
9	-0.0669632	8.6623347	-0.0707887	8.6691969	-0.0747404	8.6758113
10	-2.7694528	15.703592	-2.9286671	15.724037	-3.093199	15.74411
11	-0.2174141	72.711501	-0.229913	72.797441	-0.2428301	72.880552
12	-2.171E-05	5.6160786	-2.296E-05	5.6227004	-2.425E-05	5.6291162

A.4 Grid Connection Point Bus 9

Table A.5. Wind stabilizer reactive power loop transfer function parameters, bus 9

	Q-Loop WPSS					
	0 km. ac line		25 km. ac line		50 km. ac line	
Index	Num	Den	Num	Den	Num	Den
0	0	1E-11	0	1E-11	0	1E-11
1	3.65E-14	4.14E-09	3.89E-14	4.14E-09	4.14E-14	4.14E-09
2	3.78E-10	4.98E-07	4.04E-10	4.98E-07	4.29E-10	4.98E-07
3	1.39E-07	1.49E-05	1.48E-07	1.49E-05	1.58E-07	1.49E-05
4	1.31E-05	0.000203	1.4E-05	0.000203	1.49E-05	0.000203
5	3.57E-05	0.003664	3.8E-05	0.003665	4.05E-05	0.003666
6	0.00296	0.027466	0.003156	0.027472	0.003359	0.02748
7	0.002701	0.300781	0.002881	0.300868	0.003067	0.300963
8	0.187364	1.370376	0.199809	1.370951	0.21272	1.371572
9	0.052598	8.565163	0.056102	8.569214	0.059737	8.573518
10	2.156669	15.36749	2.300861	15.38059	2.450532	15.39429
11	0.169206	71.08871	0.18052	71.13939	0.192264	71.19171
12	1.69E-05	5.487472	1.8E-05	5.491422	1.92E-05	5.495476

Table A.6. Wind stabilizer active power loop transfer function parameters, bus 9

	P-Loop WPSS					
	0 km. ac line		25 km. ac line		50 km. ac line	
Index	Num	Den	Num	Den	Num	Den
0	0	1E-11	0	1E-11	0	1E-11
1	-2.6E-14	4.14E-09	-2.5E-14	4.14E-09	-2.4E-14	4.14E-09
2	-2.7E-10	4.98E-07	-2.6E-10	4.98E-07	-2.5E-10	4.98E-07
3	-1E-07	1.49E-05	-9.6E-08	1.49E-05	-9.2E-08	1.49E-05
4	-9.4E-06	0.000203	-9E-06	0.000203	-8.7E-06	0.000203
5	-2.6E-05	0.003665	-2.5E-05	0.003666	-2.4E-05	0.003666
6	-0.00212	0.027481	-0.00205	0.027484	-0.00196	0.027487
7	-0.00194	0.300887	-0.00187	0.300948	-0.00179	0.301014
8	-0.13433	1.371448	-0.12948	1.371755	-0.12426	1.372088
9	-0.03771	8.569466	-0.03635	8.57244	-0.03489	8.575591
10	-1.54617	15.3884	-1.491	15.39627	-1.43143	15.40436
11	-0.12131	71.09034	-0.11698	71.14061	-0.11231	71.1925
12	-1.2E-05	5.487473	-1.2E-05	5.491423	-1.1E-05	5.495476

A.5 Grid Connection Point Bus 10

Table A.7. Wind stabilizer active power loop transfer function parameters, bus 10

	P-Loop WPSS					
	0 km. ac line		25 km. ac line		50 km. ac line	
Index	Num	Den	Num	Den	Num	Den
0	0	1E-11	0	1E-11	0	1E-11
1	-1.8E-14	4.14E-09	-1.8E-14	4.14E-09	-1.7E-14	4.14E-09
2	-1.9E-10	4.98E-07	-1.9E-10	4.98E-07	-1.8E-10	4.98E-07
3	-7E-08	1.49E-05	-6.8E-08	1.49E-05	-6.7E-08	1.49E-05
4	-6.6E-06	0.000203	-6.4E-06	0.000203	-6.3E-06	0.000203
5	-1.8E-05	0.00367	-1.8E-05	0.003671	-1.7E-05	0.003672
6	-0.00148	0.027549	-0.00145	0.027558	-0.00142	0.027564
7	-0.00136	0.301759	-0.00133	0.301902	-0.0013	0.302016
8	-0.0941	1.377774	-0.09215	1.378513	-0.09006	1.379085
9	-0.02649	8.616913	-0.02595	8.622648	-0.02536	8.627265
10	-1.09038	15.56581	-1.06825	15.57844	-1.04431	15.58845
11	-0.08557	71.77173	-0.08383	71.84554	-0.08195	71.90776
12	-8.5E-06	5.541152	-8.4E-06	5.546847	-8.2E-06	5.551659

A.6 Grid Connection Point Bus 11

Table A.8. Wind stabilizer active power loop transfer function parameters, bus 11

	P-Loop WPSS					
	0 km. ac line		25 km. ac line		50 km. ac line	
Index	**Num**	**Den**	**Num**	**Den**	**Num**	**Den**
0	0	1E-11	0	1E-11	0	1E-11
1	-3E-14	4.14E-09	-3E-14	4.14E-09	-3E-14	4.14E-09
2	-3.1E-10	4.98E-07	-3.1E-10	4.98E-07	-3.1E-10	4.98E-07
3	-1.2E-07	1.49E-05	-1.1E-07	1.49E-05	-1.1E-07	1.49E-05
4	-1.1E-05	0.000203	-1.1E-05	0.000203	-1.1E-05	0.000203
5	-3E-05	0.003667	-2.9E-05	0.003668	-2.9E-05	0.003669
6	-0.00246	0.027533	-0.00243	0.027545	-0.0024	0.027553
7	-0.00224	0.301321	-0.00222	0.301508	-0.00219	0.301645
8	-0.15573	1.376909	-0.15392	1.377872	-0.1519	1.378555
9	-0.04389	8.610045	-0.04339	8.617077	-0.04282	8.622253
10	-1.80885	15.60881	-1.78848	15.62307	-1.76542	15.63311
11	-0.14198	71.76029	-0.14038	71.84135	-0.13857	71.90389
12	-1.4E-05	5.540908	-1.4E-05	5.547183	-1.4E-05	5.552031